JIMMA UNIVERSITY

JIMMA INSTITUTE OF TECHNOLOGY

FACULTY OF ELECTRICAL AND COMPUTER ENGINEERING

THESIS ON THE PARTIAL FULFILLMENT OF THE REQUIREMENTS FOR THE DEGREE OF MASTER OF

SCIENCE IN ELECTRICAL AND COMPUTER ENGINEERING (CONTROL AND INSTRUMENTATION ENGINEERING)

SPEED CONTROL OF BRUSHLESS DC MOTOR USING FUZZY BASED MODEL REFERENCE ADAPTIVE CONTROL

By Kejela A.

Advisor: Dr.Amurth R T. (PhD)

Co-Advisor: Mr. Muhidin Mohammed. (MSc)

JIMMA, ETHIOPIA

APPROVAL LATTER

JIMMA UNIVERSITY

JIMMA INSTITUTE OF TECHNOLOGY

FACULTY OF ELECTRICAL AND COMPUTER ENGINEERING

SPEED CONTROL OF BRUSHLESS DC MOTOR USING FUZZY BASED MODEL REFERENCE ADAPTIVE CONTROL

A Thesis Submitted to Jimma Institute of Technology, School of Graduate Studies, Jimma University, In Partial Fulfilment of the Requirement for the Degree of Master of Science in Electrical and Computer Engineering (Control and Instrumentation Engineering)

BY: Kejela Adane

Approved by Board Examiners

Chairman, School of Graduate Committee

Signature:_____, Date:_____

Advisor Name: Dr.Amurth R T. (PhD)

Signature: A=th. R- T. , Date: 19/09/2020

Co-Advisor Name: Mr. Muhidin Mohammed (MSc)

Signature: _____ , Date: _____

External Examiner Name: Dr. Dereje Shiferaw

Signature: _____ , Date: Sept 04/2020

Internal Examiner Name: _____

Signature:_____ , Date: _____

DECLARATION

I hereby declare that this thesis entitled "**Speed Control Of Brushless Dc Motor Using Fuzzy Based Model Reference Adaptive Control**" composed of by myself, with the guidance of my advisors, that the work contained herein is my own except where explicitly stated otherwise in the text, and that this work has not been submitted, in whole or in part, for any other degree or processional qualification.

Name **Signature,** **Date:**

Kejela Adane

Approved by:

Thesis Advisor: **Dr.Amurth R T. (PhD)**

Signature: 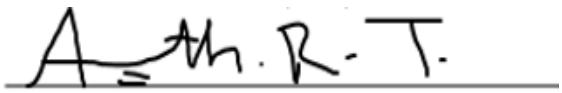 Date: 19/09/2020

Thesis Co-Advisor: Mr.Muhidin M. (MSc)

Signature,_____ Date: _____

ABSTRACT

Brushless DC motor drives are widely used in various industrial systems, such as servomotor drives, medical, automobile and aerospace industry. BLDC motors are commutated electronically and offer many advantages over brushed DC motors which include increased efficiency, longer life, low volume and high torque. Speed control of BLDC motor with drastically changing and uncertain load variation with conventional PID control system is unable to cup up with and also unable to adapt system load variation with constant gain values. So, the main objective of this thesis is to design a controller to keep the output speed of the BLDC motor constant, under different operating conditions such as parameter variations at rated speed, uncertain load disturbances and etc. In Fuzzy intelligent controller Based model reference adaptive control, the plant output is varied with respect to the output of the reference model with some adjusting mechanism in order to obtain the speed control at operating condition. The platform for modelling of BLDC motor and simulation of the control system has been done using MATLAB/Simulink Software and the result shows that intelligent based model reference adaptive controller is better in steady state performance and load rejection property than simple MIT rule and conventional PID controller and improved the existing system of the steady state response.

Keywords: Brushless DC motors, Fuzzy Logic control, Model Reference Adaptive Control, Lyapunov Stability Method, PID Controller.

ACKNOWLEDGEMENT

First of all I would like to express my deepest gratitude to my GOD. Secondly, I would like to express my deepest gratitude and appreciation to my advisors **Dr.Amurth R T (PhD)** and a **Co-**Advisor **Mr.Muhidin M (MSc).** For they excellent guidance, caring, patience, enthusiastic encouragement and useful critiques for doing this thesis. They helped me as much as possible when I present with any question they answer my question politely and without they supervision and constant help this thesis would not have been done. Besides my advisors, I'm very grateful to thanks **Mr. Abu Feyo** Coordinator of ECE Faculty and **Mr. Tesfabirhan S** Chairman of industrial control stream, for their valuable suggestions during the execution of this thesis and also for giving me moral support throughout the period of this thesis execution.

Finally, I would like to thanks my best friends for supporting me to get through the difficulty problems by solving together up to the end and for all the emotional support, camaraderie, entertainment, and caring they have provided for me.

TABLE OF CONTENT

LIST OF FIGURES

LIST OF TABLE

ACRONYMS

DSP	Digital signal proses
DC	direct current
EMDM	Electromagnetic design method
EMF	Electromagnetic force
FCM	Field-circuit method
FLC	Fuzzy logic controller
HVAC	high voltage alternative current
MRAC	Model Reference Adaptive Control
PID	Proportional integral derivative
PMBLDCM	Permanent magnet brushless dc motor
PMSM	Permanent magnet synchronous motor
PWM	pulse width modulation

LIST OF SYMBOLS

B_v - Viscous Friction Coefficient

i_x - Phase current

$f_A(\theta)$ - Back-EMF of phase A

J - Moment of inertia

K_p - Proportional constant

K_I - Integral constant

L - Stator inductance per phase

L_A - Self-inductance of phase A

M - Mutual inductance between phases

N - Turns of winding

R_x - phase resistance

R - Stator resistance per phase

T_e - Electromagnetic torque

T_L - Load torque

ω_m - Angular speed of the motor

θ - Angular position of the rotor

λ_m - Flux linkages

u_x - Phase voltage

$e_{\psi x}$ - Phase-induced EMF

$\psi_{pm}(\theta)$ - PM flux linkage of phase A

θ - Position angle of rotor

Λ_A - Permeance of self-inductance of phase A

Ω - Angular velocity of rotation

CHAPTER ONE
INTRODUCTION

1.1 Background

Two typical definitions about the brushless DC motor (BLDC motor, BLDCM) have been presented by scholars. Some of them considered that only the trapezoid-wave/square-wave brushless motors could be called BLDC motors, and sine-wave brushless motors should be called permanent magnet synchronous motors (PMSM) [1, 2].However, other scholars thought that all the motors above should be considered as BLDC motor [3].BLDCM are powered and run by DC voltage, but current commutation is achieved by electric commutation system which is solid state current commutation. The commutation instant is determined by the rotor position which is detected either by position sensors or by sensorless techniques and BLDC motors have many advantages such as [1]:

- Long operating life.
- High dynamic response.
- High efficiency.
- Better speed vs. torque characteristics.
- Higher speed range.
- Higher torque–weight ratio.

Therefore the BLDC motor has been used in many applications such as electric automotive, robotics, HVAC, electronics, computer, semiconductor, CD-ROMS and medical industries, feed drives for CNC machines, extruder drives, and in such applications BLDC motor exposed to many kinds of load disturbances. Conventional controlling methods couldn't achieve the required speed and tracking response with stable good accuracy in the condition of sudden disturbance and parameter variations. This problem can be solved by using advanced control techniques such as adaptive control, variable structure control, fuzzy control and neural network control [2].

The commutation is done electronically by controlling the power switches that are used in the inverters of BLDC motors. The commutation region of back emf should be as small as possible so as to make it difficult to commutate a phase of that motor when driven by current source inverter. The flat portion of back emf should be 120^0 for constant torque production.

Therefore a control system is a device that regulates or controls the dynamics of any other plant or process like BLDC motors. Adaptive control is one of the widely used control strategies to design advanced control systems for better performance and accuracy. Model Reference Adaptive Control (MRAC) is a direct adaptive strategy with some adjustable controller parameters and an adjusting mechanism to adjust the speed of the motor. As compared to the well-known and simple structured fixed gain PID controllers, so fuzzy based adaptive controllers are very effective to handle the unknown parameter variations and environmental changes. An adaptive controller consists of two loops, an outer loop or normal feedback loop and an inner loop or parameter adjustment loop. This thesis deals with designing of fuzzy based adaptive controller with MRAC scheme using Lyapunov controller to control the speed of brushless DC motors.

1.2 Statement of Problem

In the recent years conventional controls system are unable to follow the close loop plant system since they are a fixed gain controllers, and under different operating conditions such as parameter variations, load and disturbances also unable to sustain its original place of the process and etc. Nowadays the Fuzzy and adaptive control schemes are making their place where the conventional control system is not able to cope-up or resolve with the situation, like

- Loads, inertias and other forces acting on system change drastically.
- Possibility of unpredictable and sudden faults.
- Possibility of frequent or unanticipated disturbances.

The conventional controllers with fixed gain are unable to cop up with the problems discussed above for BLDC motor and for those different system of variable operation condition.

1.3 Objectives

1.3.1 General Objective

The general objective of this thesis is to design Speed Control of Brushless DC Motor by Using Fuzzy based Model Reference Adaptive Control.

1.3.1 Specific Objectives

- To Simulate and design Fuzzy based adaptive controller by using MATLAB/Simulink Module.
- To compare the importance of Fuzzy based model referenced adaptive controller with conventional controller.
- To check stability of brushless dc motor by using Lyapunov stability method.
- To validate the effectiveness of Fuzzy based Model Reference Adaptive controller as compared to simple MRAS and conventional controller operating at different rated speed and sudden load variation.

1.4 Scope and Limitation

- All of the models will be implemented in simulation method only using MATLAB/ Simulink software.
- The effectiveness between Fuzzy based MRAC controller and simple MRAC and conventional PID controller will be studied in terms of maximum overshoot, rise time (tr), settling time (ts),steady state error and speed variation from desired value under reference speed and load variations.
- Analyses of the controller will be carried out for constant adaptation gain and different rated speed and load variation.
- And the performance of the proposed control is not checked practical due to time and unavailability of piratical parameters on the laboratory.
- The control program is operated on a personal computer not a dedicated Machine (that means it is not on F LC machine).

1.5 Thesis Organization

The outline of this thesis is as follows. In Chapter Two Literature Review and related works about BLDC motor; In Chapter Three is the mathematical model and characteristics analysis of BLDC motor; in chapter four controllers design to regulate the speed of BLDC motor and .The simulation results followed by its analysis is described in chapter Five and Conclusion and Future works recommendation are given in chapter six.

CHAPTER TWO

LITERATURE REVIEW

DC motors are widely used in industrial applications such as electric vehicles, steel rolling mills, electric cranes, robotic manipulators, and home appliances where speed or/and position control of motor are required because of their high reliabilities, flexibilities and low costs. While, the control of the position or speed of a BLDC motor is an important concern and since then it has been studied until today. Many control methods are used for control of speed or position of DC motor and the simple and low cost controller structure is always in demand for most industrial and high performance applications. Every control theory has some advantages as well as disadvantage due to that the particular control theory methods considered as a suitable control method under specific conditions, compared to others methods of control. The control method that gives the best performances under any conditions is always in demanded for control.

Model reference adaptive control is the most recent class of control techniques, though research in adaptive control has a long and vigorous history since 1950s, it was motivated by the problem of designing an autopilots for aircraft operating at wide range of speeds and altitudes. Consequently, gain scheduling based on some auxiliary measurements of air speed was adapted. Kalman developed the concept of a general self-tuning regulator with explicit identification of the parameters of linear, single-input, single-output system and he used these parameter estimates to update an optimal linear quadratic controller. In 1960s Lyapunov's stability theory have been established as a way for improving convergence in adaptive controls methods.

Scientists have made attempts to regulate the speed of motors for many years. The conventional control method of a PID controller system with fixed gain are unable to solve the problems discussed in the statement problems. Though recently advanced fuzzy PID controllers have been developed to solve with the problems of electrical and mechanical systems. Hwang (2000) and Tang (2001) gave the concept of fuzzy PID controller. Speed control using PWM (pulse width modulation) signals was one from the earlier techniques [1]. Feedback signals from the PMBLDC motor representing speed and position are utilized to get the driving signals for the inverter switches. The nonlinear characteristics of a DC motor such as saturation and friction could degrade the performance of conventional PID controller.

Rubaai (2008) developed the DSP-Based Laboratory model of Hybrid Fuzzy-PID Controller Using Genetic optimization for high-performance Motor Drives. Later on the concept of neural network is applied to develop the PID controllers to enhance the dynamic characteristics of controller. Sun (2006) and Yao (2008) developed such PID controllers based on the artificial Neural Network technique. Still to obtain the complete adaptive nature, specific adaptive control techniques are needed.

W. Arnold, and D. Jacobson (2013) proposed a neural-network-based motor control system which has a strong ability to solve the structure uncertainty and the disturbance of the system, whereas it requires more computing capacity and data storage space.

Mohamed. A.Shamseldin, and M. Abdullah Eissa (2015) proposed MRAC with PID compensator. Contrary to the classical approach, where the modified MRAC ensure faster response and eliminate the overshoot. Also, in this work, they have designed self-tuning fuzzy PID controller which shows a good performance compared to conventional PID controller whereas they have used extra PID compensator and Modified MIT rule but still need improve stability of the system .

C. Mohankrishna et al (2016), presents a state space modeling, simulation and control of permanent magnet brushless DC motor, the motor is designed based on state space model to get information about the state of the system variables at some predetermined points along the flow of signals. By adopting this model, powerful processor requirement, large random access memory can be avoided with more design flexibility and faster results can be obtained but still the system needs to have intelligent controller to adapted load variation condition and have to reduce fast speed response to protect the motor from damage.

Adel A.El-samahy and Mohamed A.Shamseldin (2018), proposed BLDC motor tracking control using self-tuning fuzzy PID control and model reference adaptive control and the paper compares the performance of two different control techniques applied to high performance brushless DC motor And they used self-tuning fuzzy PID controller and adaptive MRAC controller with PID compensator to achieve for different speed/time tracks regardless of load disturbance and parameter variation and their control system have better performance but they ignored load disturbance and input variation and they have used additional PID compensator.

Thasneem.M.S., and Shalu George K (2018)., proposed a controller and designed to regulate the speed of BLDC motor using a conventional PID control technique and also a control technique with model reference adaptive control is used and still the proposed system have considerable percentage overshoot and high rise and settling time when compared with a conventional controller.

Murali Dasari et al (2019), they proposed Model Reference Adaptive Control for BLDC motors and designed with a PID controller tuned by GA-ANFIS. GA-Trained ANFIS framework for tuning the PID controller has been proposed. This is used along with the MRAC to deliver enhanced performance in the control of BLDC motor and the performance is validated against convention PID and self-tuning PID controllers. The result demonstrates a superior performance of the proposed approach but still they used an extra compensator to tune a PID controller and didn't consider uncertain load disturbance.

The above mentioned techniques require accurate nonlinear model for better tracking. Soft computing techniques like Genetic algorithm were introduced and Conventional feedback controllers like proportional derivative (PD) controllers, proportional-integral-derivative (PID) and hybrid fuzzy PID controllers were discussed to achieve speed control of BLDC motor [3-4]. However, major problems in applying a conventional PID controller in a position or/and speed are the effects of nonlinearity in a DC motor. Genetic Algorithm is proposed as a global optimizer to find optimized PID gains for position control of BLDC motor [5]. It has a disadvantage of high power consumption. Using fuzzy logic as a design methodology, which can be applied in developing nonlinear system for embedded control. Accommodates non-linearity without utilization of mathematical model developed the next controller [6].Speed controllers using Fuzzy based PID controllers came into existence[7].A single set of Fuzzy rules were used for controlling $K_P, K_I \; and \; K_D$values in the controller so it failed to adapt with change in parameters. The controller is designed to regulate and robust the speed of BLDC motor using a conventional PID control technique and a control technique with model reference adaptive control and also a fuzzy control techniques for error reduction by minimizing steady state error as well as percentage over shoot is used for the design system. Therefore in this thesis three advanced control strategies are going to be adopted and compared. The first control technique is conventional PID controller which shows a good performance compared to the other conventional controller. The second

technique is based on MRAC system and having MRAC system on the plant shows a reasonable performance but it has comparative rise time and steady state error. The third technique is Combining MRAC with fuzzy control theory which minimizes both the overshoots and steady state error of the control system and have ability to reject load disturbance with adapting mechanism and sustain motors long operating life as advantage.

Therefore, the basic task is to design such a control, which will ensure the minimal error between the reference model and the plant outputs despite the uncertainties or variations in the plant parameters and working conditions.

The Main approach is to design a model reference adaptive controller using Fuzzy based on Lyapunov stability theory method. This theory assures that the system at equilibrium point is asymptotically stable and is preferred for a second order system as it yield better performance than MIT Rule.

CHAPTER THREE

MATHEMATICAL MODELING AND CHARACTERISTICS

The mathematical model of the BLDC motor is fundamental for the corresponding performance analysis and control system design. The structure characteristics and working modes of the BLDC motor has been considered when we are building its model. The BLDC motor generally consists of three parts: the motor structure, the power driving circuit, and the position sensor. Moreover, there are various structures and different driving modes. In the first section of this chapter, we introduced several existing structures and driving modes of BLDC motors. The common mathematical models, which mainly include differential equation model, transfer function model, and state-space model where presented in the second section. Finally, the steady and dynamic characteristics are analyzed and the variations of current and torque during commutation are discussed in detail.

3.1 Structure and Drive Modes of BLDC

3.1.1 Basic Structure

The main design principle of a BLDC motor is to replace the mechanical commutator by using an electrical switch circuit. In traditional DC motors, the brushes are used for commutation, making the directions of the main magnetic field and the armature magnetic field perpendicular to each other when the motor is running. For the purpose of realizing commutation without mechanical contact, brushes were abandoned after the “inverted DC motor” was developed in which armature winding and magnet steel are placed on the stator and rotor sides separately. In order to control the motor’s rotation speed and direction, a rotor-position sensor, a control circuit, together with a power inverter must be included in a BLDC motor system.

Compared with other kinds of motors, the BLDC motor is excited by a square wave, so that the motor has lots of advantages, such as higher permanent magnet utilization, smaller size, larger motor torque, higher efficiency and reliability. Therefore, the BLDC motor plays an important role in product quality improvement, service life extension and energy saving. These superiorities are becoming even more evident along with the presence of higher performance and lower price of new types of NdFeB.

The BLDC motor's structure contains a stator with armature winding and a rotor with a permanent magnet, which is similar to PMSM. The cross-sectional image of a four-pole BLDC motor is shown in Figure 3.1 below.

3.1.1.1 Stator Cores

The stator structure of the BLDC motor is similar to that of a general synchronous motor or an induction motor. Single-or multiple-phase symmetric windings are embedded in the iron core, which can be connected in "Y" or "D" type. Considering the performance and the cost of the system, the Y-type is mostly used, in which the three phase windings are connected symmetrically without a neutral point. Note that in the traditional brush DC motor, the armature winding is placed at the rotor, whereas in the BLDC motor, installed at the stator side, causing less heating.

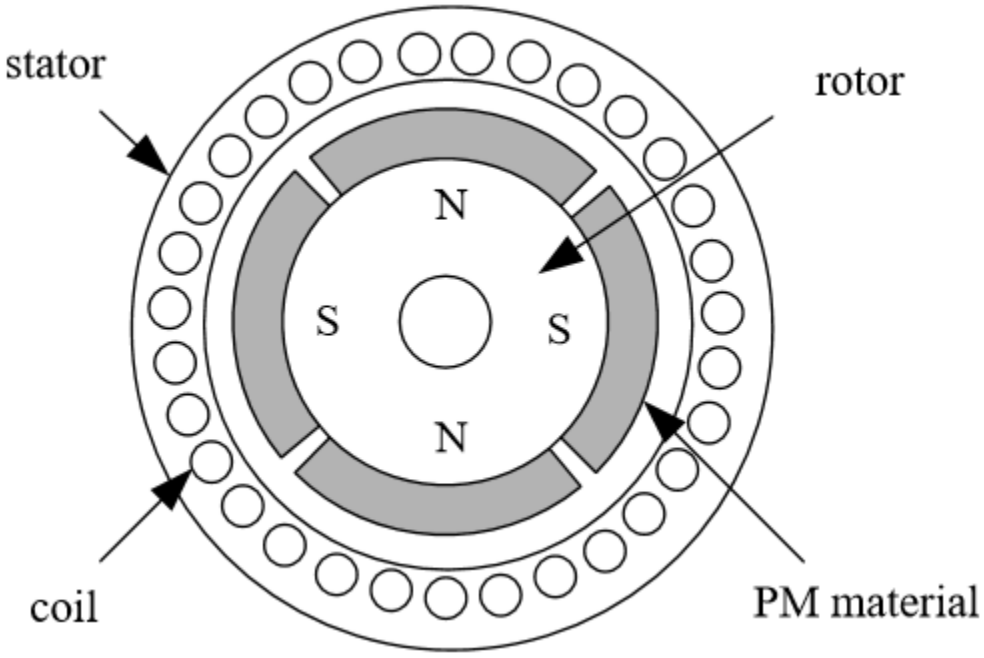

Figure 0.1 Cross-sectional image of a BLDC motor.

3.1.1.2 Windings

The common winding types used in BLDC motors are concentrated full-pitch windings, distributed full-pitch windings, distributed short-pitch windings, etc. The different types of windings can affect the waveform of the back-EMF and the performance of the motor.

(1) For the concentrated full-pitch winding, the wires of the same phase are placed in one cog, and therefore the air-gap flux density in the motor is the same. By adding the back EMF generated by

wires of each phase, we can get the waveform of the total back-EMF, which has a similar shape as the air-gap flux density. Furthermore, the platform width of the back-EMF waveform is the same as that of the air-gap flux density waveform. Thus, the concentrated full-pitch winding can produce a better trapezoidal back-EMF.

(2) For the purpose of cooling the winding effectively through the inner surface space of the stator, the coil winding can be dispersed evenly at the surface of the stator, which is called distributed winding. Under normal circumstances, it is hard for the spatial distribution of air-gap flux density to form an ideal square wave.

(3) On the other hand, application of the short-pitch winding makes it possible to shorten the connecting wires at the end of the winding. This can be helpful to save copper material and weaken the torque harmonics.

3.1.1.3 PM Rotor

The BLDC motor's rotor is constituted by permanent magnets with certain pole pairs embedded in the surface or the inside of the iron core. At present, the permanent magnets are usually made using rare-earth permanent magnetic materials like NdFeB, which have the advantages of high coercivity and remanence intensity. The permanent magnetic steels, in the BLDC motors as well as the brushed motors, are used to produce a sufficient magnetic field in the air gap. The only difference between them is that in BLDC motors, PM steels are installed on the rotor side, whereas they are placed on the stator side in brushed motors. Three typical structures of the BLDC motor rotors are as follows.

(1) Surface-mounted PM rotor. For the surface-mounted PM rotor, on the surface of the iron core there is mounted radial magnetized tile-shaped rare-earth permanent magnet. Furthermore, the tile-shaped poles can be assembled by rectangle strips so as to cut the costs of the motor. In the design procedure of the motor, the designer always adopts this structure with its pole arc width larger than 120 degree electric angle in order to generate a square air-gap flux density and decrease torque ripple.

(2) Magnet-embedded rotor. When the rectangular permanent magnets are embedded into the iron core of the rotor, we call it a magnet-embedded rotor. Since the magnetism gathering technology

can provide larger flux, the flux under one polar pitch is produced by two adjacent poles in parallel. In this case, magnetism-isolating technology or a stainless steel shaft should be adopted.

(3) Magnetic loop rotor. For the magnetic loop rotor, a rare-earth PM ring magnetized radially in multiple poles through a special way is overlapped around the iron core. Note that it is usually used in low-power motors.

3.1.1.4 Position Sensor

The position sensors installed in the motor can detect the rotor position and transform it in to an electrical signal, providing the correct commutation information for the logic switch circuit. Hence, the proper current commutation of the windings is obtained according to rotor position information, and the PM rotor will rotate continuously because of the stepping rotating magnetic field generated by the current in the air gap.

There are various kinds of position sensors and each has its own characteristics. At present, a wide range of electromagnetic, photoelectric and magnetic sensors have been used in BLDC motors. The Hall sensor, as a kind of magnetic sensor, has the advantages of compact volume, low price and convenient operation. Therefore, it is commonly used in BLDC motor control systems as the rotor-position detector.

3.1.2 General Design Method of BLDC Motor

The general methods of BLDC motor design mainly contain an electromagnetic design method (EMDM) and a field-circuit method (FCM). The EMDM is used more frequently than the FCM for its simplicity. However, the FCM can be used to get more accurate results, because it is allowed to check the magnetic field of the design scheme with the finite element method and make corresponding appropriate adjustments.

The EMDM is the traditional design method of BLDC motors. It mainly includes four steps:

1) Confirm the rotor structure according to the technical requirements;
2) Determine the magnetic load B_δ according to the rotor structure and the performance of permanent magnet;
3) Decide the electrical load A by B_δ;

4) Determine the basic size D, L according to A and B_δ. Note that this method is easy to implement in practice. But its calculation precision is relatively poor.

The FCM of BLDC motor design is based on the analysis of finite elements of magnetic field, where the magnetic and circuit parameters are obtained from the finite-element analysis and the electrical circuit, respectively. The high-precision analysis of magnetic field (generally the 2D calculation of the magnetic field meets the design requirements) is the main advantage of the method. But the amplitude and phase position of the equivalent current will change when the magnetic field is analyzed. So, the magnetic-field analysis and the circuit calculation must be carried out synchronously.

3.1.3 Drive Modes

3.1.3.1 Half-Bridge Mode

For Y-connected BLDC motors, the generally used three-phase half-bridge driving circuit is shown in Figure 3.2. In the Figure 3.2, LA, LB and LC represent the windings of phase A,B, and C, respectively, and the power switches T1,T2 and T3 are connected to the three-phase windings in series. The rotor position signals HA, HB and HC are used to drive the power switches after being amplified so as to control the motor commutation. During the commutation process, the rotating step magnetic field generated by each stator winding in the air gap has three magnetic states in the range of 360^0electrical angle, where each state holds on the 120^0 of electrical angle.

Although the three-phase half-bridge driving BLDC motor control system has the advantages of fewer drive components, lower cost, easy to control, it is seldom used because of its disadvantages of large torque ripples and low utilization of the windings. In this condition, each winding is conducted only 1/3 of the period.

The half-bridge driving BLDC motor control system schematic diagram is given in the Figure 3.2 below:

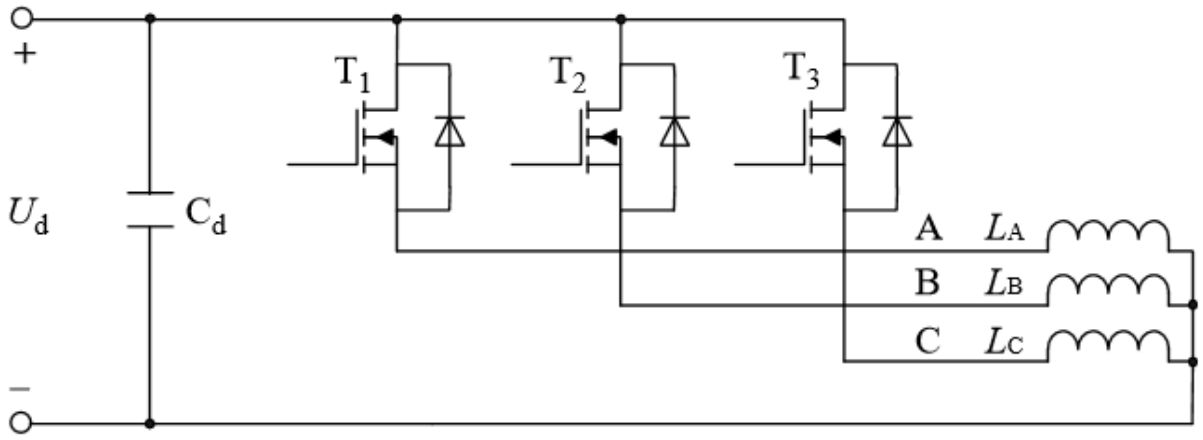

Figure 0.2 Half-bridge driving circuit [15].

3.1.3.2 Full-Bridge Mode

In the following content we introduced the full bridge driving circuit while taking the three phase Y-connected BLDC motor as an example. Figure 3.3 shows the schematic diagram of the full-bridge driving circuit. In the diagram, power switches T1, T 2, T 3, T 4, T 5 and T6 are used to turn on or turn off the currents of the windings according to the logic signals produced by Hall sensors.

The mainly used conduction modes are the two-phase conduction mode and the three phase conduction mode.

1) Two-phase conduction mode

The principle of the two-phase mode is conducting two of the motor windings all the time as well as suspending the third one. The conduction order and instant are determined by the rotor position information that is generated by the sensors. In this condition, the synthetic rotating magnetic field generated by the stator is a step field instead of a continuous one. The bridge converter commutates once the rotor rotates with $60^0$of electrical angle, and the magnetic status is consequently changed. So, there are six magnetic statuses and two phase windings are conducting in each state. The time of current flowing continuously in each winding is 120^0 electric angles.

In the two-phase mode, there is only one upper bridge switch conducted at a time, which produces the forward flowing current in the corresponding winding, resulting in a torque. Similarly, another torque is produced by the backward current because of the lower bridge switch conduction.

The sum of these torques constitutes the synthetic torque, which rotates 60^0 electrical angles at each commutation period. Therefore, the torque ripples are much smaller than that of a half-bridge driving system because the direction of torque changes six times in one cycle.

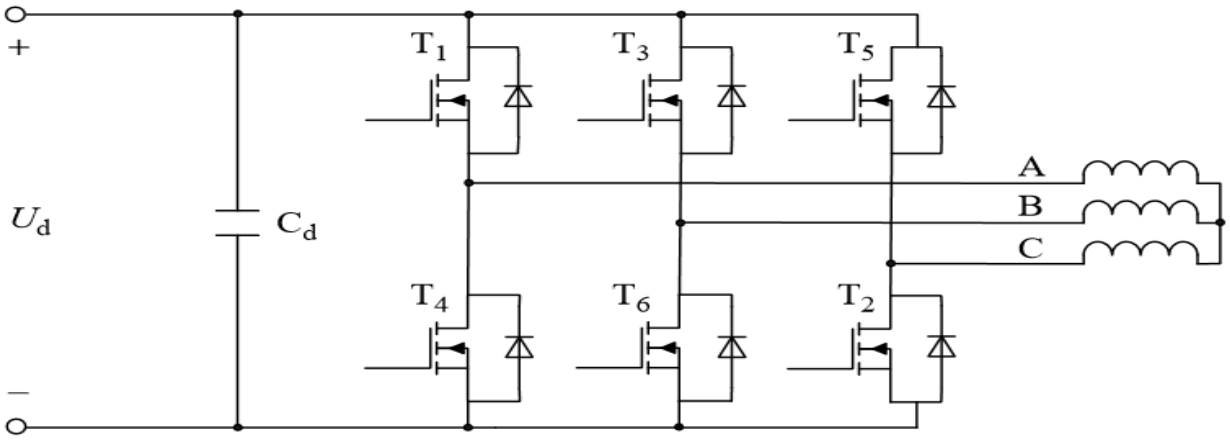

Figure 0.3 Full-bridge driving circuit.

2) Three-phase conduction mode

In the three-phase conduction mode, there are three power switches of the bridge energized every moment. Compared with the two-phase conduction mode, the three-phase conduction mode has the same driving circuit as shown in Figure 3.3. The only difference between these two modes is the order of conducting, and each power switch conducts 180^0 in the three-phase conduction mode.

The three-phase conduction mode can further increase the utilization of the windings as well as reduce the ripple torques. However, it should be noted that the three-phase conduction mode may possibly lead to the upper and lower switches of the same bridge being conducted at the same time.

The principle diagram of a Δ-connected three-phase full-bridge BLDC motor control system is shown in Figure 3.4. As shown in the figure, there are few differences between Δ–connected and Y- connected driving circuits. The only thing we need to do is consider the connection point of phase A and B in the Δ-connected motor as the point A in the Y-connected motor, while the connection point of phase B and C as B point, and the connection point of phase C and A as C point.

3.1.3.3 C-Dump Mode

In some applications of BLDC motors, good control performance, low cost and small size are all required In order to meet these requirements, a compromised method between half bridge control and full-bridge control was proposed by Walter and Stephen [16], which is called a C-Dump driving circuit. As shown in the Figure 3.5, only four power switches are used in the C-Dump driving circuit of the three-phase BLDC motor. The four-quadrant operation of the motor can be achieved through this driving mode. Compared with the full-bridge driving mode, there are fewer power switches and energy losses under the C-dump driving mode. However, larger commutation torque ripples may be produced.

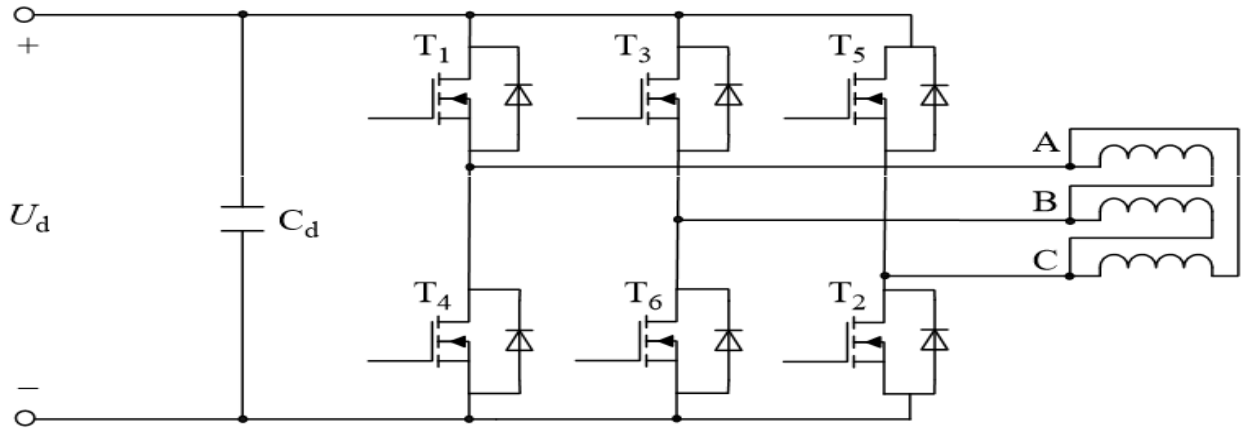

Figure 0.4 Full-bridge driving circuit for Δ–connected motor.

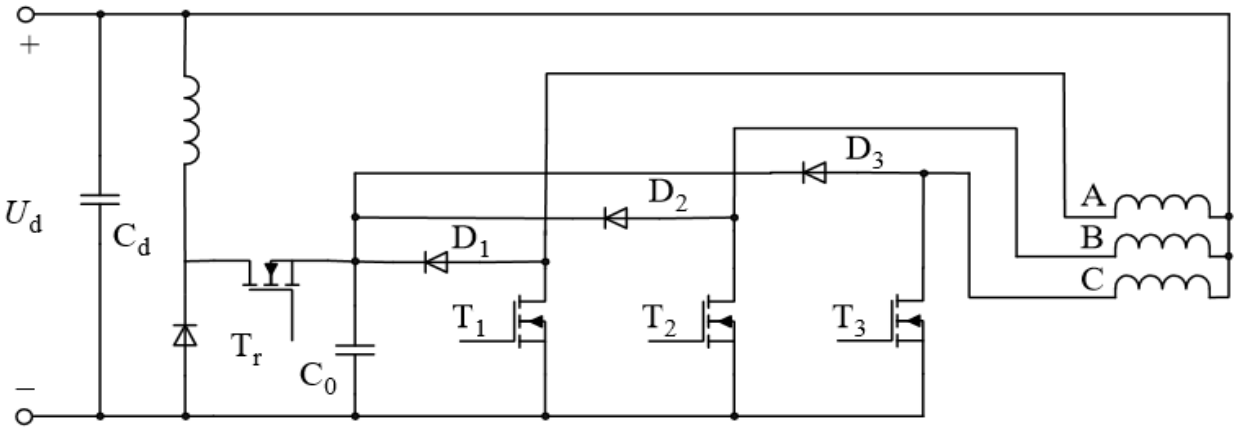

Figure 0.5 C-dump driving circuit.

Figure 3.6 shows the principle of the H-bridge power inverter. The typical feature of the H-bridge is that each winding is controlled by an H-bridge power inverter separately. The current of the BLDC motor can be controlled by this driving circuit easily. Moreover, the four-quadrant operation can also be achieved with this driving mode. Note that each H-bridge power inverter has 4 power switches for one phase winding. So, it is usually used in single-phase or two-phase BLDC motors. A delay control of the driving signals must be taken to prevent the upper and lower switches of the same bridge arm from being conducting at the same time.

This means that the switches of one side will conduct under the condition that the switches of the other side have been turned off reliably.

3.1.3.5 Four-Switch Mode

The structure of four-switch driving circuit is shown in Figure 3.7. In the topology, one bridge of the full-bridge driving circuit is replaced with two capacitances. The neutral point of the two capacitances is connected to the phase-C winding. Thus, two power switches are saved in the four-switch driving circuit so that the system has lower cost and less loss, whereas the control algorithm is more complicated [3].

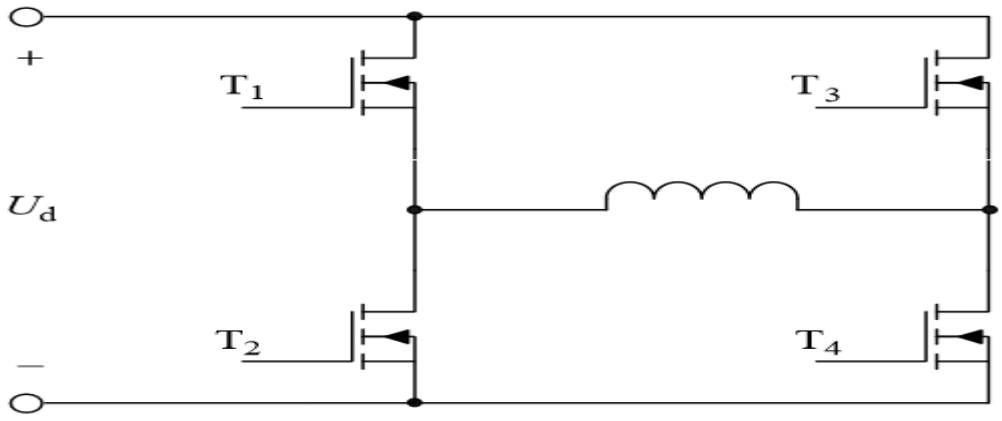

Figure 0.6 H-bridge driving circuit.

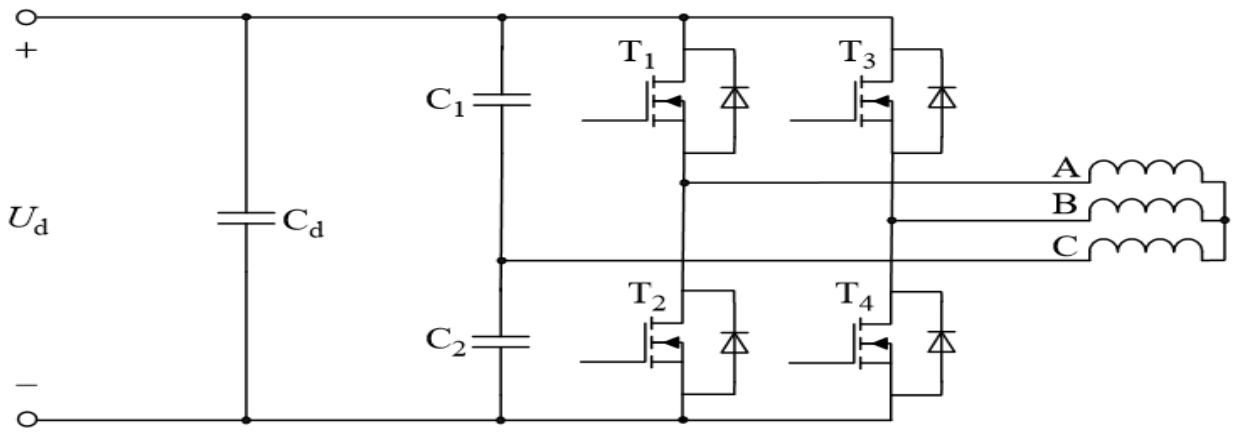

Figure 0.7 Four-switch driving circuit.

3.2 Mathematical Modeling

3.2.1 Differential Equations

In this section, the differential equation model is built for a three-phase two-pole BLDC motor. The stator has a Y-connected concentrated full-pitch winding, and the inner rotor has a non-salient pole structure. Three Hall sensors are placed symmetrically at 120^0 interval. Furthermore, the following assumptions are made to build the differential equation of the BLDC motor [17–18] by ignoring the following critical points of a control design theory.

- The core saturation, eddy current losses and the hysteresis losses of the motor.
- The armature reaction and the distribution of air-gap is a trapezoidal wave.
- The cogging effect and suppose the conductors are distributed continuously and evenly on the surface of the armature.
- Power switches and flywheel diodes of the inverter circuit have ideal switch features. Hence, the simplified schematic diagram of the motor can be obtained as shown below.

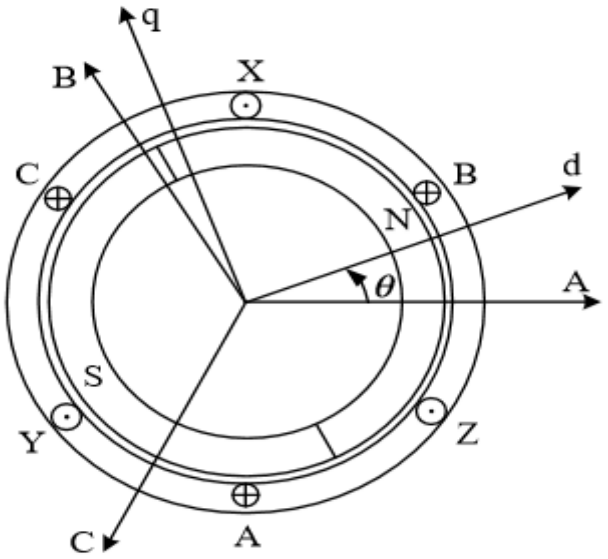

Figure 0.8 Structure of BLDC motor.

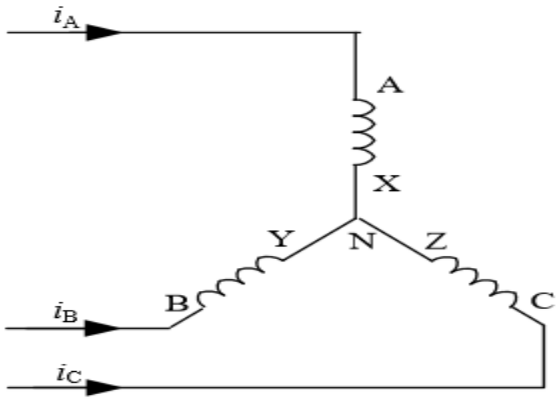

Figure 0.9 connecting type of winding.

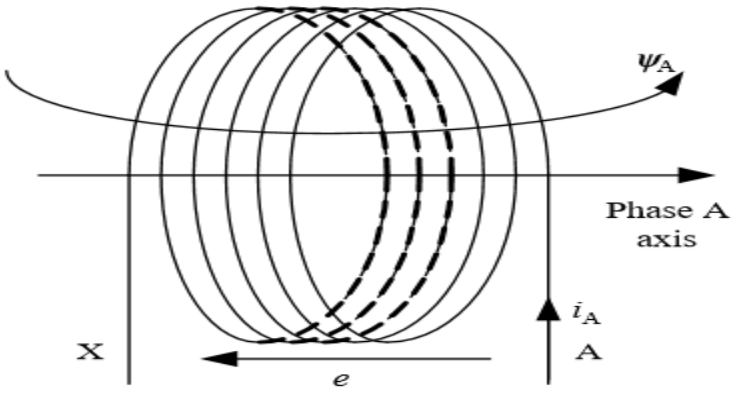

Figure 0.10 Provision of positive direction (Phase A).

Under the positive direction shown in Figure 3.10, the phase voltage of each winding, which includes the resistance voltage drop and the induced EMF, can be expressed as

$$u_x = R_x i_x + e_{\varphi x} \quad (3.1)$$

Where

u_x------ Phase voltage, in which subscript x denotes phase A, B and C;

i_x------phase current;

$e_{\psi x}$------- Phase-induced EMF;

R_x-----phase resistance. For three-phase symmetrical winding, there exists $R_A=R_B=R_C=R$

The winding-induced EMF is equal to the change rate of the flux. Since the positive direction of induced EMF and flux linkage defined is opposite to that of the right-hand screw rule, the induced EMF can be written as

$$e_{\psi x} = \frac{d_{\psi x}}{dt} \quad (3.2)$$

Taking phase A for example, the flux is given as

$$\psi_A = L_A + M_{AB} i_B + M_{AC} i_c + \psi_{pm}(\theta) \quad (3.3)$$

Where;

$\psi_{pm}(\theta)$ ---- PM flux linkage of phase A;

θ ---- Position angle of rotor, the angle between rotor d-axis and the axis of phase A;

L_A ---- Self-inductance of phase A;

M_{AB} , M_{AC} ---- mutual inductance of phase A with phase B and phase C.

The magnitude of $\psi_{pm}(\theta)$ depends on the magnetic field distribution of the PM in the air gap. The radial component of PM air-gap magnetic field distributes as a trapezoidal profile along the inner surface of the stator, is shown in Figure 3.11.

As shown in Figure 3.11, when the rotor rotates anticlockwise, the winding AX moves in the forward direction along the y-axis. Then, the effective flux of phase A will change with regard to the rotor position. When the rotor position is a, the PM flux of phase A is

$$\psi_{pm}(\alpha) = N\phi_{pm}(\alpha) \tag{3.4}$$

$$\psi_{pm}(\alpha) = \int_{-\frac{\pi}{2}+\alpha}^{\frac{\pi}{2}+\alpha} B(\theta)Sd\theta \tag{3.5}$$

Where

$\psi_{pm}(\alpha)$ ---- PM flux of phase A when the rotor position angle is a;

$B(\theta)$ ---- PM rotor radial flux density in the air gap, which is in a trapezoidal distribution along y;

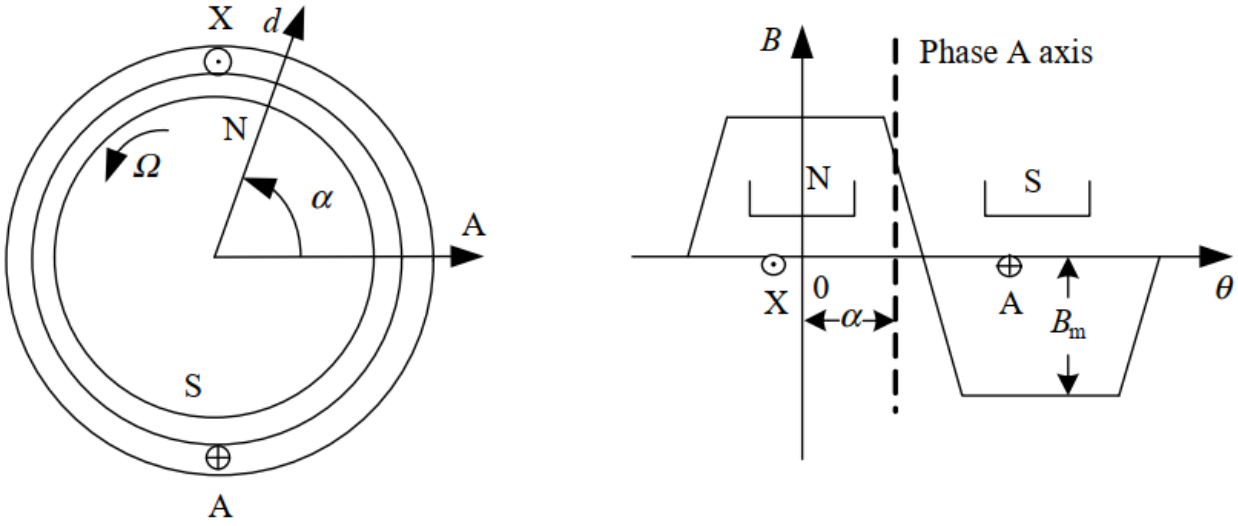

(a) Rotor position (b) Flux distribution

Figure 0.11 PM flux of phase A.

N--- Turns of winding;

S---- Product of rotor radius and effective length of conductors.

Substituting Equations (3.2)–(3.5) into Equation (3.1), we can get:-

$$u_A = Ri_A + \frac{d}{dt}(L_A i_A + M_{AB} i_B + M_{AC} i_C \psi_{pm}$$

$$= Ri_A + \frac{d}{dt}(L_A i_A + M_{AB} i_B + M_{AC} i_C) + \frac{d}{dt}[NS \int_{-\frac{\pi}{2}+\theta}^{\frac{\pi}{2}+\theta} B(x)dx]$$

$$= Ri_A + \frac{d}{dt}(L_A i_A + M_{AB} i_B + M_{AC} i_C) + e_A \quad (3.6)$$

Where e_A represents the back-EMF of phase A.

Equation (3.6) includes a derivative operation of the product of inductance and current, where the self-inductance and the mutual inductance of the winding is proportional to N^2 (N represents the number of turns) and the permanent of the corresponding magnetic circuit.

That is:-

$$L_A = N^2 \Lambda_A \quad (3.7)$$

$$M_{AB} = N^2 \Lambda_{AB} \quad (3.8)$$

Where:-

Λ_A --- Permeance of self-inductance flux in phase A;

Λ_{AB} ---- Permeance of mutual inductance flux between phase A and phase B

The permeability of salient pole rotor differs in directions of the d-axis and the q-axis, consequently the self-inductance and mutual inductance of winding changes with the rotor position [19]. Therefore, the inductance also changes with the rotor position. But for the non salient pole rotor, the flux is isotropic in all directions. Hence, the permeability of the magnetic circuit cannot be affected by rotor position. So, the self-inductance and mutual inductance will not vary with time. The effect of rotor saliency on winding inductance is shown in Figure 3.12.

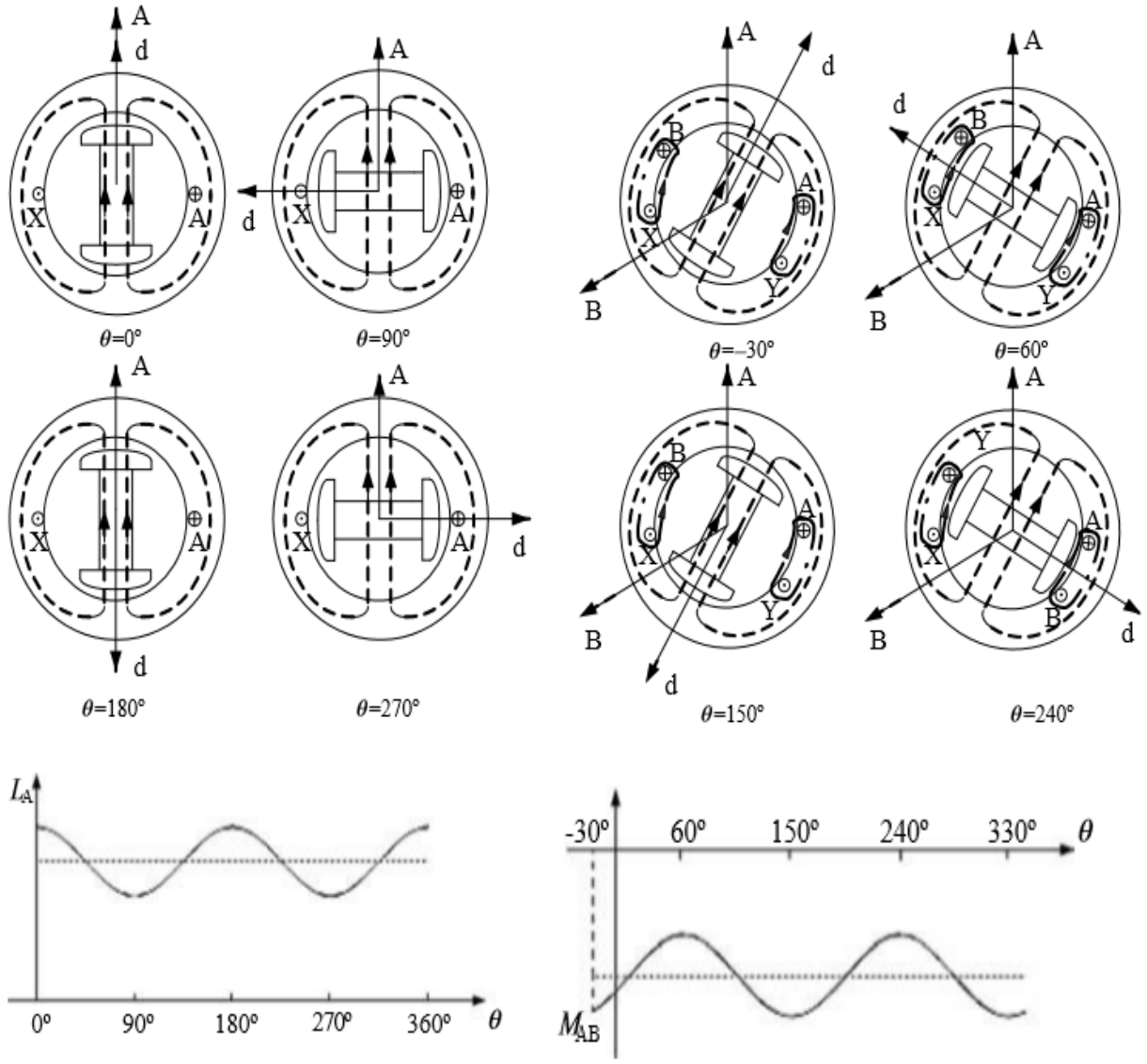

Figure 0.12 Effect of rotor saliency on magnetic circuit [15].

Generally, the surface-mounted salient-pole rotor is used for BLDC motors. In this condition, the winding inductance will not change with the time. Further, as the three-phase stator windings are symmetrical the self-inductances will be equal, and so as the mutual inductance. That is $L_A = L_B = L_C = L, M_{AB} = M_{BA} = M_{BC} = M_{CB} = M_{AC} = M_{CA} = M.$ Substituting them into Equation (3.6), we can get:-

$$u_A = Ri_A + L\frac{di_A}{dt} + M\frac{di_B}{dt} + M\frac{di_c}{dt} + e_A \qquad (3.9)$$

In which,

$$e_A = \frac{d}{dt}\left[\int_{\frac{-\pi}{2}+\theta}^{\frac{\pi}{2}+\theta} B(x)dx\right]$$

$$= NS\left[B\left(\frac{\pi}{2}+\theta\right) - B\left(-\frac{\pi}{2}+\theta\right)\right]\frac{d\theta}{dt}$$

$$= NS\omega\left[B\left(\frac{\pi}{2}+\theta\right) - B\left(-\frac{\pi}{2}+\theta\right)\right] \quad (3.10)$$

Where ω is the electrical angular speed of BLDC motor.

According to the distribution of magnetic density in the air gap as shown in Figure 9, together with B(θ) having a period of 2π and ($B(\theta+\pi) = -B(\theta)$, we can get:-

$$e_A = NS\omega\left[B\left(\frac{\pi}{2}+\theta\right) - B\left(-\frac{\pi}{2}+\theta\right)\right]$$

$$e_A = NS\omega\left[B\left(\frac{\pi}{2}+\theta\right) - B\left(\frac{\pi}{2}+\theta+\pi-2\pi\right)\right]$$

$$e_A = 2NS\omega B\left(\frac{\pi}{2}+\theta\right) \quad (3.11)$$

Then, the θ-dependent back-EMF wave of phase A is $\frac{\pi}{2}$ ahead of the distribution of the magnetic density in air gap, and e_A can be expressed as

$$e_A = 2NS\omega B_m f_A(\theta) = \omega\psi_m f_A(\theta) \quad (3.12)$$

Where;

B_m ---- Maximum value of PM density distribution in air gap;

ψ_m ---- Maximum value of PM flux linkage of each winding $\psi_m = 2NSB_m$;

$f_A(\theta)$ ---- Back-EMF waveform function of phase A.

Note that $f_A(\theta)$ has a trapezoidal distribution with the rotor position, and its maximum and minimum values are, respectively, 1 and -1 the corresponding waveform and its phase relationship with $B(\theta)$ and e_A are shown in Figure 3.13. As for the three-phase symmetrical windings, there also exist,$f_B(\theta) = f_A\left(\theta - \frac{2\pi}{3}\right)$ and$f_C(\theta) = f_A\left(\theta + \frac{2\pi}{3}\right)$.

It can be seen from Equation (3.10) that e_A is a rotating back-EMF that is produced by the winding flux linkage caused by the rotating rotor.

As the currents of the three phases satisfy

$$i_A + i_B + i_C = 0 \qquad (3.13)$$

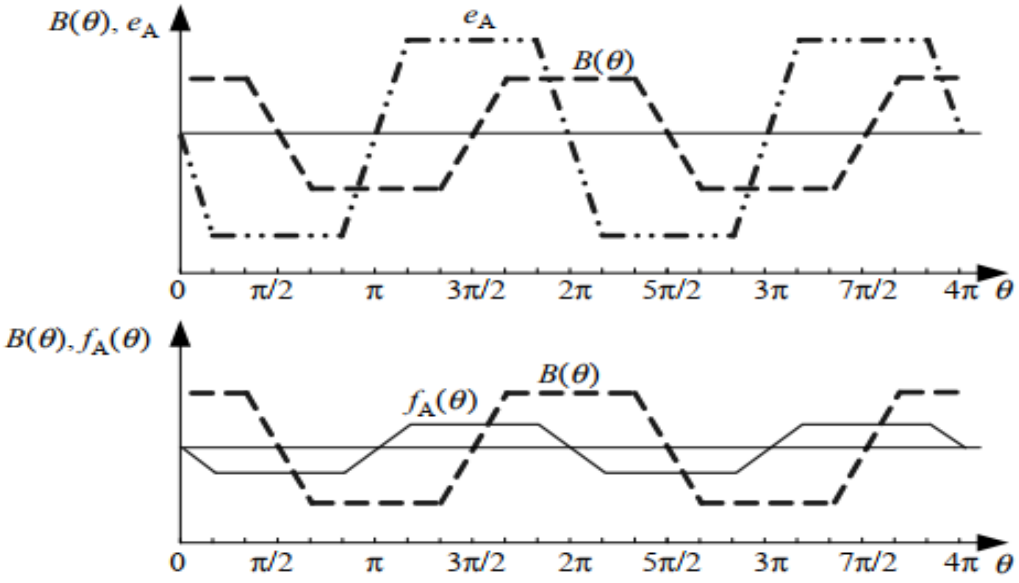

Figure 0.13 Phase relationship between$\boldsymbol{B(\theta)}$,$\boldsymbol{e_A}$ and $\boldsymbol{f_A(\theta)}$ [15].

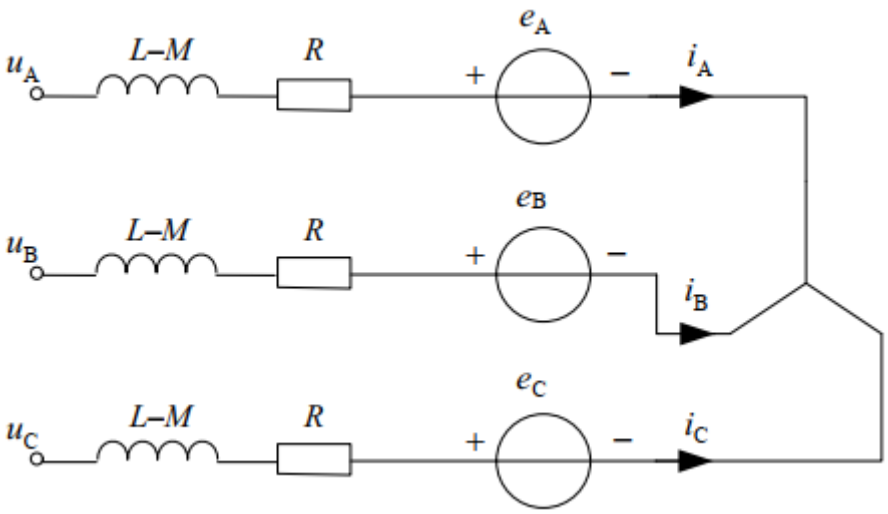

Figure 0.14 Equivalent circuit of the BLDC motor [15].

Equation (3.9) can be further simplified as

$$u_A = Ri_A + (L - M)\frac{di_A}{dt} + + e_A \tag{3.14}$$

Then, the matrix form of phase voltage equation of BLDC motor can be expressed as

$$\begin{matrix} u_A \\ u_B \\ u_C \end{matrix} = \begin{bmatrix} R & 0 & 0 \\ 0 & R & 0 \\ 0 & 0 & R \end{bmatrix} \begin{bmatrix} i_A \\ i_B \\ i_C \end{bmatrix} + \begin{bmatrix} L-M & 0 & 0 \\ 0 & L-M & 0 \\ 0 & 0 & L-M \end{bmatrix} \frac{d}{dt} \begin{bmatrix} i_A \\ i_B \\ i_C \end{bmatrix} + \begin{bmatrix} e_A \\ i_B \\ i_C \end{bmatrix} \tag{3.15}$$

According to Equation (3.15), the equivalent circuit of the BLDC motor can be shown as in Figure 3.14. In most practical applications of BLDC motors, the stator windings are Y-connected in which there is no neutral point brought out so that the phase voltages are difficult to detect. Thus, the mathematical model based on phase voltage is not applicable in some cases. In contrast, the line voltage is easy to measure. It is approximately equal to the DC bus voltage when the relevant power transistors are turned on. Therefore, the mathematical model based on line voltage is more suited to the practical system.

The line voltage equation can be obtained through subtraction calculation of the phase voltage equation as

$$\begin{matrix} u_{AB} \\ u_{BC} \\ u_{CA} \end{matrix} = \begin{bmatrix} R & -R & 0 \\ 0 & R & -R \\ -R & 0 & R \end{bmatrix} \begin{bmatrix} i_A \\ i_B \\ i_C \end{bmatrix} + \begin{bmatrix} L-M & M-L & 0 \\ 0 & L-M & M-L \\ M-L & 0 & L-M \end{bmatrix} \frac{d}{dt} \begin{bmatrix} i_A \\ i_B \\ i_C \end{bmatrix} + \begin{bmatrix} e_A - e_B \\ i_B - e_C \\ i_C - e_A \end{bmatrix} \quad (3.16)$$

Similar to DC motors, the analysis of power and torque for the BLDC motor can be carried out from the perspective of energy transfer. When the motor is operating, the power from the source is absorbed, and although a little is turned into copper loss and iron loss, most of the power is transferred through the air gap to the rotor by the torque effect. The power transferred to the rotor, which is called the electromagnetic power, equals the sum of the product of current and back-EMF of the three phases. That is

$$P_e = e_A i_A + e_B i_B + e_C i_C \quad (3.17)$$

Ignoring the mechanical loss and stray loss, the electromagnetic power is totally turned into kinetic energy, so

$$P_e = T_e \Omega \quad (3.18)$$

Where;

T_e ------ Electromagnetic torque;

Ω ------ Angular velocity of rotation.

Hence, from Equations (3.17) and (3.18), we can get

$$T_e = \frac{e_A i_A + e_B i_B + e_C i_C}{\Omega} \quad (3.19)$$

Substituting Equation (3.12) into Equation (3.19), another form of the torque equation can be represented as

$$T_e = P[\, \psi_m f_A(\theta) i_A + \psi_m f_B(\theta) i_B + \psi_m f_C(\theta) i_C \quad (3.20)$$

Where P is the number of pole pairs;

When the BLDC motor runs in the 120^0 conduction mode and the corresponding transient commutation process is ignored, the currents that have the same amplitude and the opposite direction only flow through two-phase windings of the Y-connected motor at any time. Note

that the symbols of $f(\theta)$ at the flat-top position are opposite to each other for different windings, so Equation (3.20) can be further simplified as

$$T_e = 2p\,\psi_m i_A = K_T i \qquad (3.21)$$

Where

K_T ------- The torque coefficient;

i --------- The steady phase current.

In order to build a complete mathematical model of the electromechanical system, the motion equation has to be included as

$$T_e - T_L = J\frac{d\Omega}{dt} + B_V\Omega \qquad (3.22)$$

Where

T_L --------- load torque;

J ---------- Rotor moment of inertia;

B_V -------- Viscous friction coefficient.

Thus, Equations (3.15), (3.19) and (3.22) constitute the differential equation mathematical model of the BLDC motor.

3.2.2 Transfer Function

Transfer function is one of the most fundamental idea in the control theory, and the transfer function-based modelling are widely used in automatic control fields of design and control of a plant system. Some control design and analysis methods, such as the root-locus method and the frequency-response method, are also developed based on the transfer function.

The transfer function of the BLDC motor is significant for the performance analysis and control design of the motor. Compared with the traditional brushed DC motor, the windings of the BLDC motor are energized according to the rotor position, and the motor is usually designed to be three-phase or multiphase. However, for each conducted phase winding mechanisms of back-EMF and electromagnetic torque are all identical with traditional brushed DC motor analysis methods adopted for the system. Suppose that the three-phase BLDC motor is controlled by the full-bridge driving in the two phase conduction mode and when wending of phase A and B are conducting their exist of:

$$\left\{\begin{array}{c} i_A = -i_B = i \\ \frac{di_A}{dt} = -\frac{di_B}{dt} = \frac{di}{dt} \end{array}\right\} \quad (3.23)$$

Thus, the line-voltage U_{AB} in Equation (2.16) can be rewritten as:

$$U_{AB} = 2Ri + 2(L - M)\frac{di}{dt} + (e_A - e_B) \quad (3.24)$$

Take the transient process out of consideration (i.e. ignore the trapezoid bevel edge), then the steady e_A and e_B are equal in amplitude and opposite in direction when phases A and B are turned on. So, Equation (3.24) can be expressed as

$$U_{AB} = U_d = 2Ri + 2(L - M)\frac{di}{dt} + 2e_A = r_a i + L_a \frac{di}{dt} + K_e \Omega \quad (3.25)$$

Where

U_d------ DC bus voltage;

r_a ---------- Line resistance of winding, $r_a = 2R$;

L_a -------- Equivalent line inductance of winding,$L_a = 2(L - M)$;

K_e -------- Coefficient of line back-EMF, $K_e = 2p\psi_m = 4pNSB_m$.

Equation (3.25) is exactly the armature voltage loop equation when two phase windings are excited, and the corresponding equivalent circuit is shown in Figure 3.15. Note that the equivalent circuit shown in Figure 3.15 could be adopted in three-phase half bridge driving and three-phase full-bridge driving modes of the BLDC motor with specific ke and K_T too.

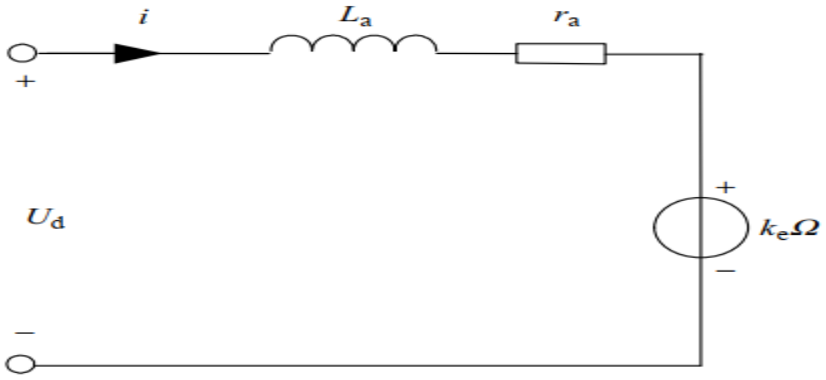

Figure 0.15 Equivalent circuit of the BLDC motor with two phase windings excited.

In Equation (3.25), if the current can be expressed by angular velocity, then we can get the transfer function of motor by obtaining the relationship between bus voltage and angular velocity. So, substituting Equation (3.21) into Equation (3.22), we get

$$K_T i - T_L = J\frac{d\Omega}{dt} + B_V\Omega \qquad (3.26)$$

First, when the BLDC motor runs with no load, the current is given as

$$i = \frac{J}{K_T}\frac{d\Omega}{dt} + \frac{B_V}{K_T}\Omega \qquad (3.27)$$

Substituting Equation (3.27) into Equation (3.25), we get

$$U_d = r_a\left(\frac{J}{K_T}\frac{d\Omega}{dt} + \frac{B_V}{K_T}\Omega\right) + L_a\frac{d}{dt}\left(\frac{J}{K_T}\frac{d\Omega}{dt} + \frac{B_V}{K_T}\Omega\right) + K_e\Omega \qquad (3.28)$$

Also, it can be rearranged as:

$$U_d = \frac{L_aJ}{K_T}\frac{d^2\Omega}{dt^2} + \frac{r_aJ+L_aB_V}{K_T}\frac{d\Omega}{dt} + \frac{r_aB_V+k_eK_T}{K_T}\Omega \qquad (3.29)$$

By Laplace transformation of Equation (3.29), the transfer function of a BLDC motor can be expressed as

$$G_u(s) = \frac{\Omega(s)}{U_d(s)} = \frac{K_T}{L_aJS^2+(r_aJ+L_aB_V)s+(r_aB_V+k_eK_T)} \qquad (3.30)$$

Thus, the structure of a BLDC motor control system with no load can be built as shown in Figure 3.16.

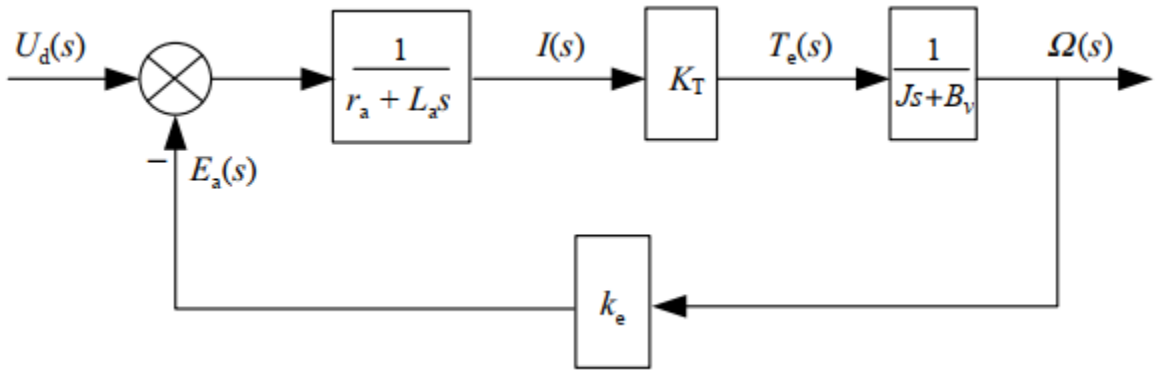

Figure 0.16 Structure of BLDC motor with no load control system.

Equation (3.30) implies that the BLDC motor can be considered as a second-order system, so it can be rearranged as:

$$G_u(s) = \frac{K_T}{r_aB_V+k_eK_T}\frac{\omega_n^2}{(s^2+2\xi\omega_n s+\omega^2)} \qquad (3.31)$$

Where;

$\omega_n = \sqrt{\frac{r_a B_V + k_e K_T}{L_a J}}$ ----- Natural frequency of the second-order system;

$\xi = \frac{1}{2}\frac{r_a J + L_a B_V}{\sqrt{L_a J}\sqrt{(r_a B_V + K_e K_T)}}$ ------ damping ratio of the second-order system.

It can be seen from Equation (2.31) that the two roots of the characteristic equation for the BLDC motor's second-order system are $s_{1,2} = -\xi\omega_n \pm \omega_n\sqrt{\xi^2 - 1}$ so the system response time is determined by ω_n and ξ. For unit step input, the convergence speed of the response curve depends on ω_n.A larger ω_n generally leads to a faster convergence speed. Meanwhile, the parameter ξ will determine the character of eigenvalues and the shape of the response curve. The system runs underdamping, critical damping and over damping states respectively, when $0 < \xi < 1$, $\xi = 1$ and $\xi > 1$. The response curves for different damping ratios are shown in Figure 3.17.

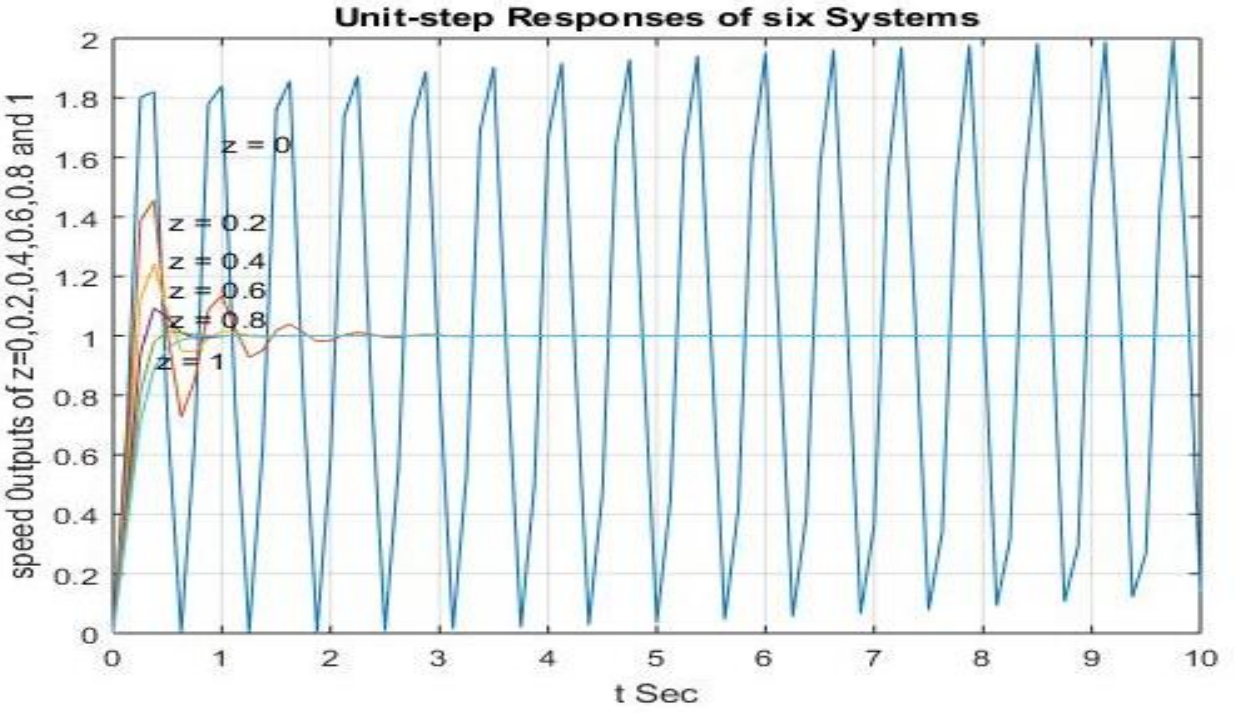

Figure 0.17 Response curves of BLDC motor.

Let the mechanical time constant be $t_m = \frac{r_a J + L_a B_V}{r_a B_V + k_e K_T}$ and the electromagnetic time constant be $t_e = \frac{L_a J}{r_a J + L_a B_V}$ Then Equation (3.30) can be rewritten as:

$$G_u(s) = \frac{K_T}{r_a B_V + k_e K_T} \frac{1}{(s^2 t_m t_e + s t_m + 1)} \quad (3.32)$$

Generally speaking, the mechanical time constant is much larger than the electromagnetic time constant, i.e.$t_m \gg t_e$, so the transfer function expressed in Equation (3.32) further can be simplified as

$$G_u(s) \simeq \frac{K_T}{r_a B_V + k_e K_T} \frac{1}{(s^2 t_m t_e + s t_m + s t_e + 1)}$$

$$= \frac{K_T}{r_a B_V + k_e K_T} \frac{1}{(s t_m + 1)(s t_e + 1)} \quad (3.33)$$

It is seen from Equation (3.33) that the transfer function of BLDC motor can be expressed by two inertia elements in series [20]. Figure 3.18 shows the corresponding speed responding process with step input. In Figure 3.18, we can learn the physical meaning of time constant in a transfer function. When a step voltage is applied to the input, first the current will respond to voltage change through the $1/(s t_e + 1)$ link, and its time constant is t_e. Then, the speed will respond to the current change through the $1/(s t_m + 1)$ link, where t_m is the corresponding time constant. Figure 3.19 has shown the interconnection between armature current and angular speed. If the effect of electromagnetic time constant is ignored, i.e. the armature inductance is negligible, then L_m can be deemed to be zero, so Equation (3.32) can be simplified into a first order model as:

$$G_u(s) = \frac{K_T}{r_a B_V + k_e K_T} \frac{1}{(s t_m + 1)} \quad (3.34)$$

The corresponding system structure diagram is shown in Figure 3.19. Further, the step response of Equation (3.34) is given by:-

$$\Omega(t) = \frac{K_T U_d}{r_a B_V + k_e K_T} \left(1 - e^{-t/t_m}\right) \quad (3.35)$$

Figure 3.18 shows the corresponding response curve of the plant.

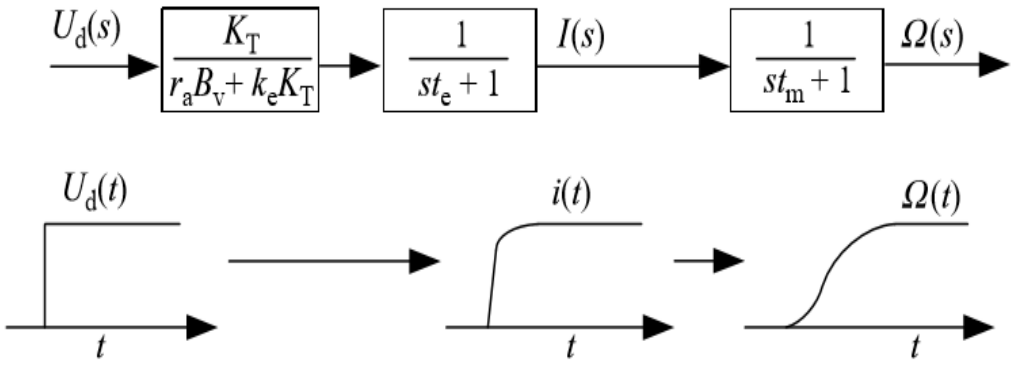

Figure 0.18 Speed responding process with step input [15].

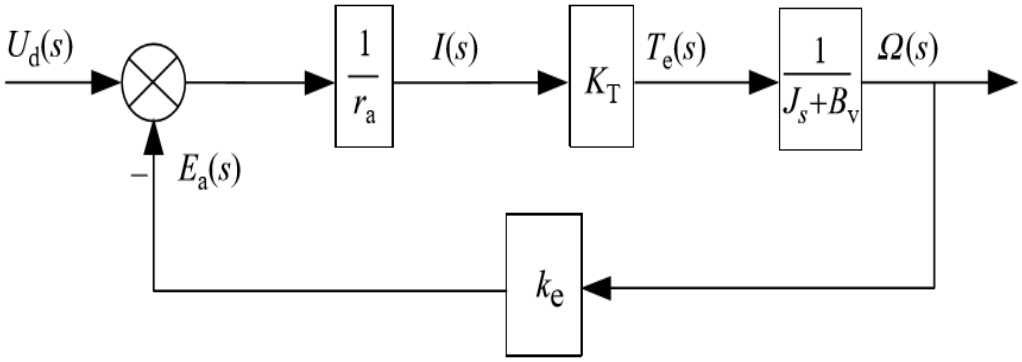

Figure 0.19 System structure diagram of BLDC motor with the armature inductance neglected.

It is known from Figure 3.20 that a smaller t_m leads to a shorter settling time of $\Omega(t)$. For a speed-control system, it is desirable that the delay time of speed response be short enough. If the mechanical time constant is big, a rational closed control system should be designed to increase the response speed. For example, a voltage or current amplifier with large gain used in an analog control system as well as the larger proportional gain of PI controller in digital control system can all increase the open-loop gain of the system. Consequently, the rise time of the speed response will be reduced. However, too large gain would bring more losses of power switches so as to reduce the efficiency of system. Furthermore, from the control viewpoint, a large proportional gain may cause oscillation and instability.

Therefore, the stability and the system response speed should be considered together in system design. The response speed should be increased under the condition of stability.

In the following, the transfer function and speed step response of a BLDC motor when the load torque is not zero will be discussed. In this condition, the load torque can be regarded as an input load variation of the system, as shown in Figure 3.21.

For such a system, the superposition principle holds. Thus, the output of the system equals the sum of outputs when $U_d(s)$ and $T_L(s)$ are applied to the system, respectively. In Figure 21, when $U_d(s) = 0$ holds, hence

$$\Omega(s) = {}^{1}/_{Js + B_V}\left[-k_e \frac{1}{r_a + L_a s} K_T \Omega(s) - T_L(s)\right] \tag{3.36}$$

$$T_L(s) = -\Omega(s)\left[\frac{(r_a + L_a s)(Js + B_V) + k_e K_K}{(r_a + L_a s)}\right] \tag{3.37}$$

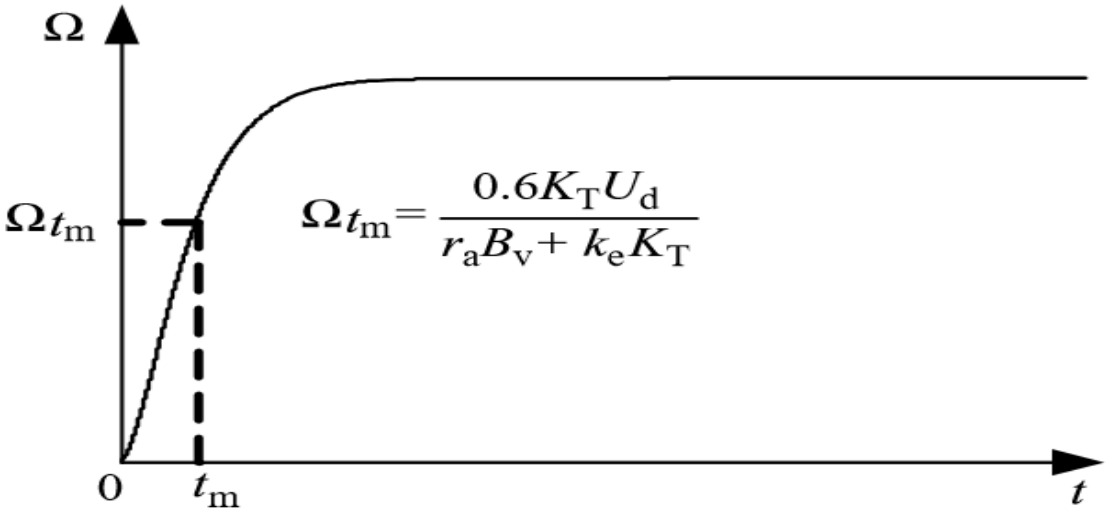

Figure 0.20 Speed step response of BLDC motor neglecting the armature inductance [15].

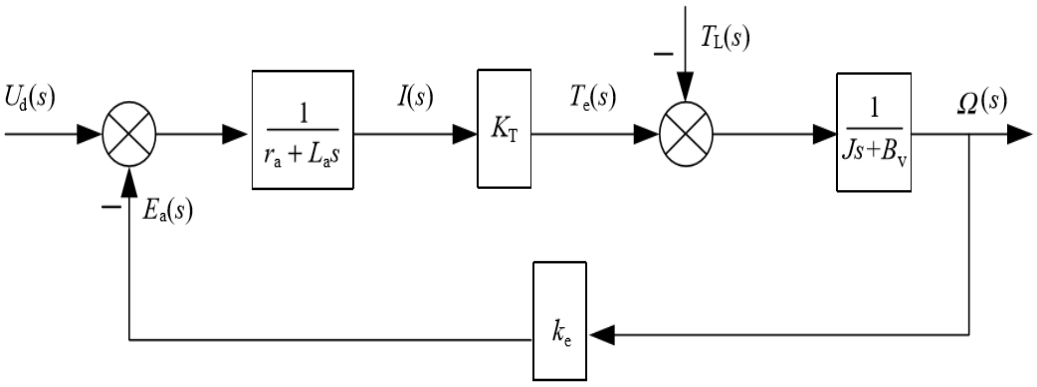

Figure 0.21 Structure diagram of BLDC motor with load torque.

Then, the transfer function between load torque and speed is

$$G_L(s) = \frac{\Omega(S)}{T_L(s)} = -\frac{r_a + L_a s}{L_a J s^2 + (r_a J + L_a B_V) s + (r_a B_V + k_e K_T)} \tag{3.38}$$

Therefore, the speed response of a BLDC motor affected together by voltage and load torque is given by:

$$\Omega(s) = G_d(s)U_d(s) + G_L(s)T_L(s)$$

Then;

$$\Omega(s) = \frac{K_T U_d(s)}{L_a J S^2 + (r_a J + L_a B_V)s + (r_a B_V + k_e K_T)} - \frac{(r_a + L_a s)T_L(s)}{L_a J s^2 + (r_{aJ} + L_{aB_V})s + (r_a B_V + k_e K_T)} \quad (3.39)$$

3.2.3 State-Space Equations

In modern control theory, the motion state of control system relies on its state equation. The state-space equation method is one of the most important analysis methods in modern control theory. From the state equation we can get all the independent variables and then determine all the motion states of the system. A group of first-order differential equations with state variables issued in the state-space method to describe the dynamic characteristics of the system. Since it is helpful to the realization of different digital control algorithms, the state-space method is becoming more and more popular in designing control systems with the fast development of computer techniques. Especially in recent years, computer on-line control systems such as optimal control, Kalman filters, dynamic system identification, self-adaptive filters and Self-adaptive control have been applied to motor control.

All these control techniques are based on the state equation. The state equations of a BLDC motor can be obtained by the algebraic transformation of the differential equation model. First, appropriate variables should be selected as state variables. The selection of state variables is not unique, but they should be independent of each other. Moreover, the number of state variables should be equal to the order of the differential equation. Currents of three phase windings and the angular speed are selected here as state variables, and the fourth-order state equation is then derived as:

$$\dot{x} = Ax + Bu \quad (3.40)$$

Where $x = [i_A \;\; i_B \;\; i_C \;\; \Omega]^T$;

$$u = [\, u_A \;\; u_B \;\; u_C \;\; T_L \,]^T ;$$

$$A=\begin{bmatrix} -\frac{R}{L-M} & 0 & 0 & -\frac{p\psi_{pm}(\theta)}{L-M} \\ 0 & -\frac{R}{L-M} & 0 & -\frac{p\psi_{pm}(\theta-\frac{2\pi}{3})}{L-M} \\ 0 & 0 & -\frac{R}{L-M} & -\frac{p\psi_{pm}(\theta-\frac{4\pi}{3})}{L-M} \\ \frac{p}{J}\psi_{pm}(\theta) & \frac{p}{J}\psi_{pm}(\theta-\frac{2\pi}{3}) & \frac{p}{J}\psi_{pm}(\theta-\frac{4\pi}{3}) & -\frac{B_V}{J} \end{bmatrix};$$

$$B=\begin{bmatrix} \frac{1}{L-M} & 0 & 0 & 0 \\ 0 & \frac{1}{L-M} & 0 & 0 \\ 0 & 0 & \frac{1}{L-M} & 0 \\ 0 & 0 & 0 & \frac{1}{L-M} \end{bmatrix};$$

In Equation (3.40), the angular position of the rotor can be detected by a position sensor. As the armature reaction is ignored, the PM flux linkage $\psi_{pm}(\theta)$ is only a function of θ, which is independent of current and speed. Hence, $\psi_{pm}(\theta)$ can be regarded as a coefficient of the equation. As θ changes with regard to time when the motor is running, matrix A is time varying. Thus, the state equation represented as Equation (3.40) denotes a time-varying multiple-input multiple-output (MIMO) continues linear system. The controllability of a linear system is the base of optimal control and optimal estimation, so it should be determined. Assume the controllability matrix is:-

$$M=[M_0\ \ M_1\ \ M_2\ \ M_3] \tag{3.41}$$

Where $M_0 = B, \quad M_i(t) = A^i B, \quad i = 1,2,3.$

Then, matrix M can be transformed to

$$M=\begin{bmatrix} \lambda & 0 & 0 & 0 \\ 0 & \lambda & 0 & 0 \\ 0 & 0 & \lambda & 0 \\ 0 & 0 & 0 & -\frac{1}{J} \end{bmatrix} \begin{matrix} M_1 & M_2 & M_3 \end{matrix} \tag{3.42}$$

Where $\lambda = {}^{1}/_{L-M}$.

The matrix M meets the condition of rank $M = 4$. So, the system represented by Equation (3.40) is controllable and all the poles of the system can be arbitrarily placed by state feedback.

3.3 Characteristics Analysis

The starting characteristics are the variation curves of the speed and current in the process of the speed rising from 0 to the stable value under constant DC bus voltage. At the instant of starting, both the speed and back-EMF are 0, and the armature current can be represented as-

$$I = \frac{U_d - \Delta U}{r_a} \qquad (3.43)$$

Where ΔU the voltage drop of the power is switches of the bridge inverter. The curves of speed and armature current in the starting process are shown in Figure 3.23. It can be seen from figure that, the voltage drop of the power switches and the armature winding resistance are too small, the starting current will be large in a short period of time. It may reach several times or more than ten times the normal operating current. Within the allowable range, the large starting current is helpful to the acceleration of the rotor so that the motor can quickly start even under full load. For example, if the motor runs under rated operating conditions, both the startup speed and back-EMF will be 0. Moreover, the armature current increases rapidly in the instant of starting. Thus, the electromagnetic torque is much larger than the load torque so that the speed increases rapidly. Consequently, the back-EMF will increase so that the growth of armature current becomes slower until it reaches the maximum. Then, the armature current begins to decrease. The decreased current will lead to a decrease of the electromagnetic torque, so the rising acceleration of the speed becomes smaller. When the electromagnetic torque and load torque achieve the dynamic balance, the speed will stay in the rating value, i.e. the BLDC motor will maintain steady-state operation. Without considering the limit of the starting current, the shape of the speed curve in Figure 3.22 is determined by the damping ratio of the motor. According to the transfer function of the motor, when the damping ratio is $0 < \xi < 1$, the system is in the underdamped condition, the speed and current will become stable after a process with overshoot and oscillation, as shown in Figure 3.23.

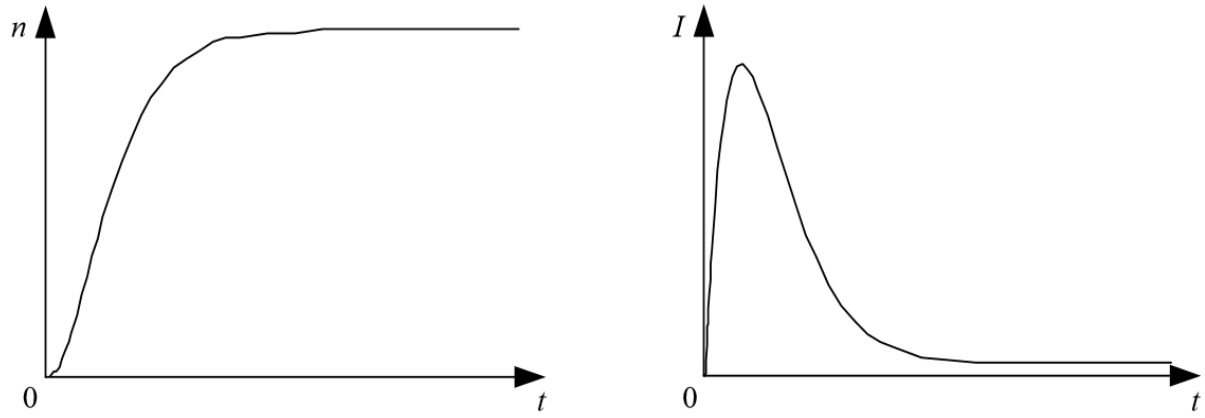

Figure 0.22 Curves of speed and current during the starting process [15].

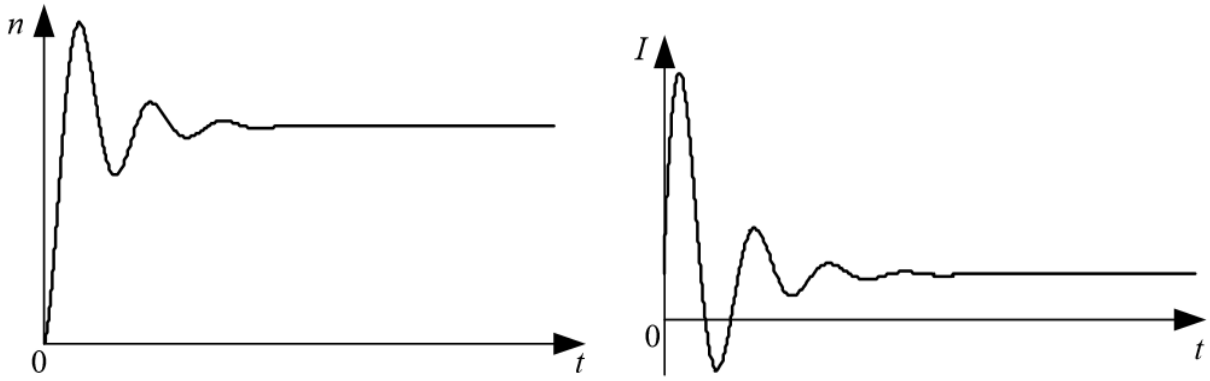

Figure 0.23 Overshoot and oscillation in starting process [15].

In the motor control system, power switches of driving circuit are more sensitive to the overcurrent. If the current exceeds its upper limit, the power switches will suffer from break down in a short period of time. For example, the enduring time of over current for IGBT is normally less than10μs. Generally, large-capacity power switches are chosen to stand the high starting current. However, the rated current of the motor is much smaller than the starting current. Thus, the current of the power switch is less than its rated value during most of the normal running. In this condition, the utilization efficiency of the switches decreases so that its cost increases. Therefore, in the design of the driving circuits, it is better to select suitable power switches according to the starting characteristics and working requirements of the motor.

In addition, the starting current has to be limited appropriately. Note that the starting current should increase as much as possible to improve the dynamic response speed when the safety of the power switches is ensured. Since the magnetic field has a trapezoidal distribution in the air gap of the BLDC motor, then if the phase winding conducts in the trapezoidal level edge of the back-EMF,

Then the back-EMF will be smaller. Thus, the armature current is becoming larger. So, compared to the traditional DC motor, the starting current of the BLDC motor may be larger. This should be considered in the design of the driving circuits.

3.3.1 Steady-State Operation

3.3.1.1 Operating Characteristics

The operating characteristics indicate the relationships between armature current, motor efficiency and output torque with a constant DC bus voltage U_d. According to Equation (3.21), the armature current will increase with the increasing load torque so that the electromagnetic torque can balance the load torque. Hence, stable running of the motor is assured.

Since the input power of the motor can be given as;

$$P_1 = U_d I = r_a I^2 + \frac{\pi}{30} k_e n I + \Delta U I \tag{3.44}$$

And

$$P_1 = P_{Cu} + P_e + P_T \tag{3.45}$$

Where n --- the motor speed;

P_{Cu} ---- The armature copper loss $P_{Cu} = r_a I^2$;

P_e ----- Electromagnetic power $P_e = k_e n I$;

P_T ----- The loss of bridge power switches ($P_T = \Delta U I$), which is related to the characteristics of power electronic switches and the voltage applied on the corresponding gate terminal of the switch. Here, it is approximately considered a constant.

As shown in Equation (3.45), the input power consists of the electromagnetic power P_e and the loss $P_{Cu} + P_T$, P_e is the power consumed to overcome the back-EMF. It can be turned into mechanical energy through the magnetic field, which will act on the rotor in the form of electromagnetic torque. So, taking the loss of load into account, the power transfer can be expressed as:

$$P_e = (T_L + T_0)\Omega = P_2 + P_0 \tag{3.46}$$

Where

T_L ---- load torque;

T_0 ----- No-load torque corresponding to no-load loss $T_0 = \frac{P_0}{\Omega}$

P_2 ----- Output power $P_2 = (T_L \Omega)$

P_0 ----- No-load loss, including the core loss and mechanical friction loss.

Thus, the efficiency of the motor is given as:

$$\eta = \frac{P_2}{P_1} = \frac{P_1 - (P_{CU} + P_T + P_O)}{P_1} = 1 - \frac{\sum P}{P_1} \tag{3.47}$$

Hence, Equation (2.47) can be further rewritten as:

$$\eta = 1 - \frac{r_a}{U_d} I - \frac{P_T + P_O}{U_d I} \tag{3.48}$$

In order to find the extreme value of Equation (3.48), the derivative of η with respect to I should be equal to 0 as:

$$\frac{d\eta}{dI} = -\frac{r_a}{U_d} + \frac{P_T + P_O}{U_d I^2} = 0 \tag{3.49}$$

Further, we can get,

$$P_T + P_O = U_d I^2 = P_{CU} \tag{3.50}$$

Note that the $P_T + P_O$ in Equation (3.50) will not change with load variation, so it is defined as the invariable loss. But the copper loss P_{CU} changes with the load variation, so it is called the variable loss. Equation (3.50) shows that when the variable loss equals the invariable loss, the maximum efficiency of the motor is achieved. Figure 3.24 shows the curves of armature current and efficiency of the BLDC motor with varied load torque and constant U_d.

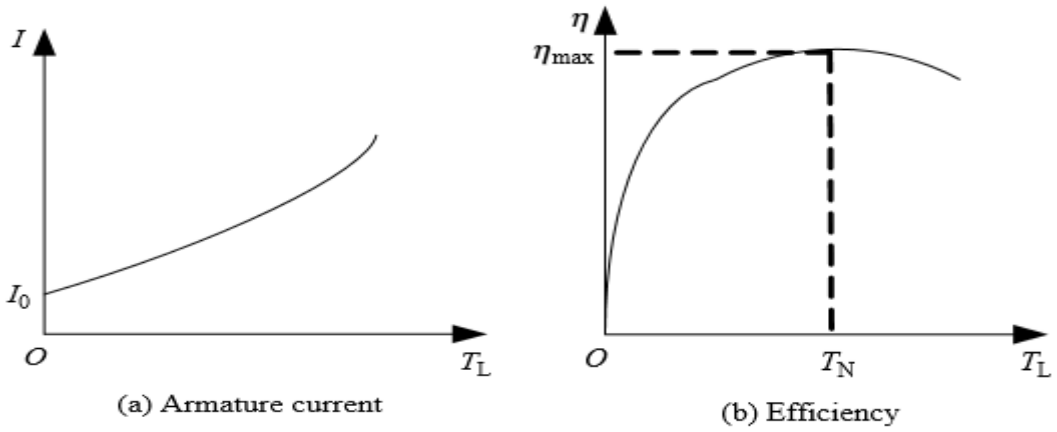

Figure 0.24 Curves of armature current and efficiency [15].

3.3.1.2 Regulation Characteristic

Regulation characteristic denotes the relationship between the speed and U_d with constant electromagnetic torque Te. If the loss of power switches is negligible, when the motor works in steady state, there exist.

$$U_d = r_a I + \frac{\pi}{30} K_e n \tag{3.51}$$

$$K_T I - T_L = \frac{\pi}{30} B_v n \tag{3.52}$$

Then:-

$$n = \frac{30K_T}{\pi K_T K_e + \pi r_a B_V} U_d - \frac{30 r_a}{\pi K_T k_e + \pi r_a B_V} T_L \tag{3.53}$$

Figure 24 shows the n –U_d curves with different electromagnetic torques, where as Te1 <Te2 <Te3 <Te4 can be seen from Figure 3.25 that there exists a dead zone in regulation characteristics. When U_d changes within the dead zone, the electromagnetic torque is not big enough to overcome the load torque to start the motor so that the speed is always zero. Only when the U_d is greater than the threshold voltage can the motor start and run in the steady state. Moreover, the greater the U_d , the bigger the steady-state speed.

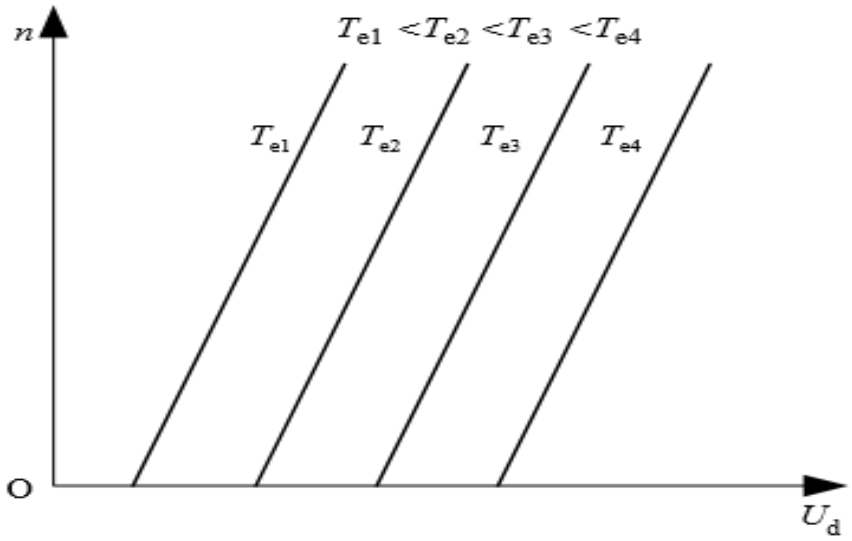

Figure 0.25 Regulation characteristics of BLDC motor [15].

3.3.1.3 Mechanical Characteristic

Mechanical characteristics denote the relationship between speed and electromagnetic torque with constant U_d. It can be derived from Equation (3.51) that

$$T_e = K_T \frac{30U_d - \pi k_e n}{30r_a} \tag{3.54}$$

Such that;

$$n = \frac{30}{\pi} \frac{K_T U_d - r_a T_e}{30r_a} \tag{3.55}$$

From Equation (3.55), we can obtain curves of mechanical characteristics with different U_d, as shown in Figure 3.26. In the figure, $U_{d1} > U_{d2} > U_{d3} > U_{d4}$ is the curve result.

Note that Equation (3.55) is a linear equation. In practice, due to influences from the variable loss and the armature reaction, the curve of mechanical characteristics is only considered as approximately linear. As shown in Figure 3.26, with a certain DC bus voltage U_d, the speed of the motor decreases on increasing the electromagnetic torque. Moreover, the curve will be shifted upward as U_d increases. Since the power electronic switches with nonlinear saturation characteristics are used for the commutation of BLDC motors, the voltage drop of the power switch will increase rapidly with increasing armature current when the motor runs near the stalled condition. So, there will be a significant downward bending phenomenon at the end of the curve of the mechanical characteristics, as shown in figure. As discussed above, the mechanical characteristics of BLDC motor are similar to those of a separately excited DC motor. The no-load point of the mechanical characteristics may be altered by changing the DC bus voltage.

Therefore, the speed control of a BLDC motor is usually carried out by means of PWM modulation.

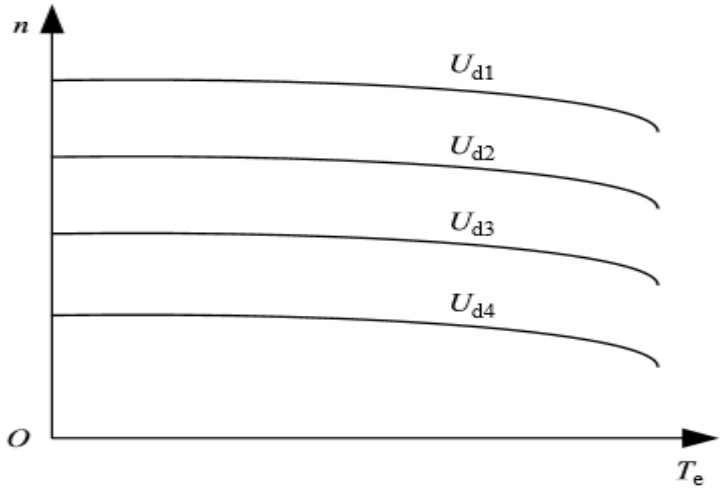

Figure 0.26 Mechanical characteristics of BLDC motor [15].

CHAPTER FOUR

CONTROLLER DESIGN OF BLDC MOTOR

BLDC motor speed control plays an important role in modern motor control. The control methods are usually divided into two main types: open-loop and closed-loop ones. Dual closed-loop speed control is common in control systems. The inner loop is the current or torque loop, while the outer loop is the velocity or voltage loop. When the motor works in normal mode or runs below the rated speed, the input voltage of the armature is changed through PWM modulation strategy; while the motor is operated above the rated speed, we usually weaken the flux by means of advancing the exciting current or auxiliary flux to achieve the aim. A BLDC motor speed-control system generally involves many techniques. In this chapter, we mainly focus on the realization of the dual-closed-loop speed control, the intelligent speed-control strategies, and MRAC based BLDC speed control system and the combination of each control once again.

4.1 PID Controller Method

PID has wide industrial applications as it need only less parameters to be tuned. It eliminates the steady state error by integral action and anticipates the change in output by derivative action. For tuning of parameters in PID controller a lot of techniques are available. Zeigler Nicholas Tuning method is the most popular method for tuning of PID controller. It depends mainly on step response of the system. The typical structure of PID control is shown in Figure 4.1. The standard PID controller calculates the deviation $\mathrm{e(t)}$ between the reference value and the actual value. Then, the plant is controlled by the variable $\mathrm{u(t)}$ with a linear combination of proportional–integral–derivative terms. The corresponding PID control law in continuous form can be expressed as

$$\mathrm{u(t)} = K_P\left(e(t) + \frac{1}{T_I}\int_0^t e(t)\,dt + T_D\frac{de(t)}{d(t)}\right) \qquad (4.1)$$

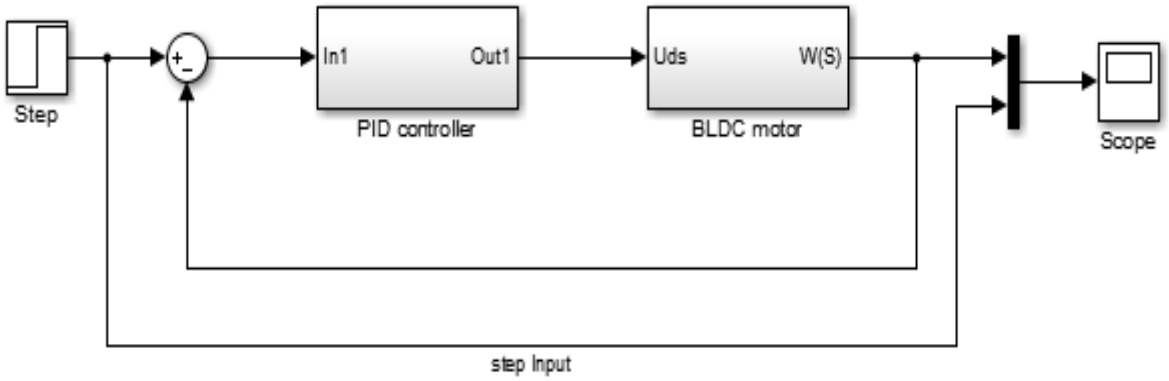

Figure 0.1 Diagram of a PID control system of BLDC motor.

Where KP is the proportional gain, TI is the integral time constant and TD is the differential time constant. In practical control system, not all PID controllers are composed of three terms: proportional, integral and differential. PID controllers contain various structure forms, such as proportional controller, proportional–integral controller and proportional–derivative controller, and so on. Among them, the proportional–integral controller is the most commonly used one in the BLDC motor control system. The differential term can effectively reduce the overshoot and maximum dynamic deviation, but it will make the controlled plant easily affected by high-frequency disturbances. And the Simulink block diagram of the PID control system is given below.

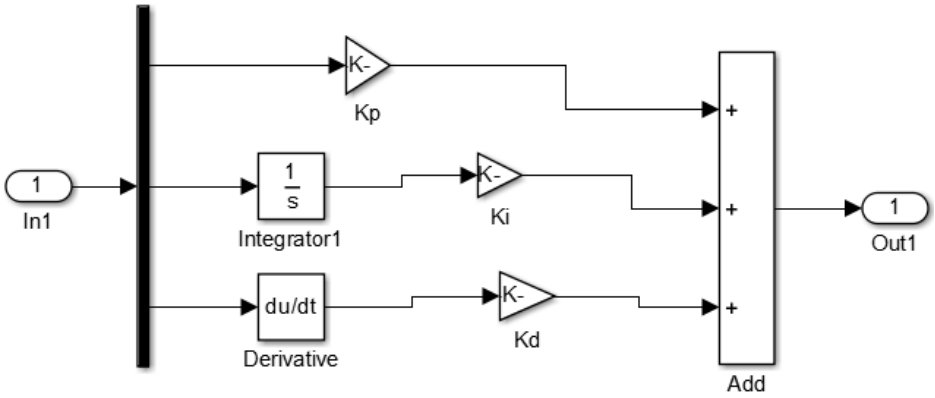

Figure 0.2 Internal Simulink block diagram of PID controller Structure

4.1.1 Zeigler Nicholas Method

From Figure 4.2 of the PID control structure diagram the Ziegler Nicholas method calculation is derived below and our Goal is to choose K_p, K_I, and K_d values appropriately by using oscillation. Ziegler Nichols is an iterative, online method to choose each value and there is no need of modeling required therefore, from equation (4.1) U(t) is derived:

$$u(t) = k_p e(t) + \frac{k_p}{T_i}\int_0^t e(t)d(t) + k_p T_d \frac{de(t)}{d(t)} \qquad (4.2)$$

From equation (4.2), K_I and K_d values are from those value Ti and Td:

$$K_I = \frac{k_p}{T_i}\int_0^t e(t)d(t) \qquad (4.3)$$

$$K_d = k_p T_d \frac{de(t)}{d(t)} \qquad (4.4)$$

To determine the Ziegler Nichols parameters for a PID controller, by oscillation method and adjusting the parameter until we get a certain critical system and adjusting the parameters within the simulation and based on the Ziegler Nichols table below we find out the parameters as given below.

Table 0.1 Ziegler Nichols parameter

Controller	Kc	τ_i	τ_d
P	0.5Kcu	-	-
PI	0.455Kcu	0.83Pu	-
PID	0.6Kcu	0.5Pu	0.125Pu

From the table and oscillation method we determined the period or the oscillation period of the PID tuner w=0.5403, hence the ultimate gain or frequency is given as:

$P_U = \frac{2\pi}{w} = 2 * \frac{3.14}{0.5403} = 11.623$ And Kcu=1.491 obtained from oscillation method.

$$\tau_i = 0.5Pu = 0.5 * 11.623 = 5.8115$$

$$\tau_d = 0.125 * 11.623 = 1.453$$

From equation (4.3) and (4.4).

And using oscillation method once again we can find PID controller gain parameters with small and small value estimation is given by kp=5.7748, ki=1605.29 and kd=0.00468 which is a tray and error method mostly.

4.2 Model Reference Adaptive Controller

Adaptive Control process is the one that continuously and automatically measures the dynamic behavior of plant, compares it with desired output and uses the difference to vary adjustable system parameters or to generate the actuating signal in such a way as to obtain optimal performance. An adaptive control system has two loops. One is the normal feedback with process and controller and the other loop consists of the adjustment loop. The parameter adjustment loop is often slower than the normal feedback loop. It can adapt to any change in the speed which occurs due to variation in load or due to external disturbances and the model reference adaptive controller main system block diagram is given below.

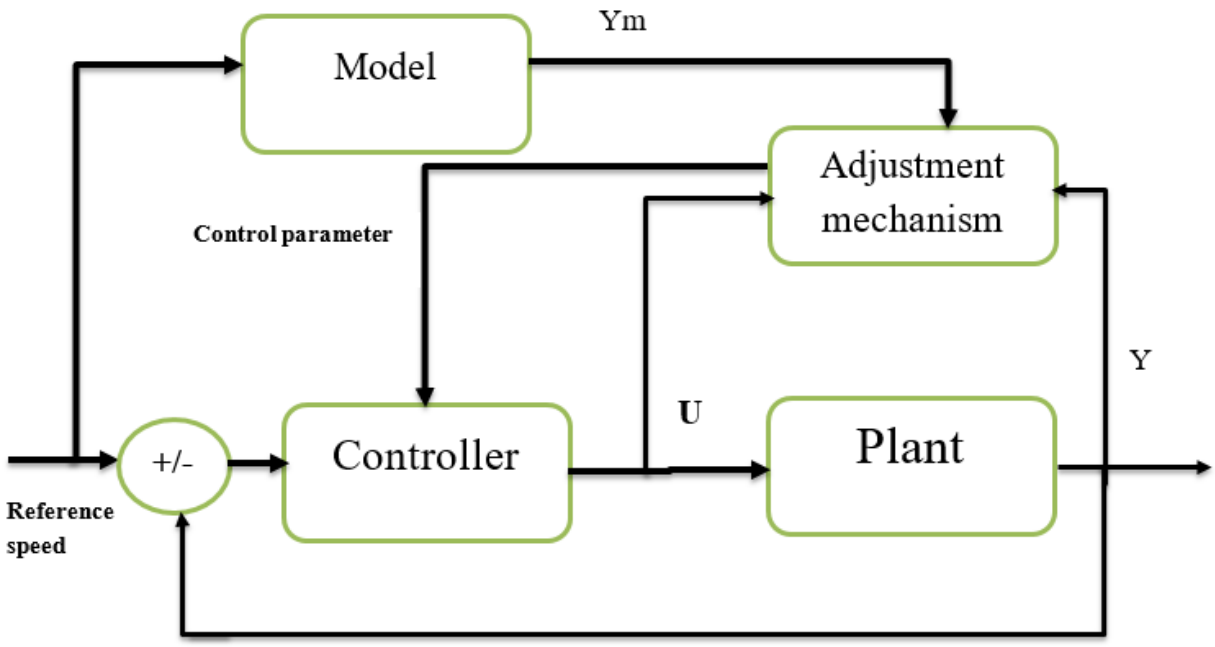

Figure 0.3 Block diagram of a model-reference adaptive system (MRAS).

In model reference adaptive controller, controller is designed to force the system or plant to behave like reference model. Model output is compared to the actual output, and the difference is used to adjust the feedback controller parameters MRAS has two loops :inner loop an ordinary control loop consisting of plant and regulator, an outer loop or adaptation loop that adjust the control

parameters in order to reduce the error between model and plant output to zero. Mathematical techniques like MIT rule and Lyapunov theory are used to develop adaptation mechanism.

4.2.1 MRAC based MIT Rule

This rule is developed in Massachusetts Institute of technology and is used to apply the MRAC approach to any practical system. In this rule the cost function or loss function is defined as gradient error.

$$J(\theta) = {}^{1}/_{2}\, e^2 \qquad (4.5)$$

The partial derivative term ∂e/ ∂θ, is called the sensitivity derivative of the system. This shows how the error is dependent on the adjustable parameter, θ. There are many alternatives to choose the loss function J, like it can be taken as mode of error also. Similarly $\frac{d\theta}{dt}$, can also have different relations for different applications.

Required general MIT gradient equations:

Process: $\boldsymbol{G(s) = \frac{y}{u}}$ (4.6)

Model: $\boldsymbol{G_m(s) = \frac{y_m}{r}}$ (4.7)

Control law: $\boldsymbol{u(t) = f(u_c, y)}$ (4.8)

Get Close loop from (4.6) and (4.8): $\boldsymbol{\frac{y}{r}}$ (4.9)

Error: $e = y - y_m$ (4.10)

$$\frac{\partial e}{\partial \Theta} = \frac{\partial y}{\partial \Theta} \qquad (4.11)$$

MIT rule: $\frac{d_\Theta}{dt} = -\gamma e \frac{\partial e}{\partial \Theta} = -\gamma e \frac{\partial y}{\partial \Theta}$ (4.12)

The BLDC motor process is a second order element with the following transfer function:

From equation (3.31)

$$G_u(s) = \frac{K_T}{r_a B_V + k_e K_T} \frac{\omega_n^2}{(s^2 + 2\xi\omega_n s + \omega_n^2)}$$

$$= \frac{\alpha_1}{s^2 + \alpha_2 s + \alpha_3} \tag{4.13}$$

For the reference model, a second order transfer function is selected as:

$$G_m(s) = \frac{y_m(s)}{r(s)} = \frac{\omega_n^2}{s^2 + 2\xi\omega_n s + \omega_n^2} \tag{4.14}$$

The control law is chosen as:

$$u(t) = k_1 r(t) - k_2 y(t) - k_3 \dot{y}(t) \tag{4.15}$$

By inserting Equation (4.13) into Equation (4.15), the MIT rule is applied, where p is the differential operator which is P=S therefore y (t) becomes:

$$y(s) = G_u(s)u(s) = \frac{\alpha_1}{s^2+\alpha_2 s+\alpha_3}\left(k_1 R(s) - k_2 y(s) - k_3 s\dot{y(s)}\right)$$

$$y(s) = \frac{\alpha_1 K_1 R(s)}{s^2+(\alpha_2+\alpha_1 k_3)s+\alpha_3+\alpha_1 k_2}$$

$$y(t) = \frac{\alpha_1 K_1 r(t)}{p^2+(\alpha_2+\alpha_1 k_3)p+\alpha_3+\alpha_1 k_2} \tag{4.16}$$

As a consequence, the error is:

$$e = y - y_m$$

$$e(t) = \left(\frac{\alpha_1 K_1 r(t)}{p^2+(\alpha_2+\alpha_1 k_3)p+\alpha_3+\alpha_1 k_2} - \frac{\omega_n^2}{s^2+2\xi\omega_n s+\omega_n^2}\right) r(t) \tag{4.17}$$

The sensitivity derivatives are obtained by taking the partial derivatives of the error and considering the controller parameters:

Therefore:

$$\frac{\partial e}{\partial k_1} = \frac{\alpha_1 r(t)}{p^2 + (\alpha_2 + \alpha_1 k_3)p + \alpha_3 + \alpha_1 k_2} \equiv y_m \tag{4.18}$$

$$\frac{\partial e}{\partial k_2} = \frac{-{\alpha_1}^2 k_1 r(t)}{(p^2 + (\alpha_2 + \alpha_1 k_3)p + \alpha_3 + \alpha_1 k_2)^2}$$

$$= -\frac{\alpha_1 y(t)}{p^2 + (\alpha_2 + \alpha_1 k_3)p + \alpha_3 + \alpha_1 k_2} \tag{4.19}$$

$$\frac{\partial e}{\partial k_3} = \frac{-{\alpha_1}^2 p k_1 r(t)}{(p^2 + (\alpha_2 + \alpha_1 k_3)p + \alpha_3 + \alpha_1 k_2)^2}$$

$$= -\frac{\alpha_1 \dot{y}(t)}{p^2 + (\alpha_2 + \alpha_1 k_3)p + \alpha_3 + \alpha_1 k_2)^2} \quad (4.20)$$

Due to the fact that the process parameters are unknown, none of the above three equations can be used. The below approximation is required in order to overcome such an impediment:

$$p^2 + (\alpha_2 + \alpha_1 k_3)p + \alpha_3 + \alpha_1 k_2$$

$$p^2 + 2\xi\omega_n p + \omega_n^2 \quad (4.21)$$

$$\frac{d_\theta}{dt} = \frac{d_k}{dt} = -\gamma e \frac{\partial e}{\partial k} = -\gamma e \frac{\partial y}{\partial k} \quad (4.22)$$

In conclusion, the adjustment for the controller parameters is:

$$\frac{dk_1(t)}{dt} = -\gamma \left(\frac{1}{p^2 + 2\xi\omega_n p + \omega_n^2} r(t) \right) e(t) \quad (4.23)$$

$$\frac{dk_2(t)}{dt} = \gamma \left(\frac{1}{p^2 + 2\xi\omega_n p + \omega_n^2} y(t) \right) e(t) \quad (4.24)$$

$$\frac{dk_3(t)}{dt} = \gamma \left(\frac{1}{p^2 + 2\xi\omega_n p + \omega_n^2} \dot{y(t)} \right) e(t) \quad (4.25)$$

After mathematical modeling the MIT rule, the simulation block diagram is given in the Figure 4.4 below as we know ‘p’ is a differential operator:

Where; $K_1 = K_P, K_2 = K_I, K_3 = K_D$ of PID controller gains.

And parameter α_1 is introduced in the adaptation gain γ.

Assuming a critically damped second order system is chosen as reference model with damping ratio as 1 and natural frequency as 1000 whose transfer function is given by

$$G_m(s) = \frac{y_m(s)}{r(s)} = \frac{1000000}{s^2 + 2000s + 1000000} \quad (4.26)$$

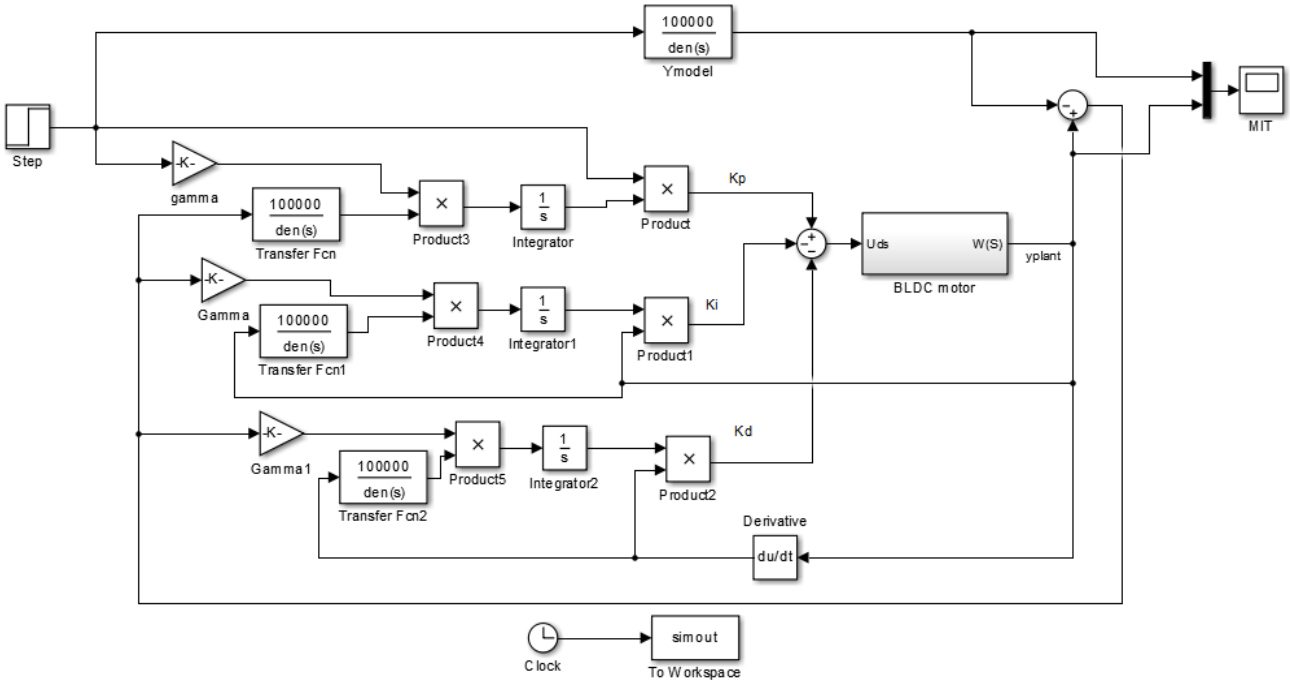

Figure 0.4 MATLAB Simulink module of MIT rule

The above MIT design is designed with a reference signal of step input to analysis the model how much is tracking the plant signal with estimated parameter.

4.2.2 Design of MRAC using Modified MIT Rule

Normalization can be used to protect against dependence on the signal amplitudes.

With $$\varphi = \frac{\partial e}{\partial \Theta} = \frac{\partial y}{\partial \Theta} = \frac{\partial y}{\partial \mathrm{k}} \qquad (4.27)$$

Where; φ Normalization constant,

The MIT rule can be written as:

$$\frac{d\Theta}{dt} = \frac{dk}{dt} = -\gamma\varphi e \qquad (4.28)$$

The normalized MIT rule is then become:

$$\frac{d\Theta}{dt} = \frac{dk}{dt} = \frac{-\gamma\varphi e}{\alpha^2 + \varphi^T\varphi} \qquad (4.29)$$

From equation (4.16) we can get the close loop transfer function with differential operator ‘p’ becomes:

$$y(t) = \frac{\alpha_1 K_1 r(t)}{p^2 + (\alpha_2 + \alpha_1 k_3)p + \alpha_3 + \alpha_1 k_2} \qquad (4.30)$$

The sensitivity derivatives are obtained by taking the partial derivatives of the error and considering the controller parameters and as we know $\frac{\partial e}{\partial \theta} = \frac{\partial y}{\partial k} = \frac{\partial y}{\partial \theta}$.

Hence:

$$\frac{\partial e}{\partial k_1} = \gamma \left(\frac{1}{p^2 + 2\xi\omega_n p + \omega_n^2} r(t) \right) e(t) \cong y_m = G_m r \qquad (4.31)$$

$$\frac{\partial e}{\partial k_2} = \gamma \left(\frac{1}{p^2 + 2\xi\omega_n p + \omega_n^2} y(t) \right) e(t) = -G_m y \qquad (4.32)$$

$$\frac{\partial e}{\partial k_3} = \gamma \left(\frac{1}{p^2 + 2\xi\omega_n p + \omega_n^2} \dot{y}(t) \right) e(t) = -G_m \dot{y} \qquad (4.33)$$

In conclusion, with approximation and the adjustment for the controller parameters is:

$$\frac{dk_1}{dt} = \frac{-\gamma y_m e}{\alpha + y_m^2} \qquad (4.34)$$

$$\frac{dk_2}{dt} = \frac{\gamma G_m y e}{\alpha + (G_m y)^2} \qquad (4.35)$$

$$\frac{dk_3}{dt} = \frac{\gamma G_m \dot{y} e}{\alpha + (G_m \dot{y})^2} \qquad (4.36)$$

Therefore the modified MIT rule Simulink block diagram is given in Figure 4.5 below as the derived mathematical equation of the modified MIT rule with $K_P, K_I \; and \; K_D$ values of $K_1, K_2 \; and \; K_3$ respectively.

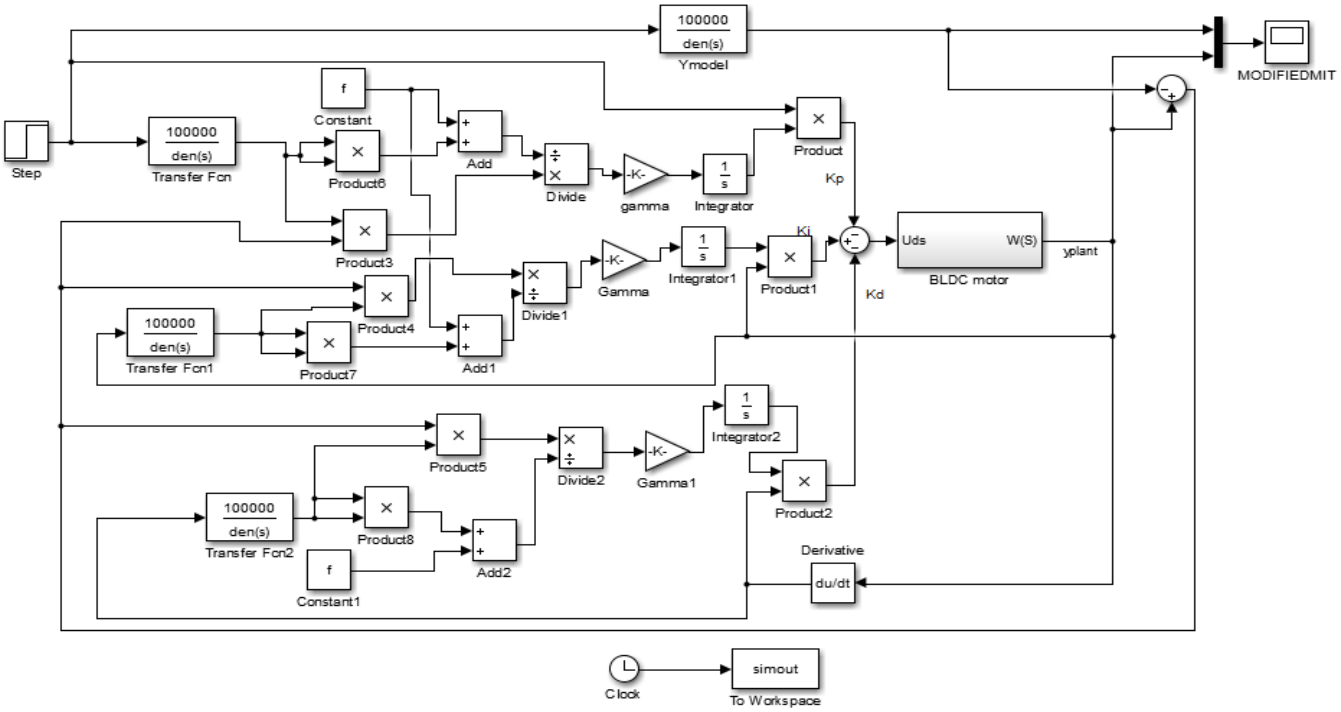

Figure 0.5 Simulink model of Modified MIT rule

4.2.3 MRAC with Lyapunov Stability Method

Model Reference Adaptive control with Lyapunov Stability method is generally used for first and second order systems. An advantage of this method is that a different adaptation law is not required even if we change the reference model or the plant, unless the performance seems to be insufficient. The Lyapunov method attempts to find the Lyapunov function and an adaptation mechanism such a way that the error between plant and model goes to zero. Also this method ensure stability to the system.

For the above mention system the controller law is defined by equation (4.15). The error is given by equation (4.17).

The Lyapunov function is described $v(e, \theta_1, \theta_2, \theta_3)$. This function should be positive semi definite and is zero when error is zero. For stability according to Lyapunov theorem the derivative $^{dv}/_{dt}$ must be negative. The derivative $^{dv}/_{dt}$ requires the values of $d\theta1/dt, d\theta2/dt$ and $d\theta3/dt$. If the parameters are updated then so $^{dv}/_{dt}$ is negative semi definite. This shows that V(t) = V(0) and e, θ1, θ2 and θ3 must be bounded and also Lyapunov removes the filter of MIT rule and uses the

simplified mathematical model which is given below after we derived using Lyapunov rule of the given form.

The Lyapunov Function is taken as:

$$v(e,\theta_1,\theta_2,\theta_3) = v(e,k_1,k_2,k_3) \tag{4.37}$$

$$v(e,k_1,k_2,k_3) = {}^{1}/_{2}\,(e^2 + \tfrac{1}{by}(bk_3 + a - a_m)^2 + \tfrac{1}{by}(bk_2 + a - a_m)^2 + \tfrac{1}{by}(bk_1 - b_m)^2) \tag{4.38}$$

$$\frac{dk(t)}{dt} = -\gamma\left(\frac{p}{p+4}r(t)\right)e(t) \cong -\gamma\big(r(t)\big)e(t) \tag{4.39}$$

According to Lyapunov, the system is said to be stable when ${}^{dv}/_{dt}$ is negative definite. So in order to make the system stable the parameters are updated as:

$$\frac{dk_1(t)}{dt} = -\gamma\big(r(t)\big)e(t) \tag{4.40}$$

$$\frac{dk_2(t)}{dt} = \gamma\big(y(t)\big)e(t) \tag{4.41}$$

$$\frac{dk_3(t)}{dt} = \gamma\big(\dot{y}(t)\big)e(t) \tag{4.42}$$

Therefore, The Lyapunov Simulink block diagram accordingly is given in Figure 4.6.

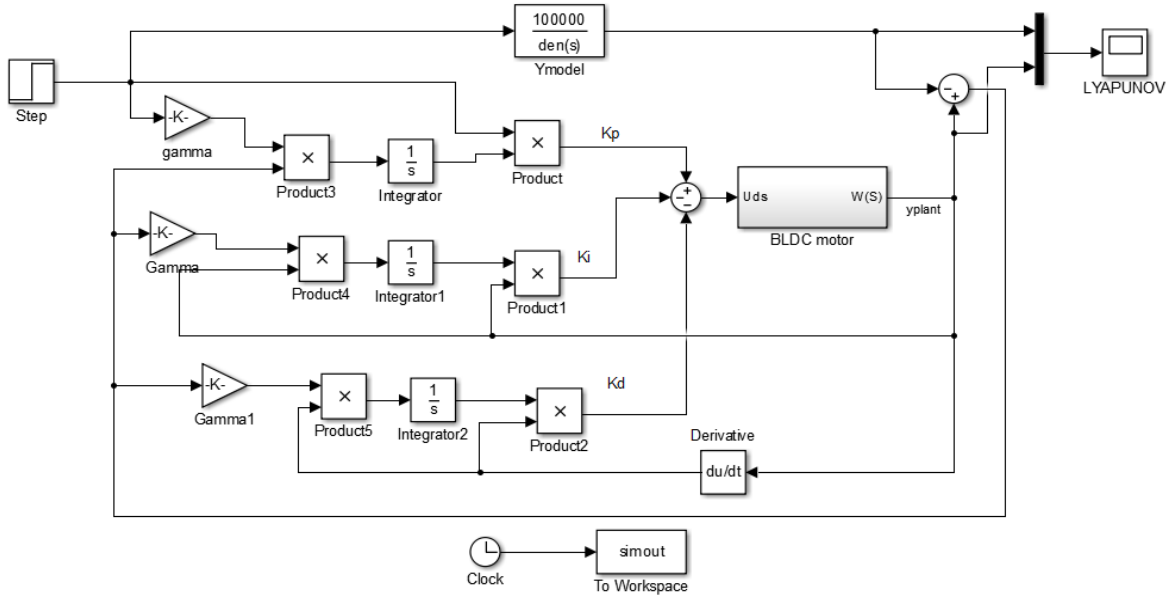

Figure 0.6 System block diagram of Lyapunov method.

4.3. Applying Of Fuzzy Logic Controller

As shown in Figure 4.7 below, a typical fuzzy-control system is composed of a fuzzy controller and a plant. The fuzzy controller involves four components: fuzzification, knowledge database (including the database and rule base), fuzzy inference and defuzzification. Fundamentally, fuzzy control can reflect human reasoning. It is an intelligent control method that is independent of the precise mathematical model of the controlled object. Whether the controlled object is linear or nonlinear, a fuzzy controller can be implemented effectively with good robustness and adaptability.

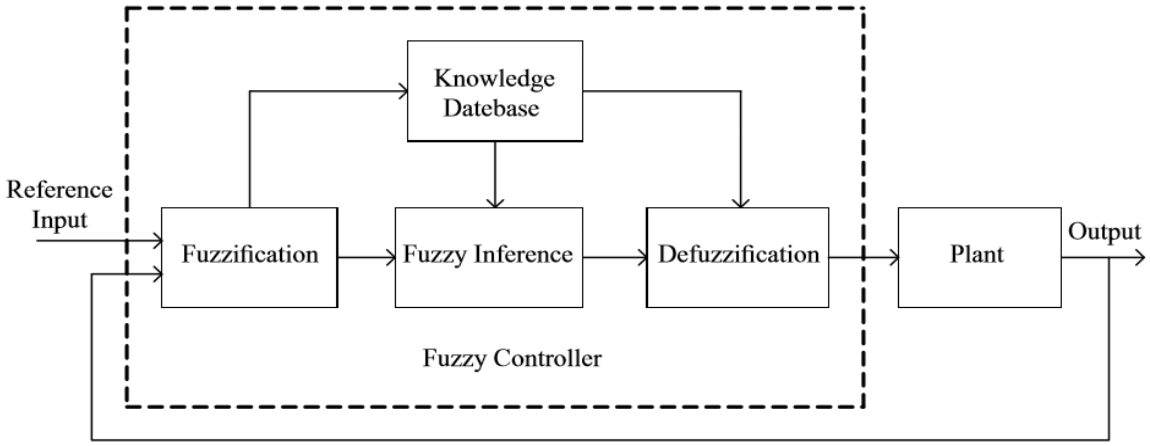

Figure 0.7 Typical diagram of a fuzzy-control system [15].

Due to the appearance and development of fuzzy theory, fuzzy control has been used widely in motor-control applications. Since the motor load varies greatly in many motor applications, good speed-regulation ability is often essential in all working conditions. Considering the limitation on algorithm time consumption, nonlinear control methods based on fuzzy logic are ideal choices for motor control [5–8]. Currently, the fuzzy-control methods for BLDC motors can be mainly divided into three categories: standard fuzzy controller, fuzzy PID switch controller and optimized fuzzy controller.

4.3.1. Configuration of FLC

- Principal components of Fuzzy logic controller:
- Fuzzification block or Fuzzifier
- Knowledge base
- Decision making block
- Defuzzification block or Defuzzifier

The structure of Fuzzy controller is shown below.

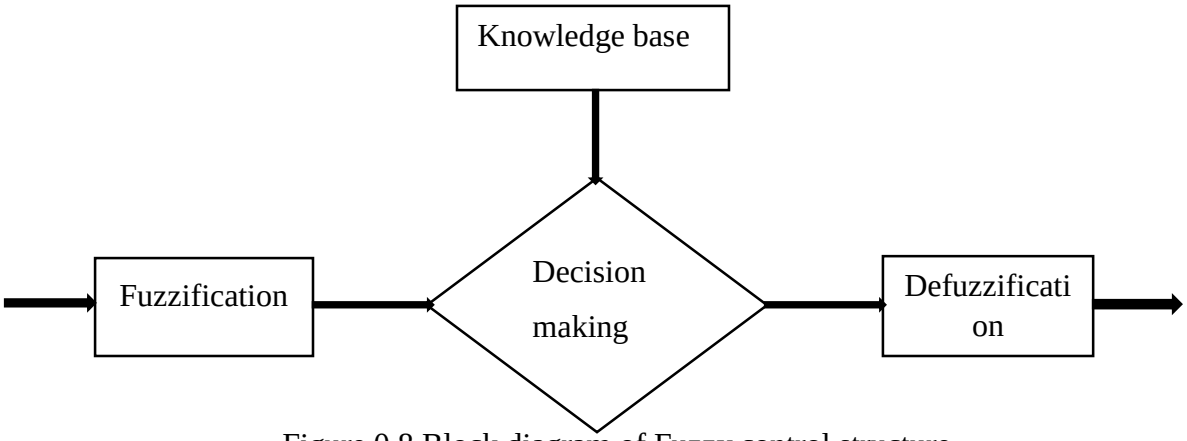

Figure 0.8 Block diagram of Fuzzy control structure

4.3.2 Fuzzifier

As discussed previously fuzzy logic based on linguistic variable but since input given to the FLC block is in numeric form so first thing to be done is to convert the numerical data/variable into linguistic variable. And this task is performed by the Fuzzifier. So Fuzzifier converts the numerical variable given to the FLC into linguistic variable. This Fuzzification task includes choosing proper MF for the variables so that the crisp inputs can be converted into fuzzy sets.

4.3.3. Knowledge base

Fuzzy inference engine or the knowledge base is the process that relates input fuzzy sets to output fuzzy sets using if-then rules and fuzzy mechanism to derive a reasonable output form crisp or fuzzy inputs. There are two types of fuzzy inference systems: Mamdani-type and Sugeno-type. Mamdani fuzzy inference system is the most commonly used method; since it has the advantages of intuition, wide acceptance and suitability to human input.

The following steps summarize the algorithm of Mamdani (max-min) inference engine:

Step 1: Computing the degree of fulfillment by:

$$\beta i = \max[\mu\mathcal{A}'(x) \Lambda \mu\mathcal{A}'(x)], i = 1,2, \dots, K \quad (4.43)$$

Step 2: Deriving the output fuzzy setsBi':

$$\mu B'(y) = \beta i \Lambda \mu\mathcal{B}i\ (y), y\epsilon Y, i = 1,2, \dots, K \quad (4.44)$$

Step 3: Aggregating the output fuzzy sets β 'i into a single fuzzy set β ' is:

$$\mu Bi'(y) = max\mu\mathcal{B}i'(y), y\epsilon Y, 1 < i < K \quad (4.45)$$

4.3.4 Decision Making Block

It is the most important component of a fuzzy controller because it is the block that decides the output depending upon the input. Based on fuzzy concepts, data and rule bases, it provides reasonable output.

4.3.5 Defuzzifier

İt performs the task just opposite to that of Fuzzifier. So the task of Defuzzifier is to convert the linguistic variable into crisp one. There are different types of Defuzzification techniques.

- Centroid of Area (COA)
- Bisector of Area (BOA)
- Mean of Maximum (MOM)
- Smallest of Minimum (SOM)
- Largest of Maximum (LOM)

Among these methods, the most commonly used is the centroid Defuzzification. This technique was developed by Sugeno in 1985, and it had very accurate results compared with other methods. The centroid Defuzzification method which is shown in Figure 4.9 and expressed as follows:

$$x^* = \int \mu i(x) x\, dx \Big/ \int \mu i(x)\, dx \quad (4.46)$$

Where:

x* is the Defuzzifier output

$\mu i(x)$ Is the aggregated membership function

x Is the output variable

Rule1 If x is A then N is D Rule2 If y is B then N is E

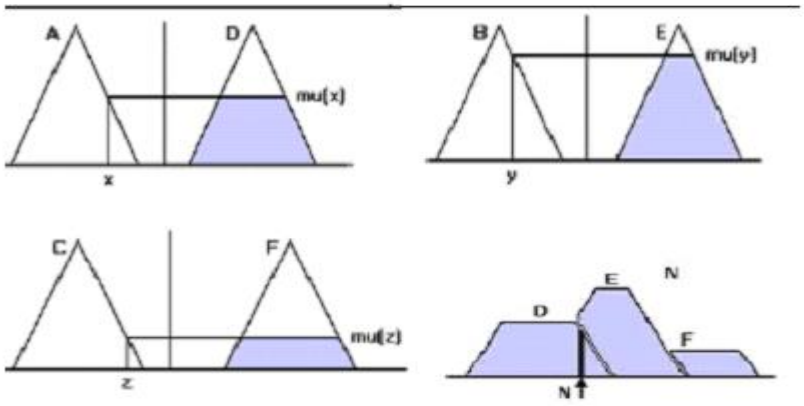

Rule 3 If z is C then N is F Defuzzification crisp value = N

Figure 0.9 Block diagram of Centroid Defuzzification using max-min inference [15].

4.3.6 Fuzzy Logic-Based Controller

Modern electric drives require monitoring the shaft speed of the motor continuously to assure that it follows preselected tracks. Fuzzy control system could be designed to achieve this goal. Fuzzy control system could replace human experience using fuzzy rule-based system by converting linguistic control into automatic control approach. One of FLC advantages is that it shows high performance control without requiring mathematical model of the system. The implementation of FLC could be summarized in the following steps:

I. Determination which of system dynamic parameters will be used as input, and which will be used as output of the fuzzy controller. For example: rotor speed and rotor acceleration are the inputs, while voltage and frequency are the outputs.

II. Choosing proper linguistic fuzzy variables to describe the membership functions for input and output variables of the fuzzy controller. These variables are used to transform numerical values into fuzzy quantities. For example: (NL) is used for (negative large), and (PM) is used for (positive medium).

III. Building the fuzzy control rules that relate input variables to output variables using (if-then) statements.

IV. Finally, a fuzzy centroid is used to calculate the fuzzy control output.

4.3.7 Speed Control Using FLC

In the case of motor speed control, the two needed input variables for FLC is: the motor speed error (E) and its derivative, which represents the change of speed error (CE). Whereas, the controller output is the change in frequency (CF) of the voltage supply fed to motor. Speed error and change of speed error could be defined as follows:

$$E = V_{ref} - V_{act} \tag{4.47}$$

$$CE = \frac{dE}{dt} \tag{4.48}$$

Where $V_{ref}$the desired motor speed and V_{act} is the measured motor speed.

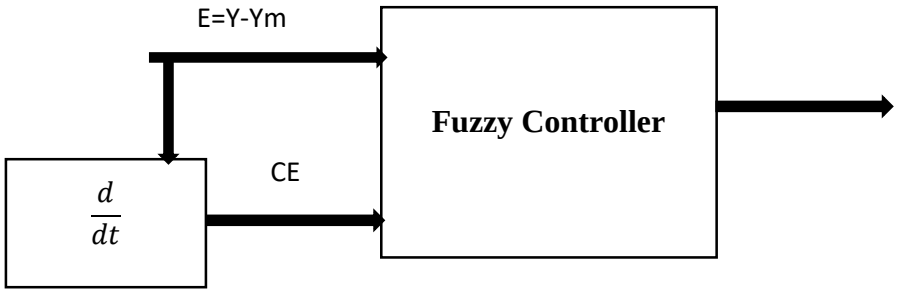

Figure 0.10 Block diagram of Fuzzy control system.

In fuzzy controller design, three main regions could be defined for each of the two input fuzzy variables, and the same number for the output variable. These regions are: negative, zero, and positive. In the input side (E and CE), these regions are used to determine the required frequency of voltage supply based on predefined regions at the output side. Such frequency enables the motor speed to follow a desired reference track.

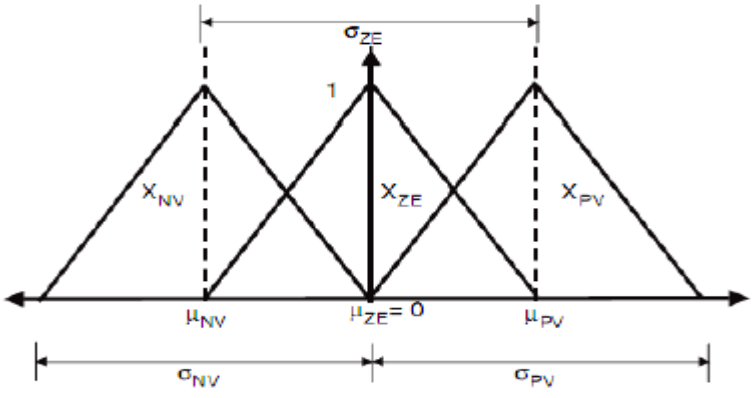

Figure 0.11 Triangular membership functions example [15].

Positive and negative regions are usually divided into sub regions, such as (positive big) and (negative medium). In general, an odd number of membership functions are used to partition a region in fuzzy logic applications, often five or seven.

4.3.8 Design methodology of fuzzy logic inference system on MATLAB TOOLBOX

Steps to design a Fuzzy Logic Controller at a blank M File editor window are shown as follows:

- Selecting the input to the FLC
- Selecting proper MFs both for input and output variables
- Fuzzification of the input variable
- Preparing a Fuzzy rule base for the controller
- Selecting proper Defuzzification technique
- Defuzzification of output that is to be given to the system for desired operation.

4.3.9 Selecting and Designing Membership Functions

The Table 2 gives the fuzzy set and Membership function for speed error below.

A. For speed error (E)

Table 0.2 Fuzzy set and MFs for input speed error (E)

Fuzzy set	Range of MFs	Membership Function chosen
NL(Large Negative)	-0.8 to -0.8 -0.8 to -0.6 -0.6 to -0.4	Trapezoidal
NM(Medium Negative)	-0.4 to -0.2 -0.2 to -0.02	Triangular
NS (Small Negative)	-0.2 to -0.1 -0.1 to 0	Triangular
ZE (Zero)	-0.02 to 0 0 to 0.02	Triangular
PS (Small Positive)	0 to 0.1 0.1 to 0.2	Triangular
PM (Medium Positive)	0.02 to 0.2 0.2 to 0.4	Triangular
PL(Large Positive)	0.4 to 0.6 0.6 to 0.8 0.8 to 0.8	Trapezoidal

B. For change in (derivative of) speed error:

Table 3 below shows the MFs for input change in speed error.

Table 0.3 Fuzzy set and MFs for input change in speed error (E)

Fuzzy set	Range of MFs	Membership Function chosen
NL(Large Negative)	-0.8 to -0.8 -0.8 to -0.6 -0.6 to -0.4	Trapezoidal
NM(Medium Negative)	-0.4 to -0.2 -0.2 to -0.02	Triangular
NS(Small Negative)	-0.2 to -0.1 -0.1 to 0	Triangular
ZE(Zero)	-0.02 to 0 0 to 0.02	Triangular
PS(Small Positive)	0 to 0.1 0.1 to 0.2	Triangular
PM(Medium Positive)	0.02 to 0.2 0.2 to 0.4	Triangular
PL (Large Positive)	0.4 to 0.6 0.6 to 0.8 0.8 to 0.8	Trapezoidal

4.3.10 Designing Membership Functions for Change in Control:

Table 4 given below shows Fuzzy set and MFs for output change in speed.

Table 0.4 Fuzzy set and MFs for output change in control

Fuzzy set	Rang of MFs	Membership Function chosen
NL (Negative Large)	-1.0 to -1.0 -1.0 to -0.8	Trapezoidal
NLM(Negative Large Medium)	-1.0 to -0.8 -0.8 to -0.6	Triangular
NM (Negative Medium)	-0.8 to -0.6 -0.6 to -0.4	Triangular
NMS(Negative Medium Small)	-0.6 to -0.4 -0.4 to -0.2	Triangular
NS (Negative Small)	-0.4 to -0.2 -0.2 to 0	Triangular
ZE (Zero)	-0.2 to 0 0 to 0.2	Triangular
PS (Positive Small)	0 to 0.2 0.2 to 0.4	Triangular
PMS (Positive Medium Small)	0.2 to 0.4 0.4 to 0.6	Triangular
PM (Positive Medium)	0.4 to 0.6 0.6 to 0.8	Triangular
PLM(Positive Large Medium)	0.6 to 0.8 0.8 to 1.0	Triangular
PL (Positive Large)	0.8 to 1.0 1.0 to 1.0	Trapezoidal

4.3.11 Rule Base

There are 7 speed error variables and 7 changes in speed error variables are taken, so there are total 49 rules which are governed the decision making mechanism. The most important step in designing fuzzy system is the design of the rule base. It consists of a number of fuzzy IF-THEN rules that define the behavior of the system. The Table 5 below shows the corresponding rule base table for the proposed fuzzy control system. The top row of the matrix indicates the fuzzy sets of the error variable E and the left column indicates the change in error variable CE and the output variable U is shown in the body of the matrix.

Table 0.5 Rule base table

CE / E	NL	NM	NS	ZE	PS	PM	PL
NL	NL	NL	NLM	NM	NMS	NS	ZE
NM	NL	NLM	NM	NMS	NS	ZE	PS
NS	NLM	NM	NMS	NS	ZE	PS	PMS
ZE	NM	NMS	NS	ZE	PS	PMS	PM
PS	NMS	NS	ZE	PS	PMS	PM	PLM
PM	NS	ZE	PS	PMS	PM	PLM	PL
PL	ZE	PS	PMS	PM	PLM	PL	PL

Procedure to simulate the fuzzy controller in MATLAB:

- First rules have to coded and written in m-file and saved with .FIS extension.
- Then the FIS editor will be opened by typing fuzzy in the command window.
- Then the required FIS file has to be imported by browsing.
- After the loading of FIS file the controller is ready to be operated. All the above procedures are explained with figure in below.

After giving the fuzzy command in the command window, then Figure 4.12 FIS Editor window will be opened as shown below.

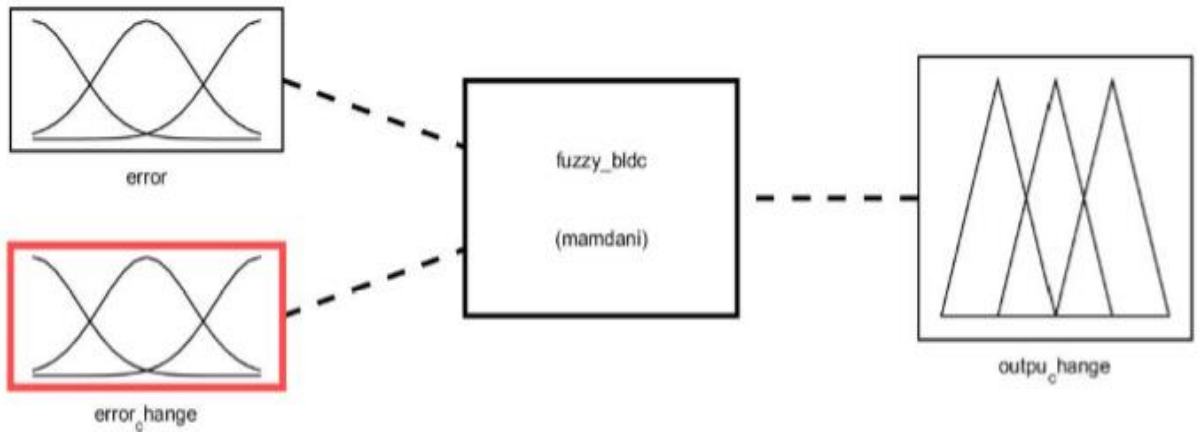

Figure 0.12 FIS Editor Window.

Then after importing the FIS file FIS Editor: rules window will be opened as shown in Figure 4.13 below with input of error and change of error.

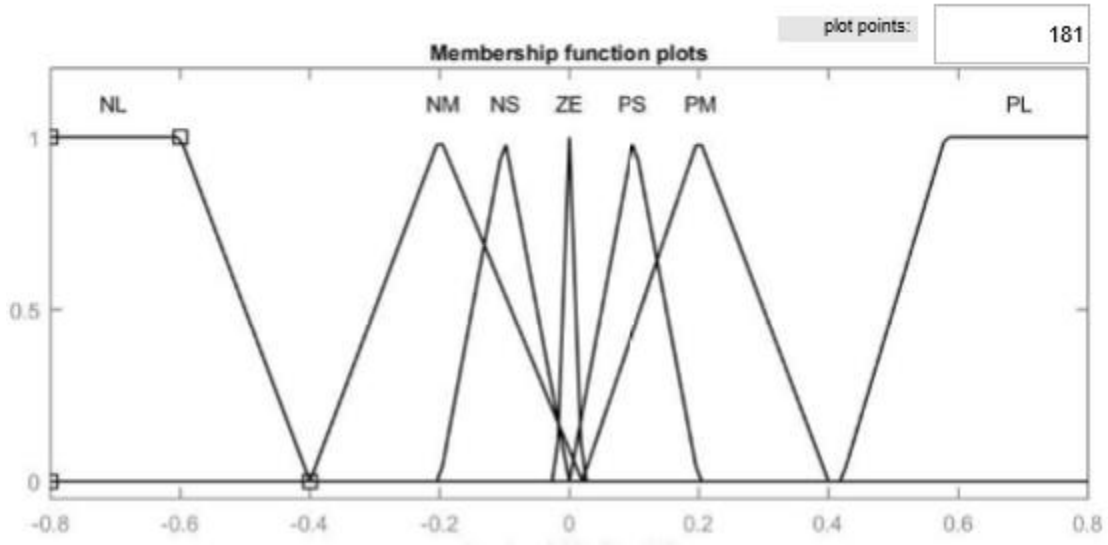

Figure 0.13 membership function plots of input error and change of error.

Similarly membership function of output change can also be seen below in Figure 4.14

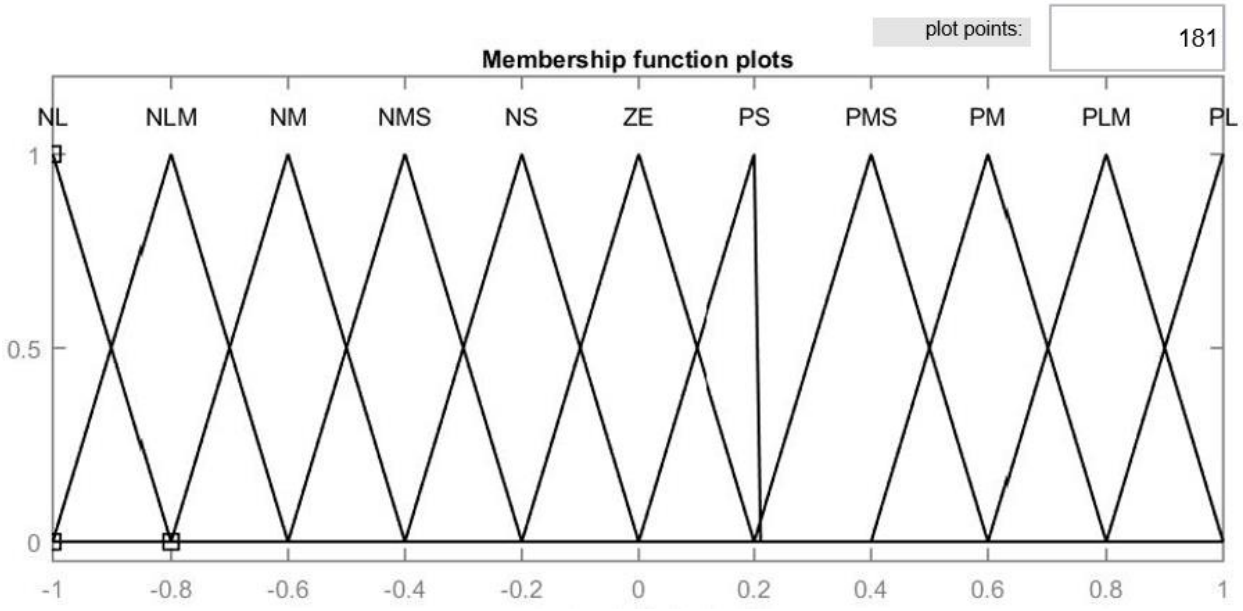

Figure 0.14 Membership Function of output change.

- In the FIS Editor window: rules view window, by clicking on view, rules and surface can also be seen below in Figure 4.15 and 4.16.

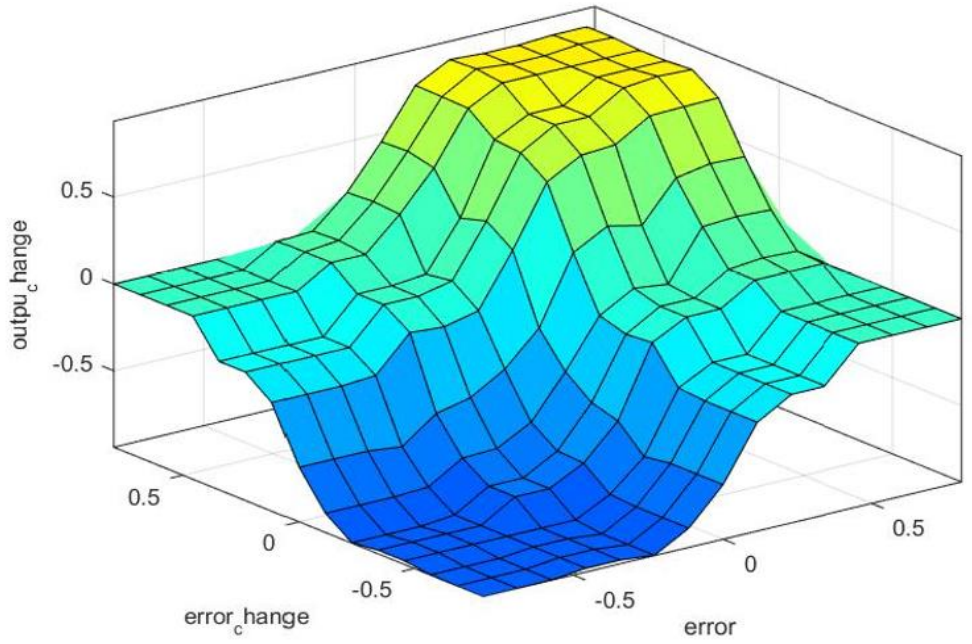

Figure 0.15 3-dimensional view of control surface.

Rule View of the control also can be shown Figure 4.16 below at a given value of error and change of error with relative change of output.

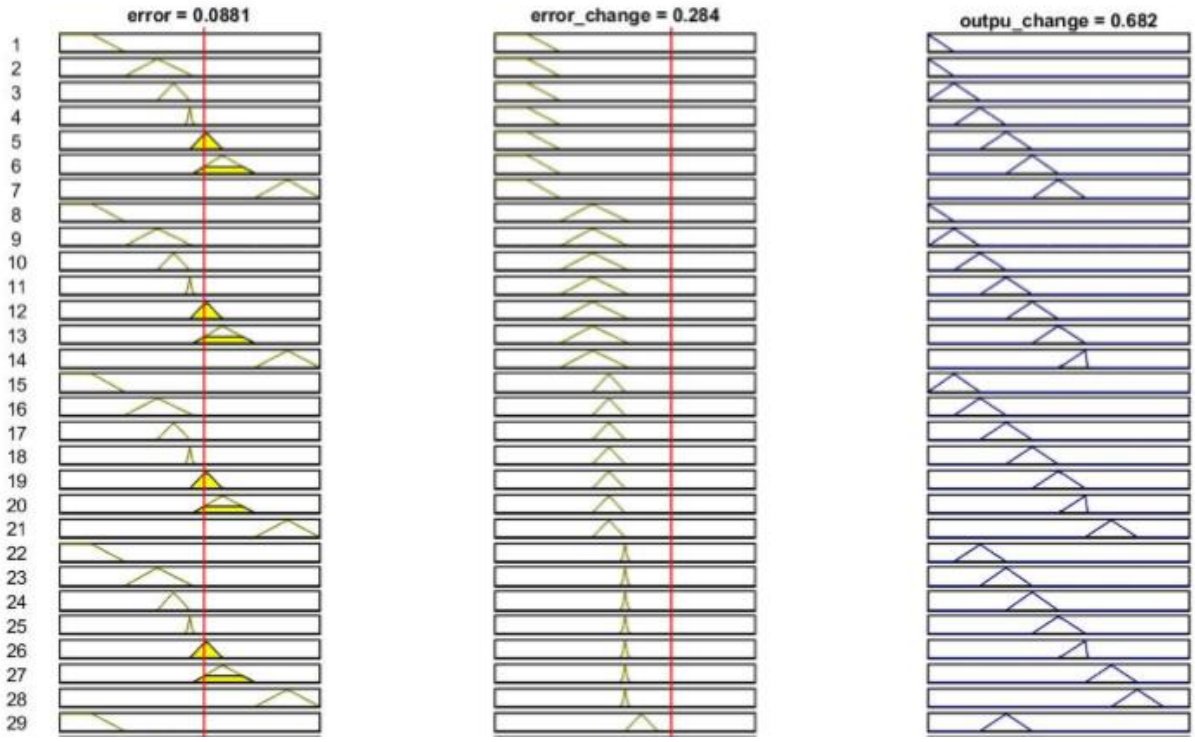

Figure 0.16 Rule Viewer with input E= 0.0881 and CE=0.264, Change of control=0.682.

4.4 Proposed Controller Design

The Figure 4.17 given below shows the proposed system design of the drive system of BLDC motor. Drive system includes the BLDC motor, inverter, controller and three Hall Effect sensors. Reference speed to which the motor is to be regulated is given as input to the controller. The rotor position is detected by using the three Hall Effect sensor signals and is fed back to the controller along with actual speed of BLDC motor. The controller generates the control signal based on the Fuzzy based model reference adaptive control law which is used for speed regulation and adapting purpose. This controls uses Application of fuzzy systems to nonlinear system hybrid model reference adaptive control design is proposed in this thesis. Model reference adaptive control are in general considered being applicable to plants that are mathematically understood and where the fuzzy system experienced human operators or behavioral learner are available.

Then a controller is constructed assuming that the MRAC system approximately represents the true plant as well as the model. Feedback linearization techniques for nonlinear control system design have been developed in the last two decades [8] [9]. However, these techniques can only

be applied to nonlinear systems whose parameters are known exactly. If the nonlinear system contains unknown or uncertain parameters then the feedback linearization is no longer utilizable. In this situation, the adaptive strategies are used to simplify the problem and to allow a suitable solution.

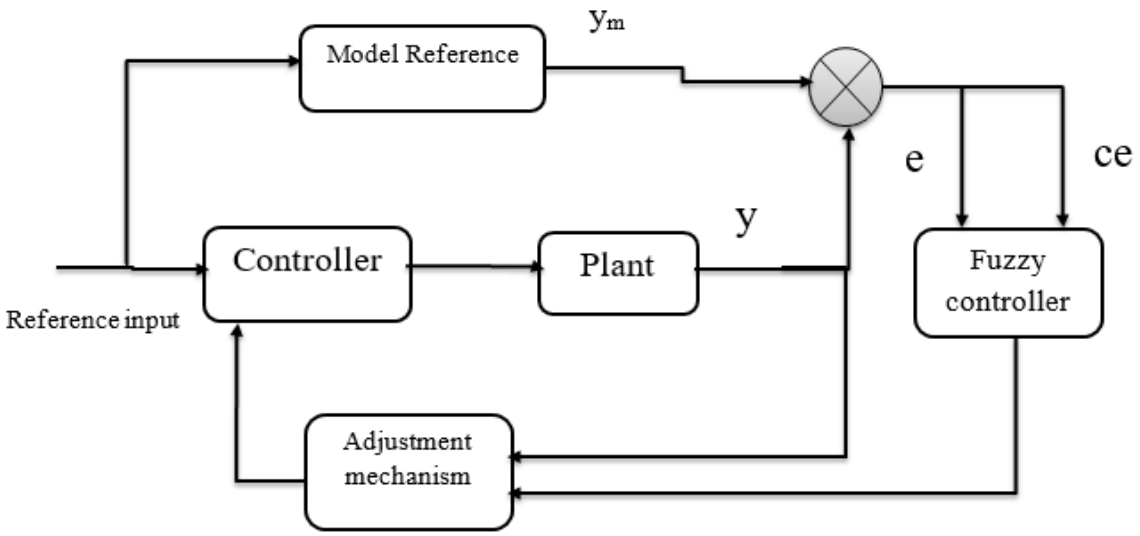

Figure 0.17 Complete proposed System design.

4.4.1 Proposed System Simulink Block Diagram

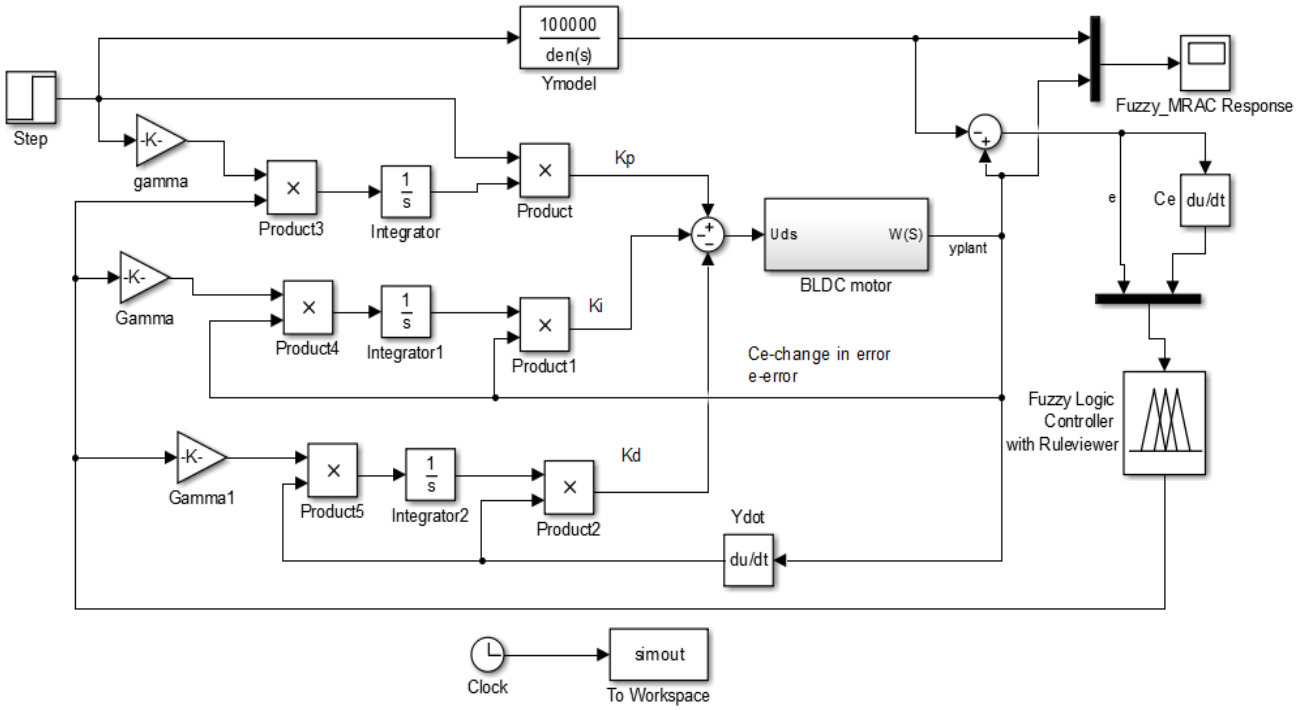

Figure 0.18 Proposed System Simulink Block Diagram.

4.4.2 Dynamic BLDC motor specification

Specifications of BLDC motor used for simulation is given in table 6 below.

Table 0.6 BLDC specification [10]

PARAMETERS	VALUES
Rated Power	6000W
Rated Voltage	315V
Rated Current	20A
Rated speed	1500 rpm
Rated Torque	30N-m
Stator Resistance	0.43Ω
Stator Inductance	0.00255H
Inertial Constant	0.0011
Viscous Friction Coefficient	0.05

CHAPTER FIVE

RESULT AND DISCUSSION

A Brushless DC motor drive system was modeled. Adaptive controller with MIT rule and Lyapunov Stability Method with Fuzzy was designed and applied to the model and a compared with the results of the conventional PID and simple MRAS controller as well as open loop response. All the simulations were carried out in MATLAB/ Simulink. Step input was given as the reference to study the response of controller with sudden load change.

5.1 Open Loop Response

The Open loop response of the plant is given in the Figure 5.1 with Simulink model and the load response of the plant with load torque is given below to characterize how much the plant resists a load torque and a base for close loop response characterization property.

5.1.1 Open Loop Model

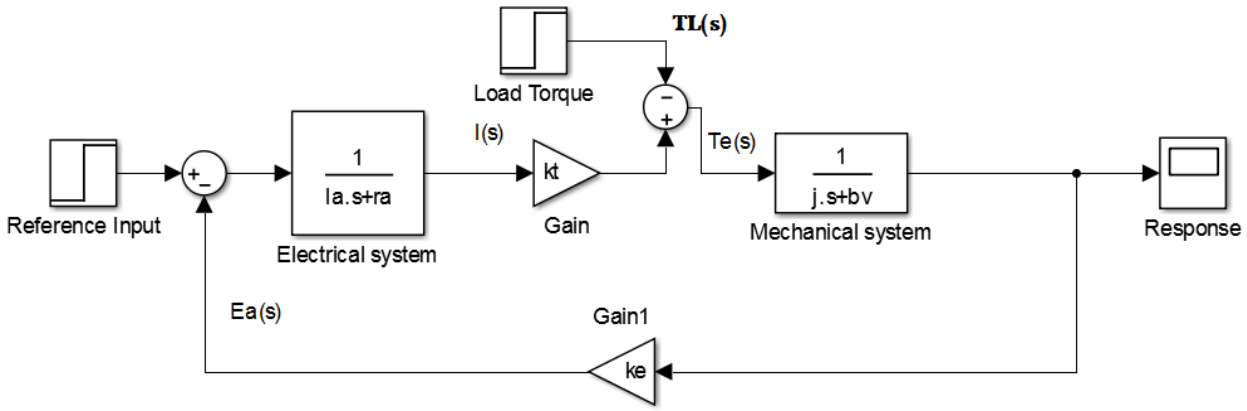

Figure 0.1Open loop Simulink model

Therefore, from the above Simulink model we have examined the open loop response with no load and with load condition and the load torque is varied from 100_300Nm and rated speed is 1500rpm is given for examination.

5.1.2 Open loop response

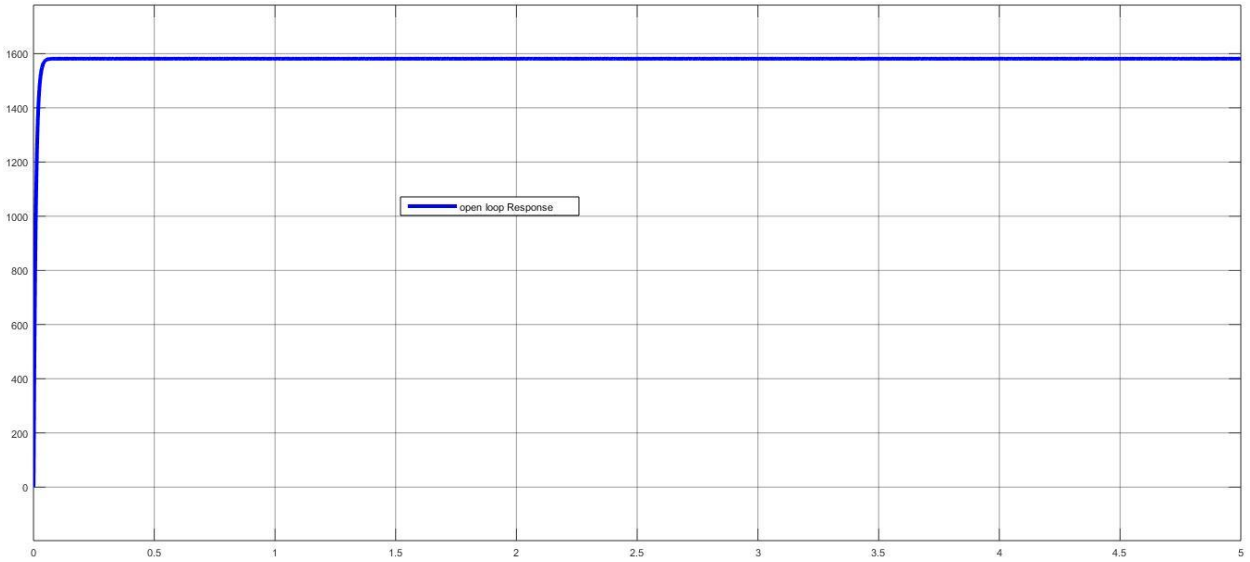

Figure 0.2 No load Open loop response

From the Figure 5.2 above we noticed that the plant response with a percentage overshoot of 0.495%, Rise time of 19.253ms and settling time of 12.871ms to operate as open loop.

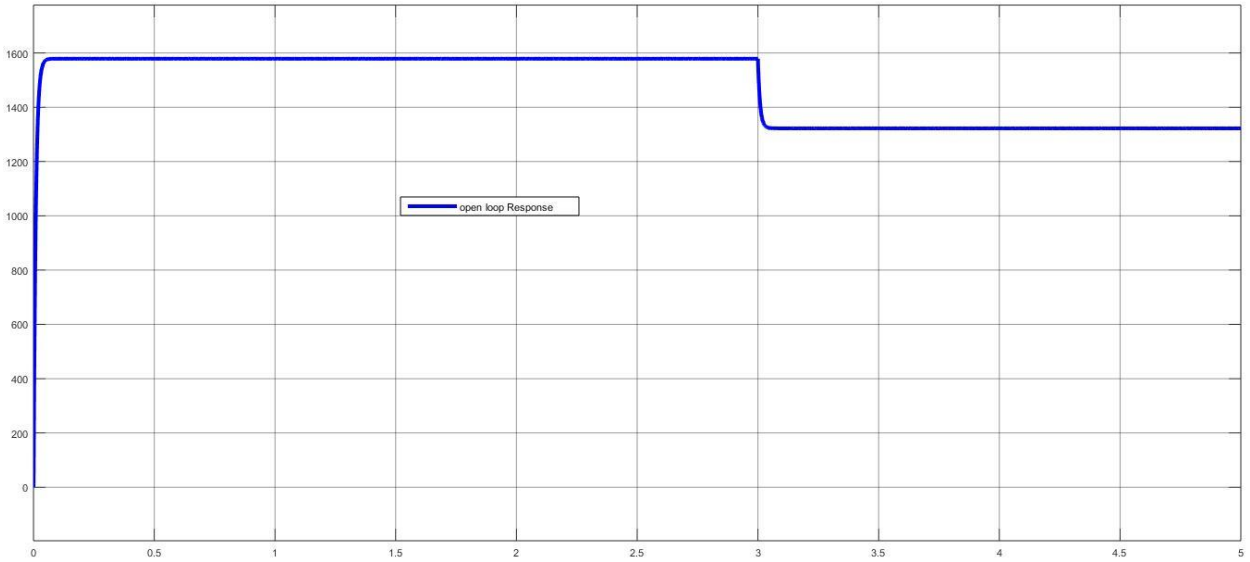

Figure 0.3 Open loop Response with Load torque 300Nm response

From open loop Load torque 300Nm response we have observed that the plant never come to the original place after applied and continues where load torque applied and the plant response with open loop Rise time of 19.253ms, Settling time of 12.871ms and with some increscent of a percentage overshoot 0.495% to operate as open loop with load torque of 300Nm at 3seconds.

5.2. Response of PID Controller

The controller parameters for the conventional PID controller are found such that it guarantees required tracking and also maintains the stability of the overall system when compared to open loop response. Zeigler Nicholas method of tuning is used to find the controller parameter which cope with the steady state error, overshoot and settling time requirements. The designed controller parameters are kp =5.7748, ki=1605.29, kd=0.00468 for speed tracking performance. The step responses of the conventional PID controller for the system with variation in speed from 1000 rpm to 1500 rpm and a load torque of rated 300Nm is applied as shown below in Figure 5.4 and Figure 5.5 respectively, High overshoot up to 1200-2000 rpm is observed for the system to sustain the operating condition of the plant. In order to reduce overshoot the controller with Model Reference Adaptive control technique is designed below.

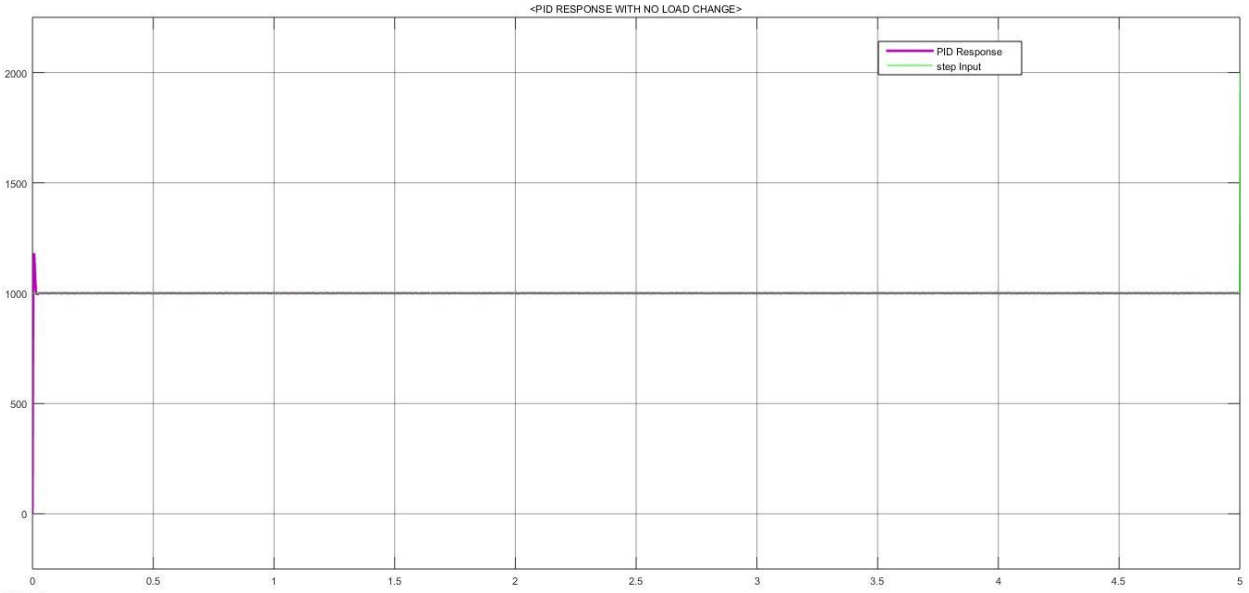

Figure 0.4 No Load Response of PID controller at 1000rpm

At rated speed with no load response of the plant, the close loop controller response of a conventional PID controller applied on the plant responses with a settling time of 12.284ms, Rise time of 2.552ms and a percentage over shoot of 18.452%.

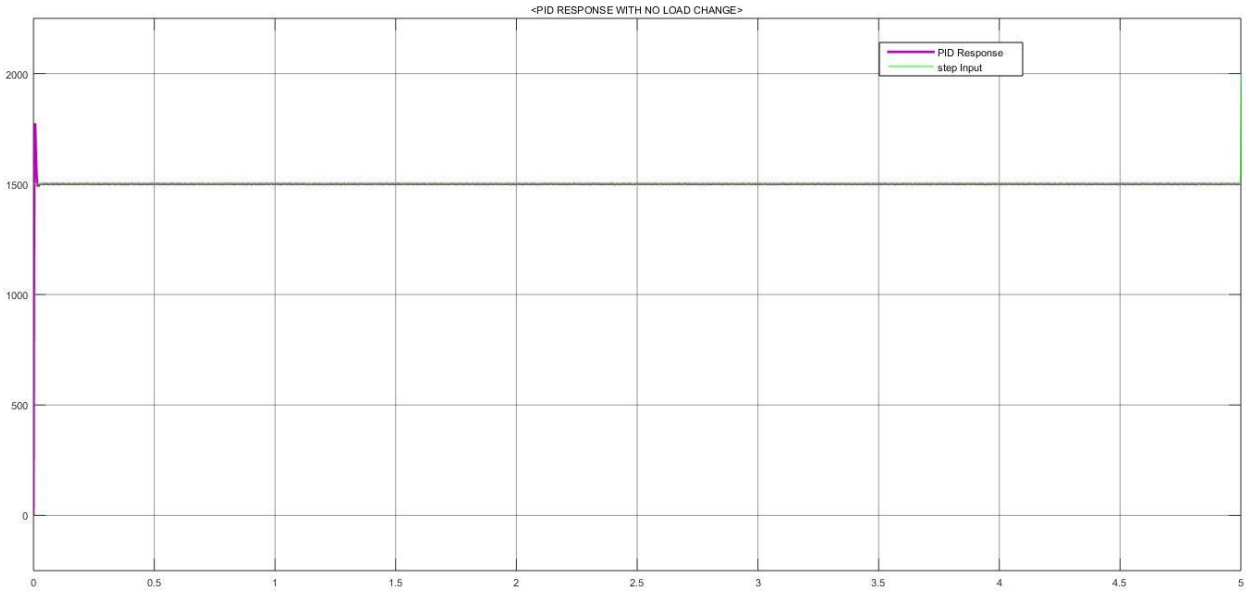

Figure 0.5 No Load Response of PID controller at 1500rpm

At rated speed with no load response of the plant increases, the close loop controller response of a conventional PID controller applied on the plant responses also increases in some condition with a settling time of 12.131ms and decreases with some condition of Rise time of 2.552ms and a constant percentage over shoot of 18.452% is observed with no load condition which indicates that changing rated input speed does not have fundamental change so we have been considered only on load change condition.

5.2.1 Response of PID Controller with Sudden Load Change

In order to validate the performance of the proposed controller setup is subjected to different test cases, like sudden change in load and sudden change in speed. The results of which are presented here in Figure 5.6 at 1000rpm and 1500rpm motor operation is in order to validate the model with a sudden load change applied at 3 seconds with rated speed of load torque. Initially the motor is run at no load and then the speed curve points to the no load operation.

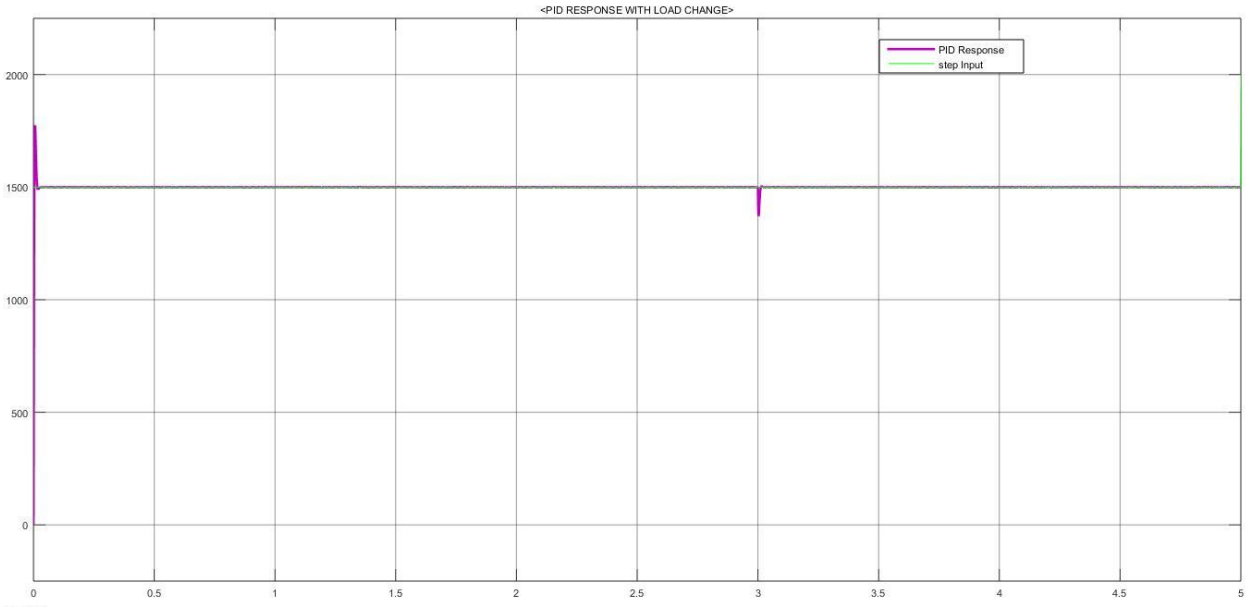

Figure 0.6 Response of PID controller at 1500rpm with sudden load change

5.3 Response of Model Reference Adaptive control

The Model Reference Adaptive controller is designed as discussed in the above sections. Error between the reference speed and actual speed is forced to zero using adaptation mechanism. The responses of the system when MRAC with MIT, modified MIT rule and Lyapunov stability method is applied with variation of speed from 1000 rpm to 1500 rpm is shown in Figure given below, For Adaptive controller with MIT rule we can see that the disturbances and overshoot are considerably reduced, thus reducing the steady state error and settling time. But we have same considerable overshoot.

5.3.1 No load response of model reference adaptive control

The following output shows the no load response of a model response adaptive controller with characteristics compression of steady state response.

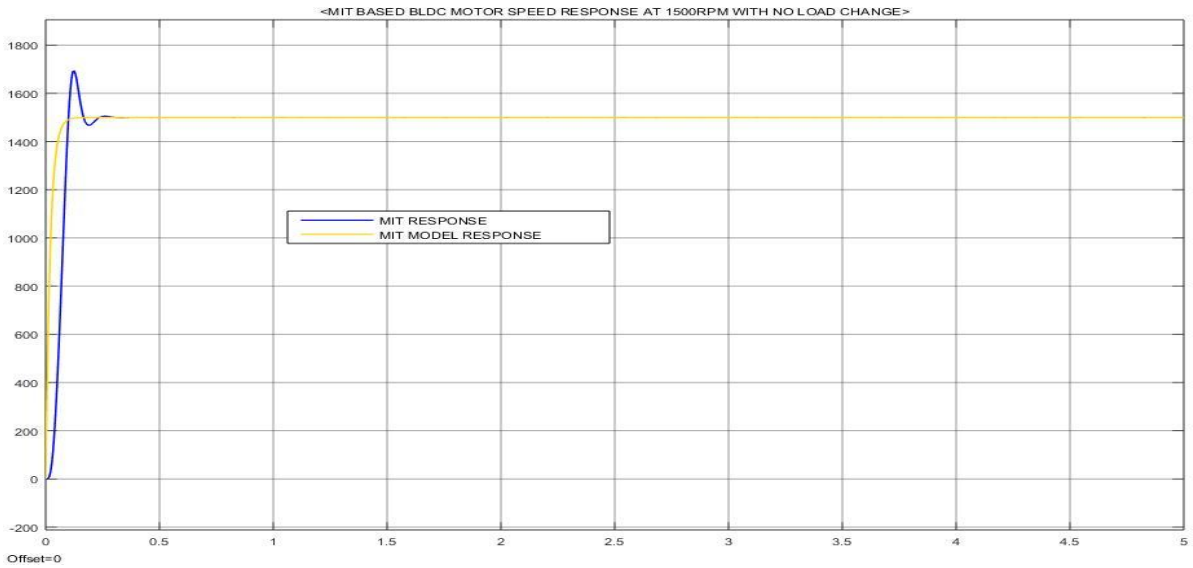

Figure 0.7 Response of Model Reference Adaptive controller With MIT rule at 1500rpm

From the response graph we have observed that the close loop response of the plant with model reference adaptive control is have some considerable change compared to with conventional PID controller with performance characteristics response of robustness hence the Rise time is 56.63ms,Settling time 0.4580s and a percentage overshoot of 13.0687% is observed.

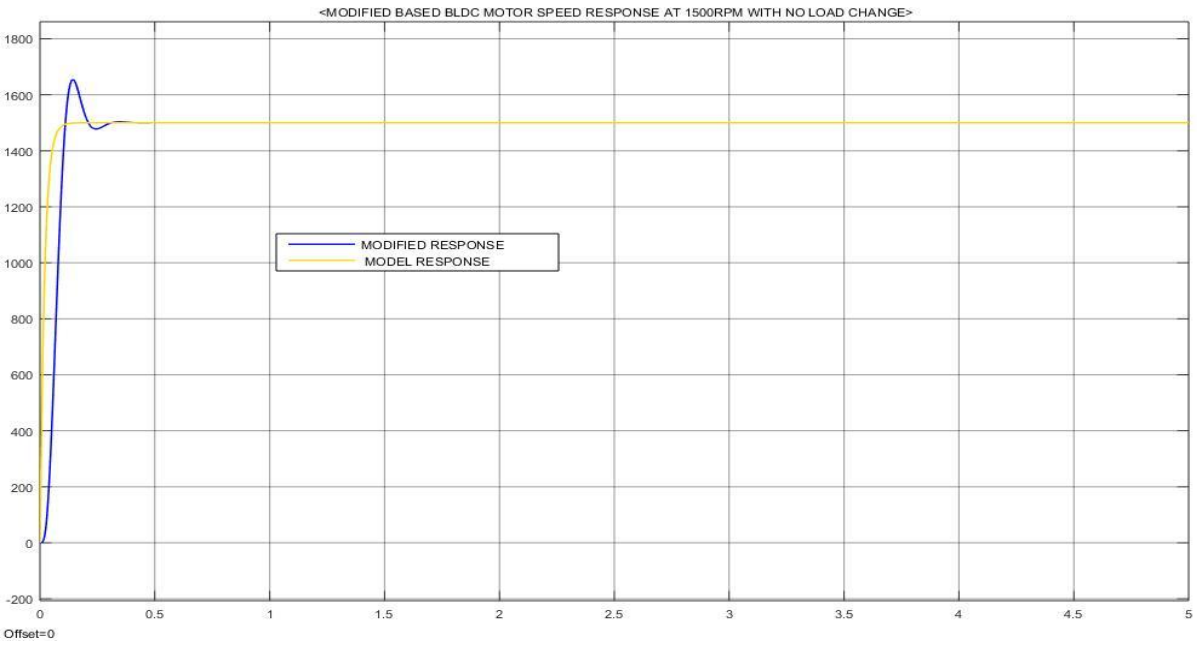

Figure 0.8 Response of Model Reference Adaptive controller with modified MIT rule at 1500rpm

From the response graph we have observed that the close loop response of the plant with model reference adaptive control with Modified MIT rule is have some considerable change compared to with MIT rule controller with performance characteristics response of robustness and the Rise time is 63.039ms,Settling time 0.485s and a percentage overshoot of 10.556% is observed witch is the Modified MIT rule have the ability to reduce the noise and some offset value or an overshoot compered to MIT rule.

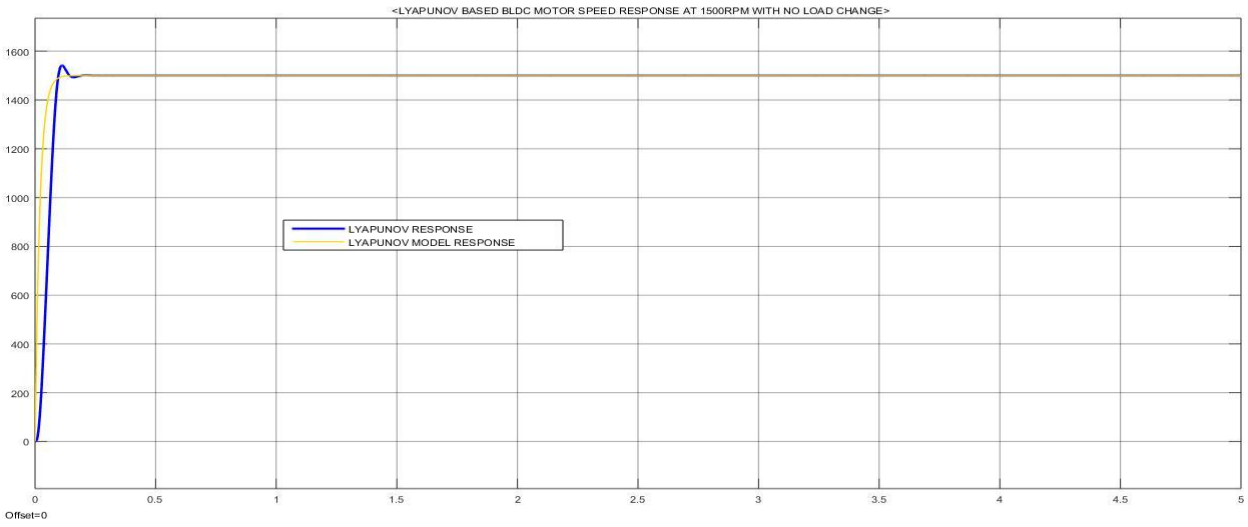

Figure 0.9 Response of Model reference Adaptive controller with Lyapunov Stability method at 1500rpm

From the above Lyapunov stability method response of close loop control system, we have observed that the response of the plant is stable and almost adapting the model response and responding a stable response of the characteristics of robustness compared to the two model reference adaptive controller and the Rise Time is 59.612ms, settling time 0.195s and a percentage overshoot of 2.577% is observed at no load condition.

5.3.2 Response of Model Reference Adaptive control with Sudden Load Change

In order to validate the performance of the proposed controller setup is subjected to different test cases, like sudden change in load and sudden change in speed as we said before. The results of which are presented here in Figures below at 1000rpm and 1500rpm motor operation. In order to validate the model at a sudden load change is applied at 3.0seconds. Initially the motor is run at no load and then the speed curve points to the no load operation at the applied time of load.

5.3.2.1 MIT Rule Sudden Load Change

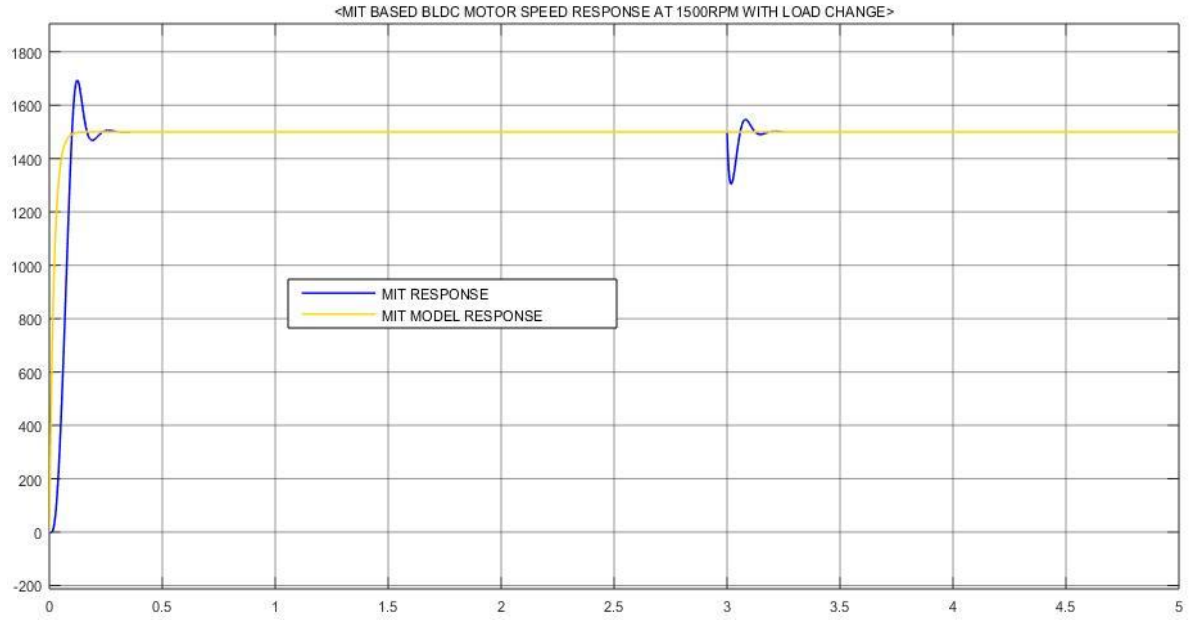

Figure 0.10 MIT rule sudden load change at 1500rpm and 300Nm

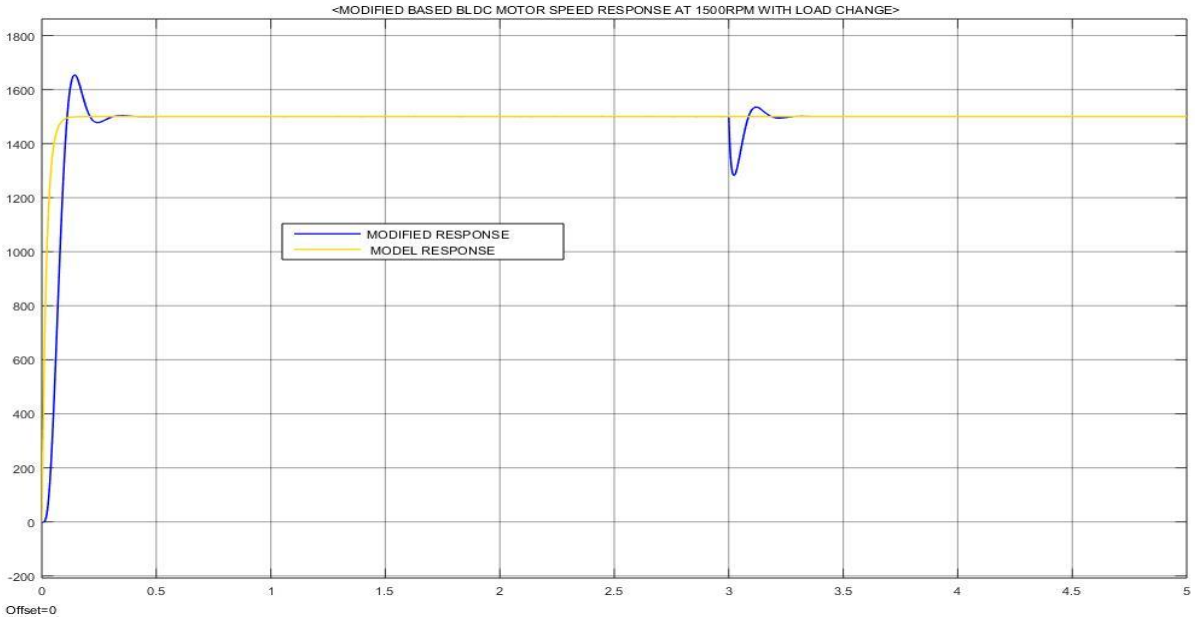

Figure 0.11 Modified MIT rule sudden load change at 1500rpm and 300Nm

5.3.2.2 Lyapunov Stability Method Sudden Load Change

As explained above sudden load change in the plant response at rated speed of the plant is given below with different input speed of the plant and a rated torque rated speed.

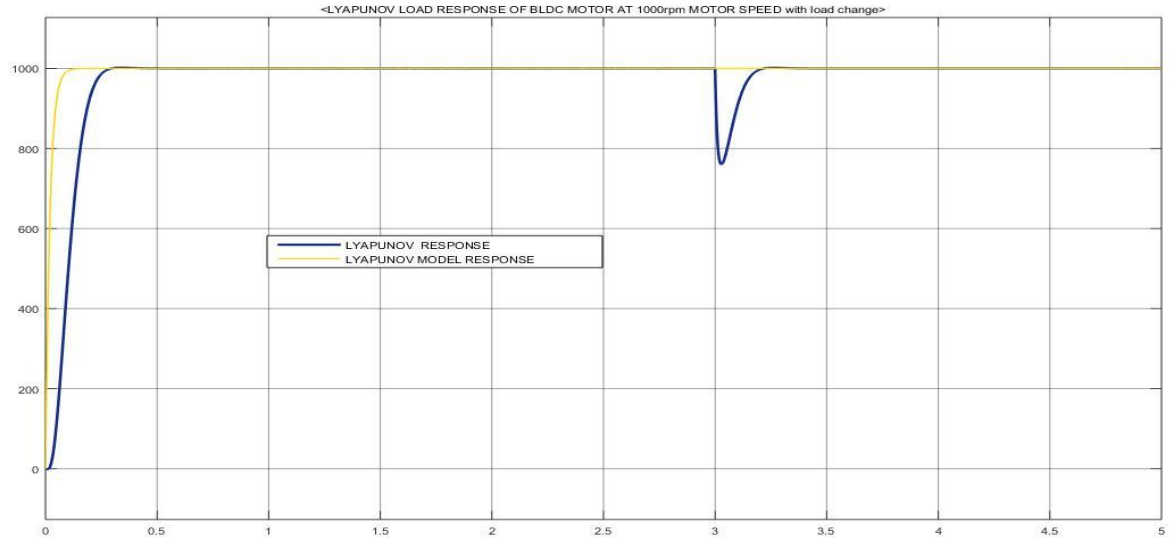

Figure 0.12 Lyapunov stability method sudden load change at 1000rpm and 300Nm Load

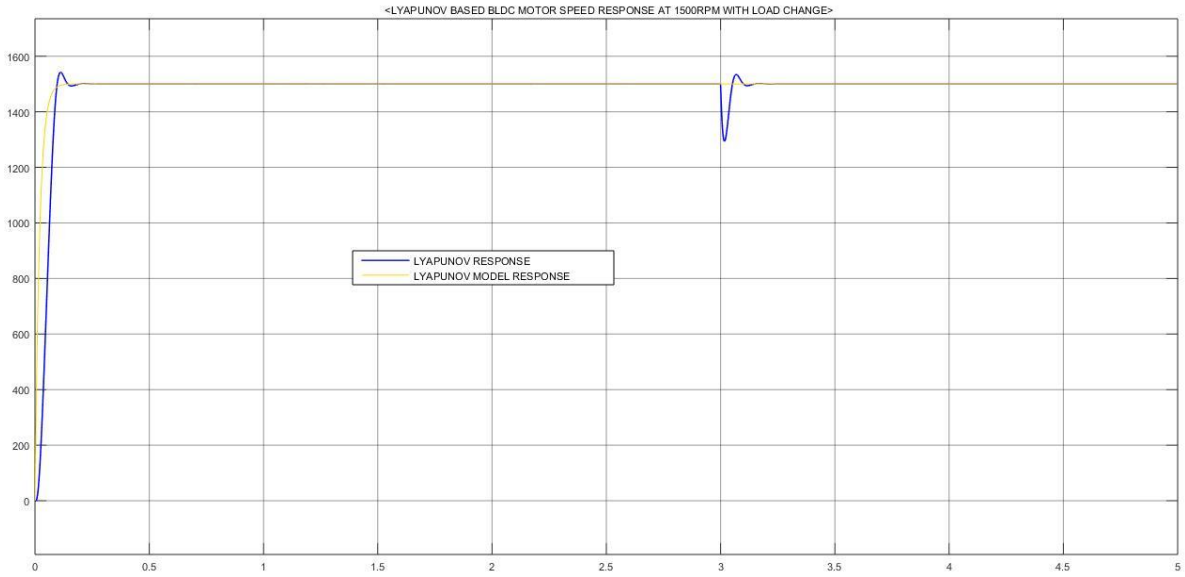

Figure 0.13 Lyapunov stability method sudden load change at 1500rpm and 300Nm Load

5.3.2.3 Lyapunov Stability Method Sudden Load Change Gain and Error response

The effect of the load change in the motor on the performance of the controllers was studied by changing the rated speed from 1000rpm to 1500rpm. The response of the Gain and Errors is shown in Figures given below Figure 5.14 and 5.15 and Figure 5.16 and 5.17 respectively.

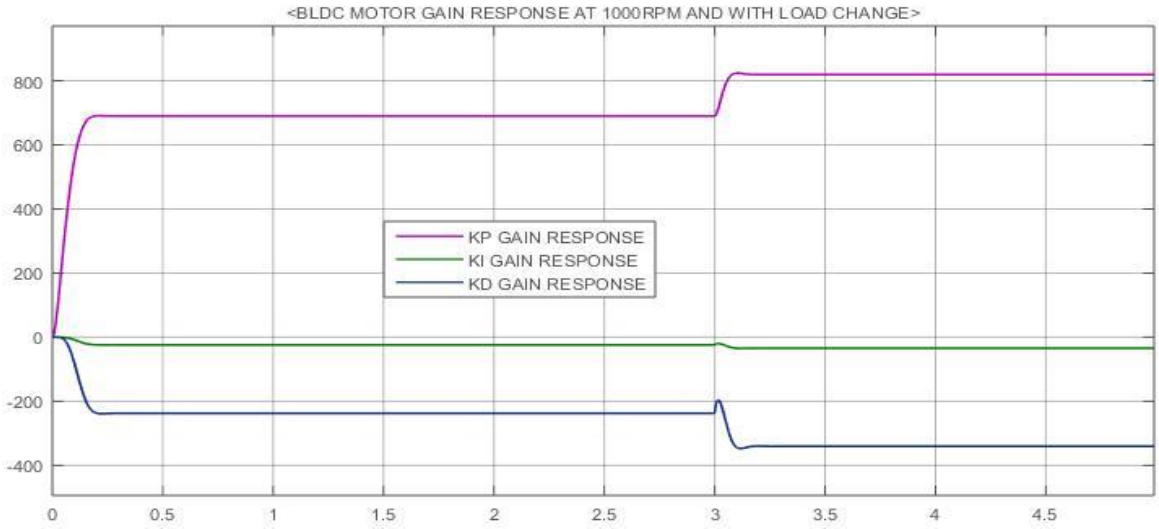

Figure 0.14 Lyapunov stability method sudden load change Gain response at 1000rpm

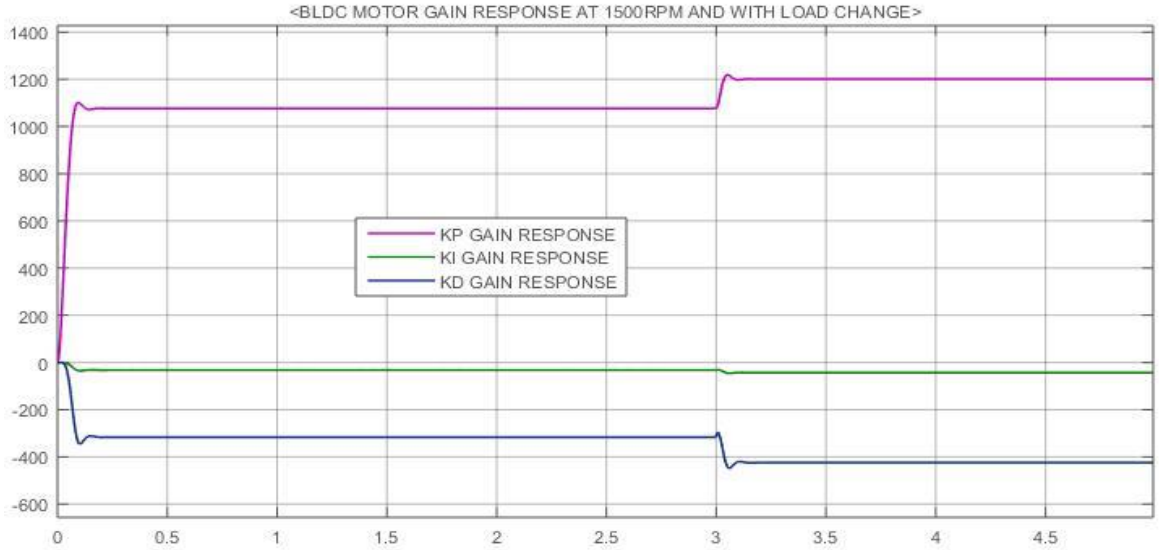

Figure 0.15: Lyapunov stability method sudden load change Gain response at 1500rpm

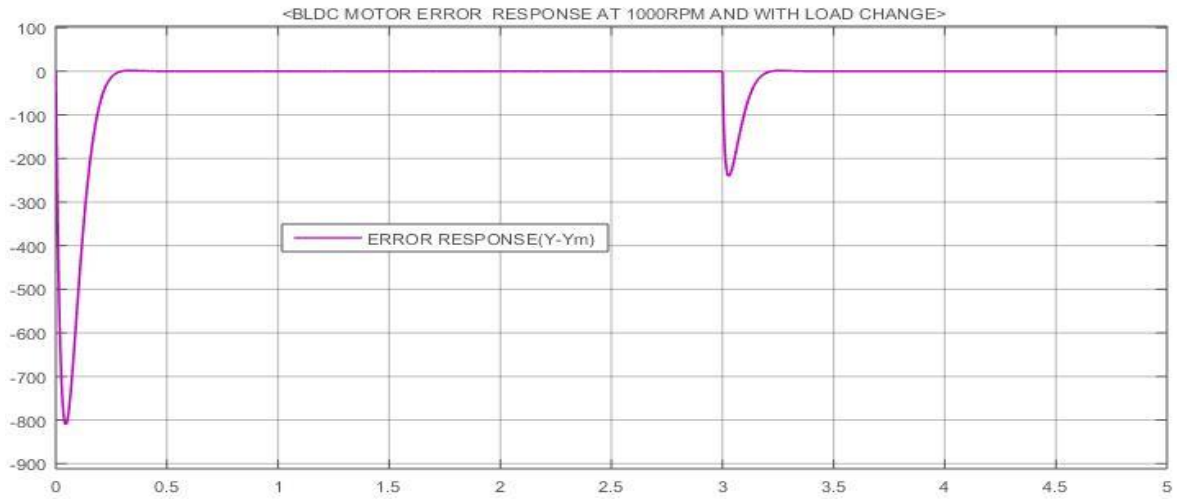

Figure 0.16 Lyapunov stability method sudden load change, change in error response at 1000rpm

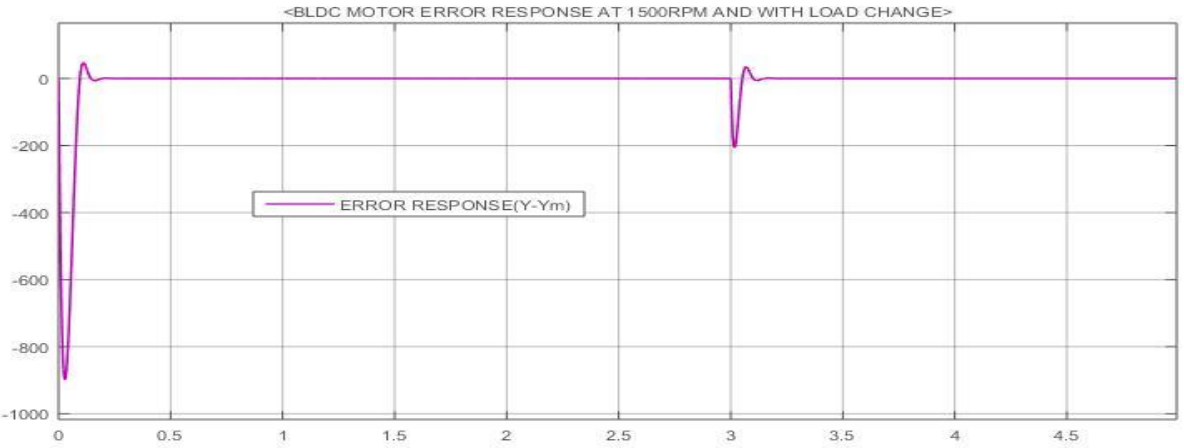

Figure 0.17 Lyapunov stability method sudden load change, change in error response at 1500rpm

5.4 Lyapunov Stability Method Sudden Load Change speed tracking response

Analyzing the addictiveness of the controllers is performed using a sine wave signal with a time period of 0.5 s and with constant amplitude. This can be interpreted as a repeated step response with each step lasting for a duration of 5 s and 50 Hz frequency duration. While it is common to use a single step function to examine ordinary of stability method to show how much tracks the speed response well is given in the given Figure 5.18-5.20 below with Gain and change of error response given respectively.

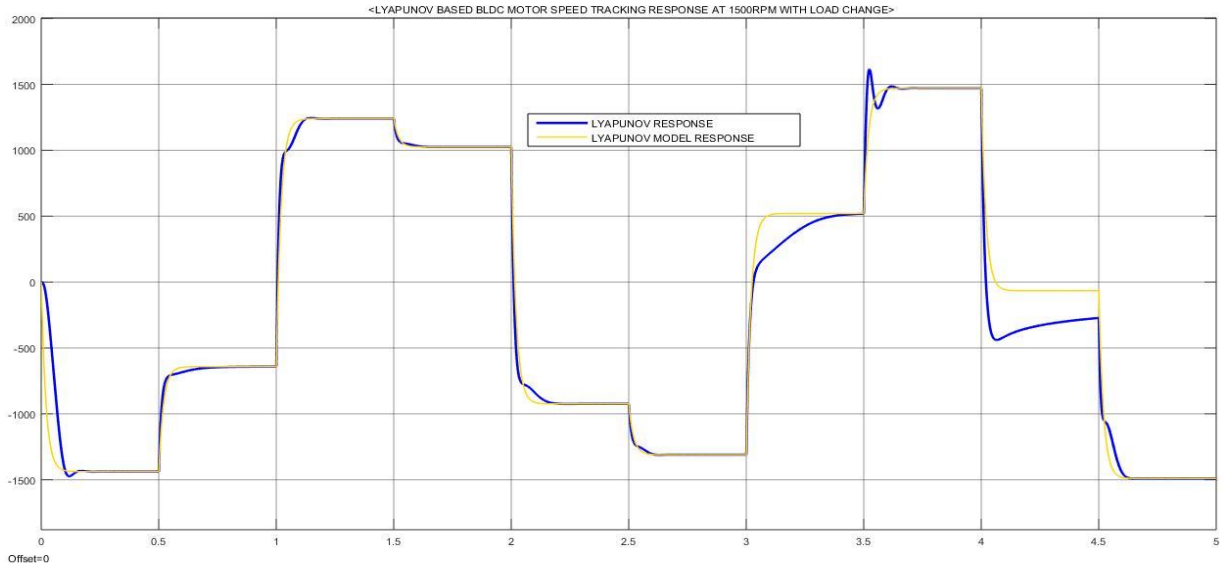

Figure 0.18 Lyapunov stability method sudden load change, speed tracking response at 1500rpm

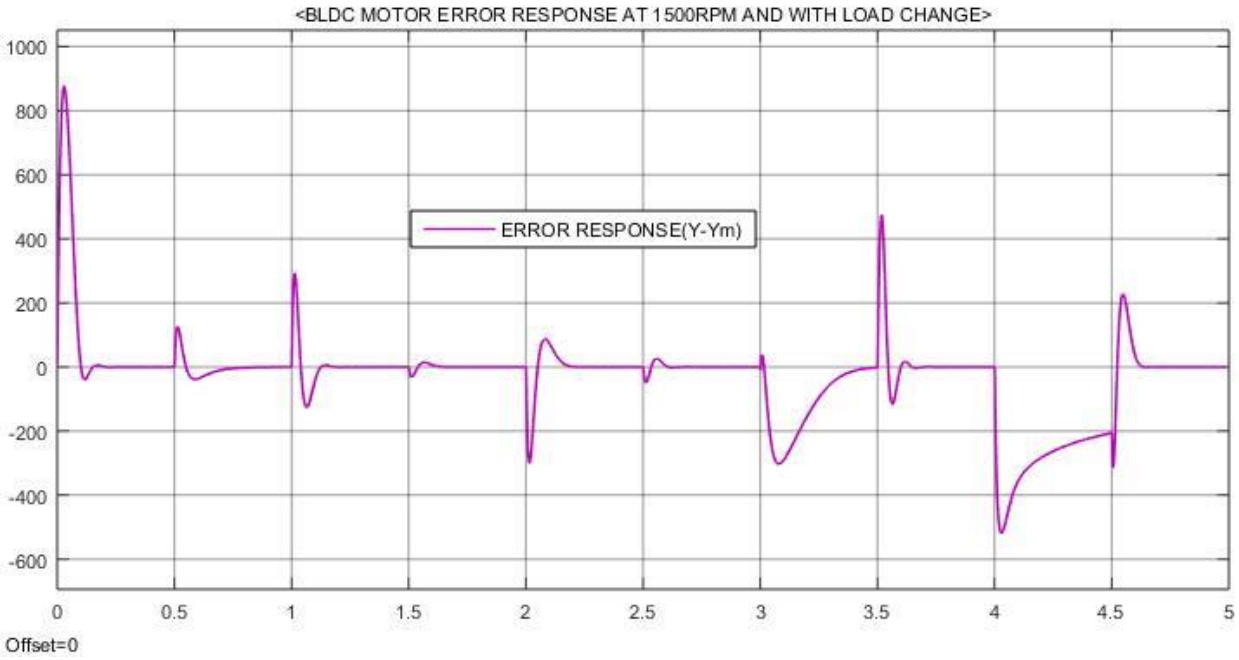

Figure 0.19 Lyapunov stability method sudden load change, tracking change in error response at 1500rpm

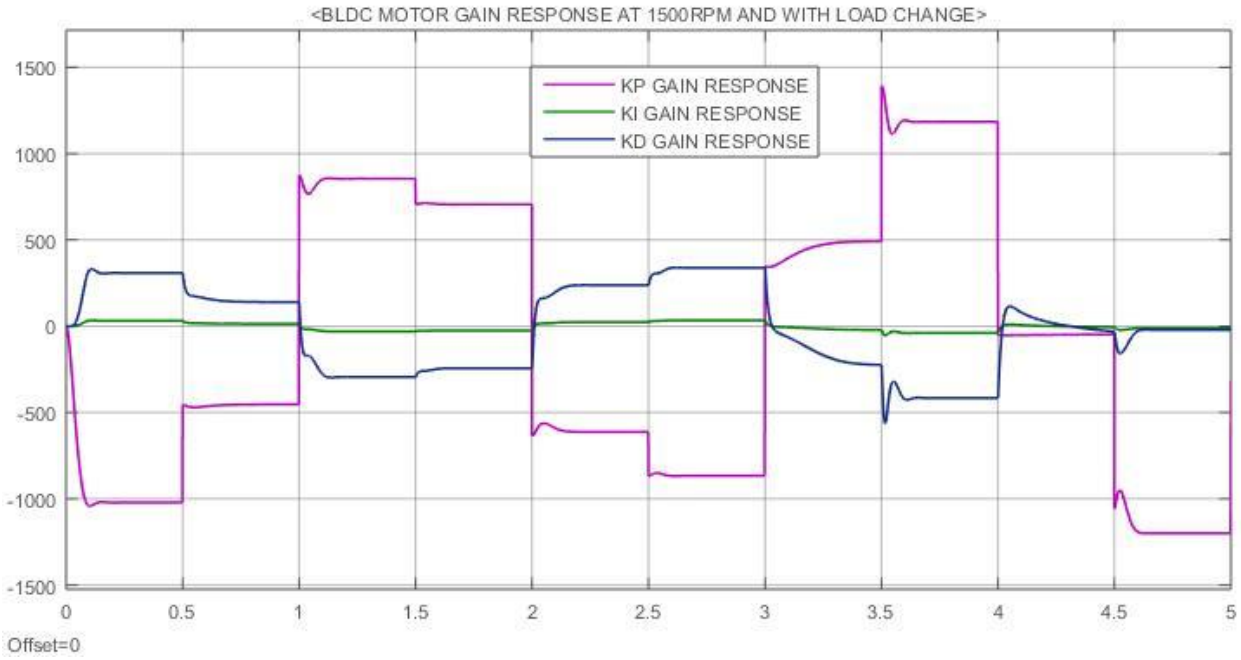

Figure 0.20 Lyapunov stability method sudden load change Gain tracking response at 1500rpm

From the above Figures as we saw that the Lyapunov stability method shows a great speed tracking response and almost a zero change error between the plant and reference model which is a best requirement as a control system and a good Gain change is observed totally.

5.5 Response of Fuzzy Based Model Reference Adaptive Control

In order to investigate the effect of the proposed controller and to compare its performance with the conventional PID controller and simple MRAC controller, the Simulink model of the system employing these controllers was simulated and tasted and given in the Figures below with no load condition and with load condition is clearly established and an improved performance of the system is equipped with the proposed Fuzzy based MRAC controller with no load and with load of rated speed.

5.5.1 Fuzzy Based Model Reference Adaptive Control at No Load Condition

The overshoot of the system equipped with the proposed Fuzzy based MRAS controller is considered almost zero as compared to a percentage overshoot of simple MRAS and conventional PID controlled system during no-load condition.

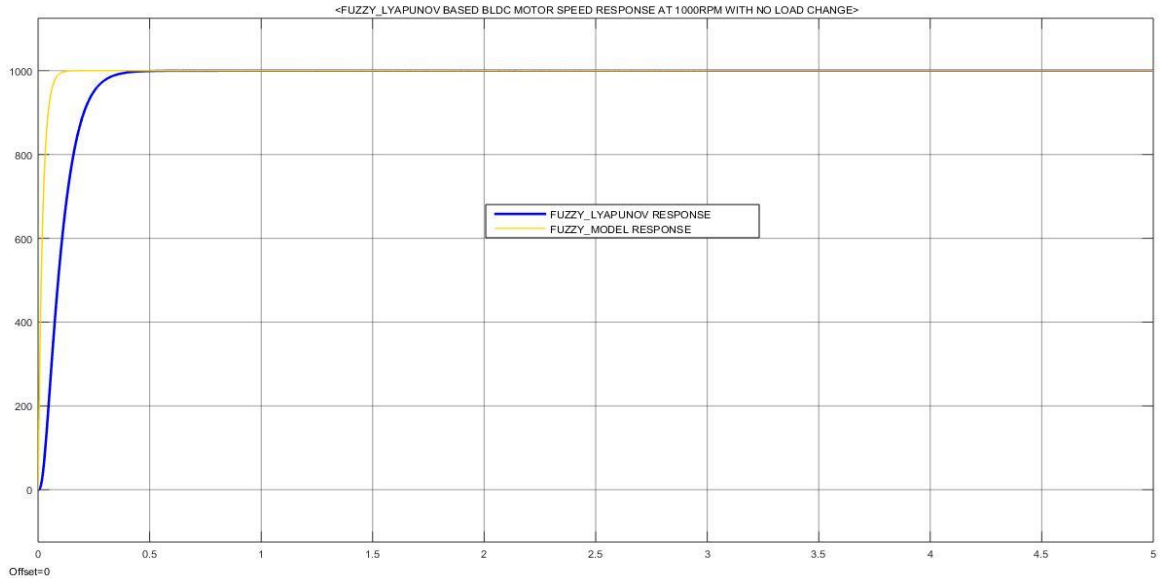

Figure 0.21 Fuzzy based MRAS controller at no load speed of 1000rpm

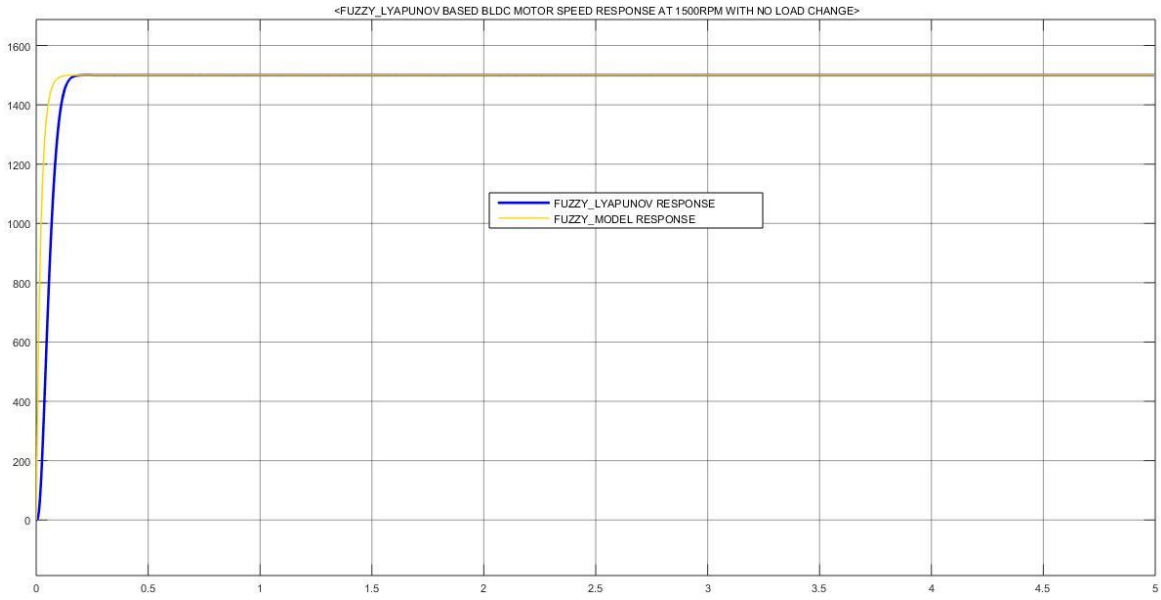

Figure 0.22 Fuzzy based MRAS controller at no load speed of 1500rpm

From the above two Figures we have observed that the response of the close loop control system is stable and almost all adaptive with a comparative response of steady state response. While a Fuzzy control system is a learning system with lunges tic variable and witch is a human learning tool therefore the steady state response of the Fuzzy based MRAC system with no load applied on the plant, so Rise time is 0.169seconds,settling time is 0.491seconds and percentage over shoot is 0.501% at rated speed of 1000rpm.

And a Rise time is 0.0784seconds, settling time is 0.20seconds and a percentage overshoot of 0.505% at rated speed of 1500rpm is observed comparatively good robust response of the plant at no load respectively.

5.5.2 Fuzzy Based Model Reference Adaptive Control at Load Condition

The Figure 5.23 and 5.24 below given indicates that how much the proposed system handles a load variation with the given rated speed of the plant when compared to with the others.

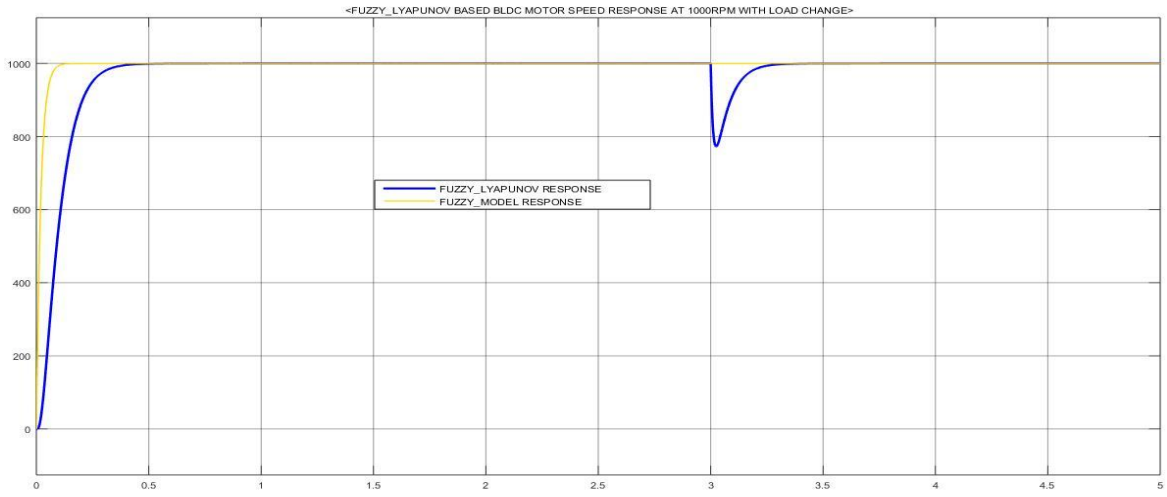

Figure 0.23 Fuzzy based MRAS controller with load change and rated speed of 1000rpm

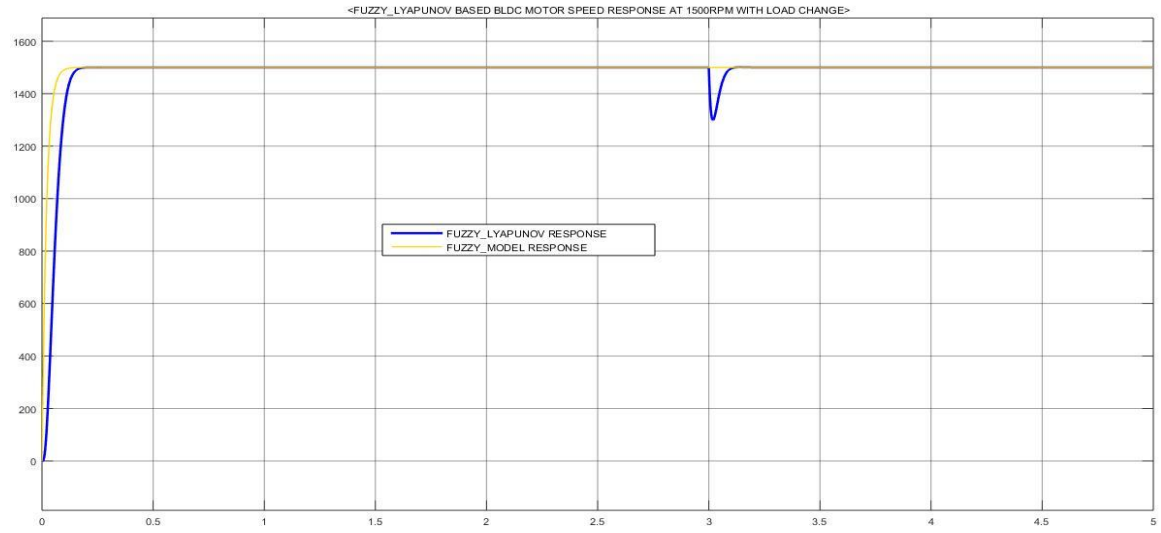

Figure 0.24 Fuzzy based MRAS controller with load and rated speed of 1500rpm

Hence the above Figures 5.23 and 5.24 show some considerable undershoot and a good speed response and good load rejection and stable response as adaptive control system and learning system.

5.6 Fuzzy Based Model Reference Adaptive Control at Unpredictable and Sudden Load Change

In order to further evaluate the response of the proposed controller configuration it has been evaluated under changing motor inertia and rated speed simultaneously at certain time. By increasing rated torque to 100Nm to show how much the system resists the unpredictable load disturbance or uncertain load disturbance and maintain the exact motor performance or operating condition. The following Figures 5.25and 5.26 shows the Simulink block diagram of system design with uncertain load disturbance and result performance at 1000rpm and 1500rpm rated speed and 100Nm of rated torque.

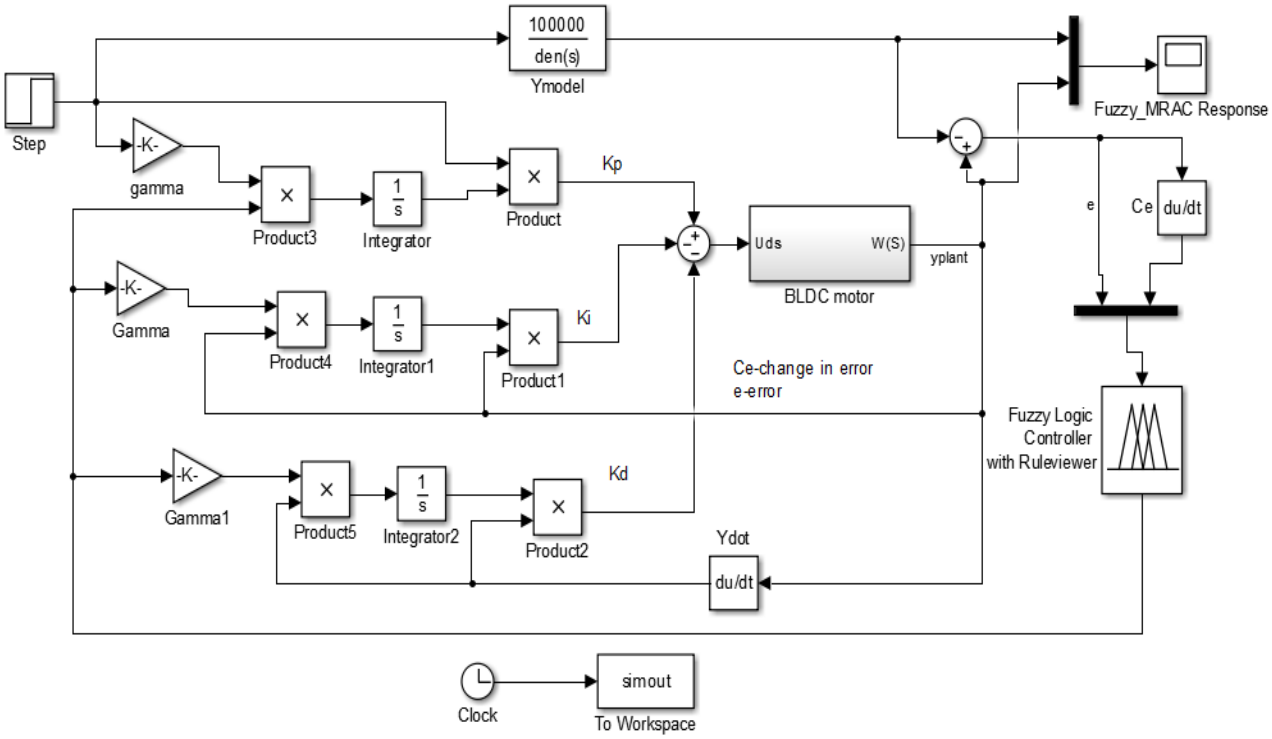

Figure 0.25 Fuzzy based MRAC system with uncertain load change Tds

5.6.1 Sub block diagram of BLDC motor with uncertain load

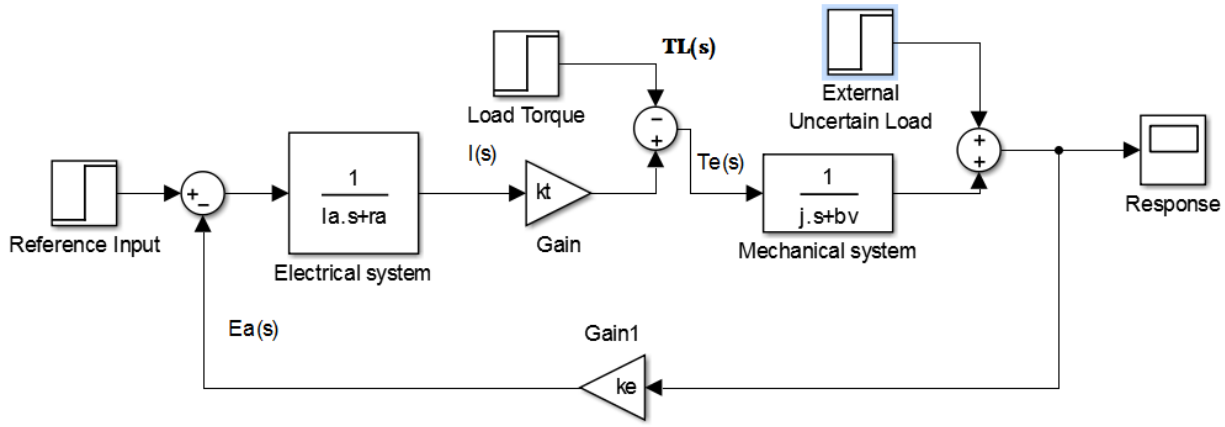

Figure 0.26 Sub block diagram of BLDC motor with uncertain load change Td(s)

5.6.2 MATLAB Simulink Result of Uncertain Load Change at Rated Speed and 100Nm Rated Torque

Figure 5.27 and Figure 5.28 depicts the output of the controller for uncertain load change in rated torque and it can be observed from the figures of controller output varies rapidly with the change in inertia. The rise time is sudden increase with small change and can help in enhancing the speed of response of the controller to maintain the constant speed of the rated speed.

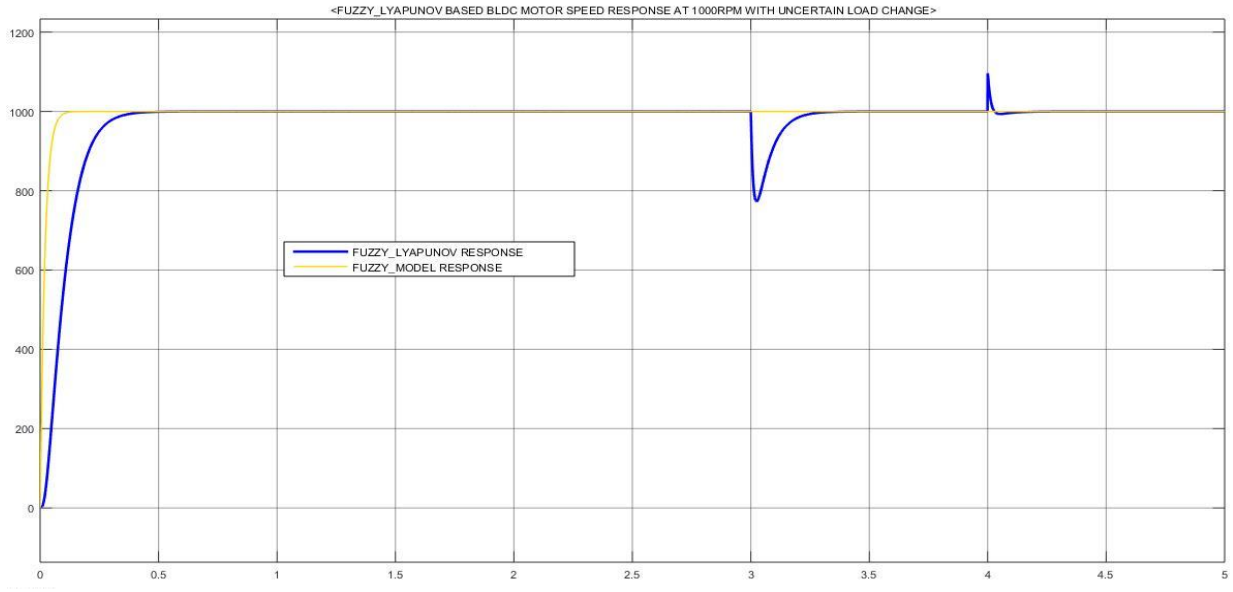

Figure 0.27 speed response of Fuzzy based MRAS controller at External sudden load and rated speed 1000rpm

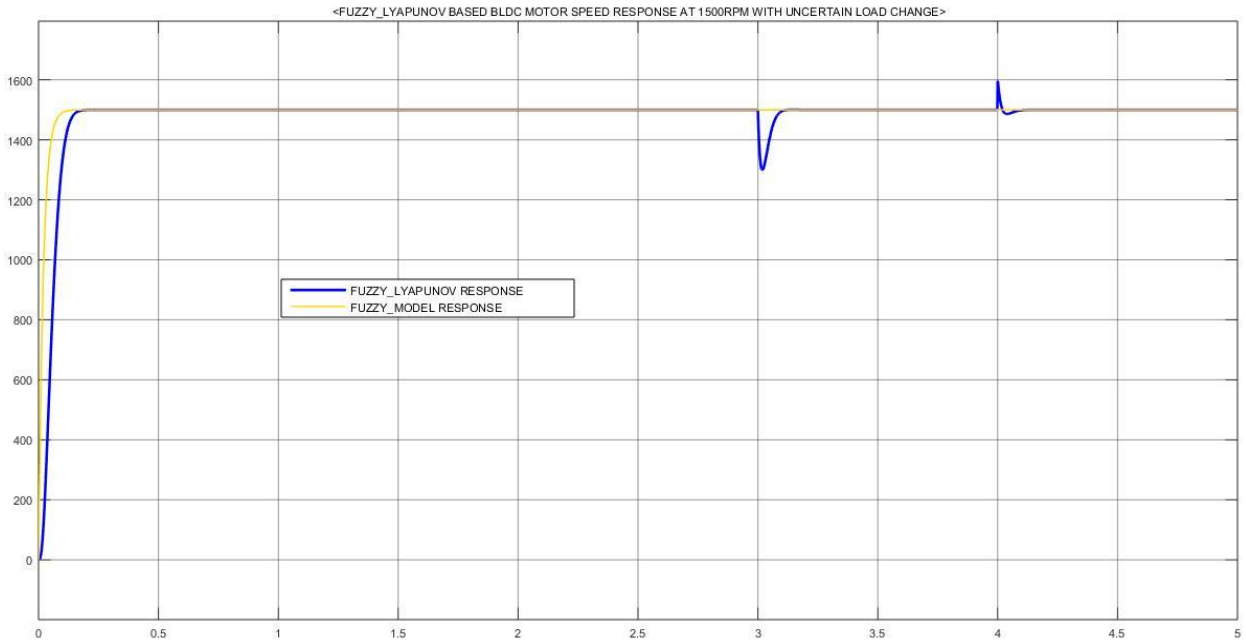

Figure 0.28 speed response of Fuzzy based MRAS controller at External sudden load and rated speed 1500rpm

As shown in the above the performance of the fuzzy based MRAC controller with load condition of speed and Torque. The uncertain and sudden load torque applied on the system is 100-300 Nm and applied at 3 and 4seconds to the close loop control system and it shows high stable response and fast load rejection due to that the offset overshoot also reduced instantly.

5.6.3 Proposed System result tracking and result compression

The given the following result shows how much the proposed control system sustain a load variation and track the reference model with a given speed and frequency oscillation to show the stability of the system with tracking speed and almost a zero error as a close loop control system. Therefore the following figures show the tracking speed response and some controller result compression of the system.

5.6.3.1 No Load Tracking Response of proposed controller

The following figures show how much the proposed system sustain load variation and give a stable response with compared to the others at steady state response of the plant at rated speed 1500rpm.

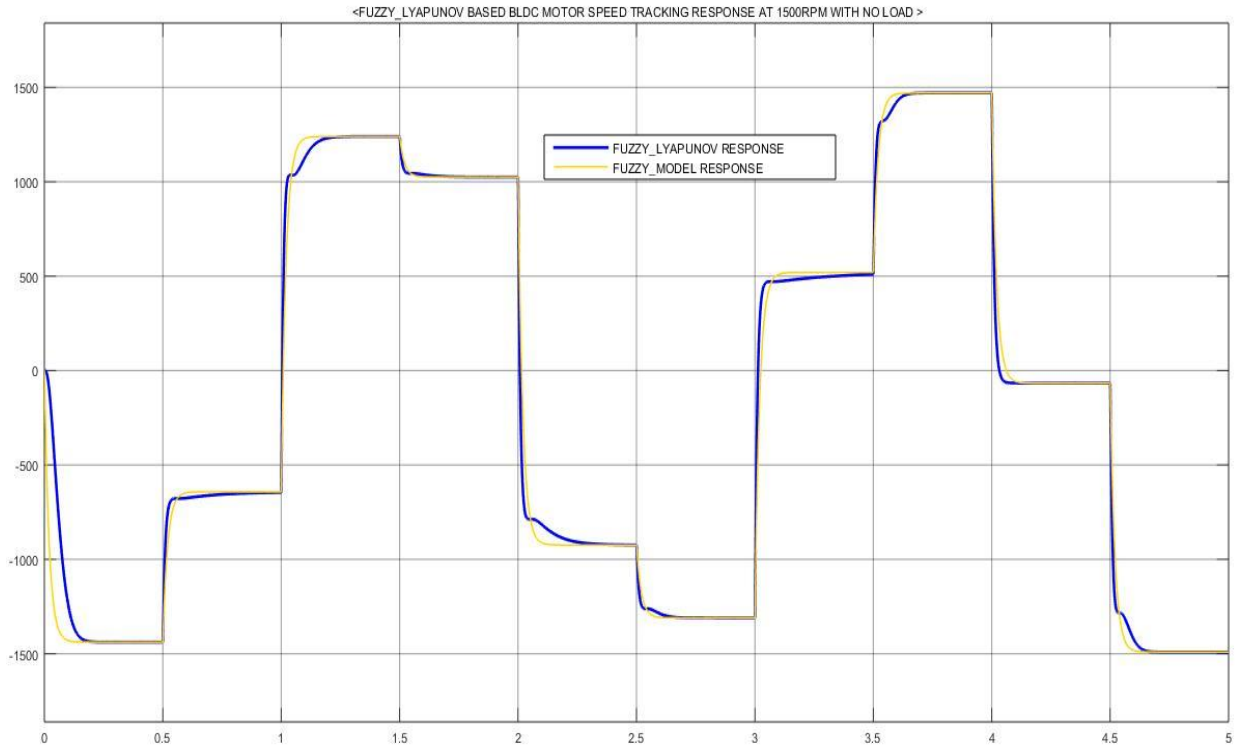

Figure 0.29 No load speed tracking response of Fuzzy based MRAC system with rated speed of 1500rpm

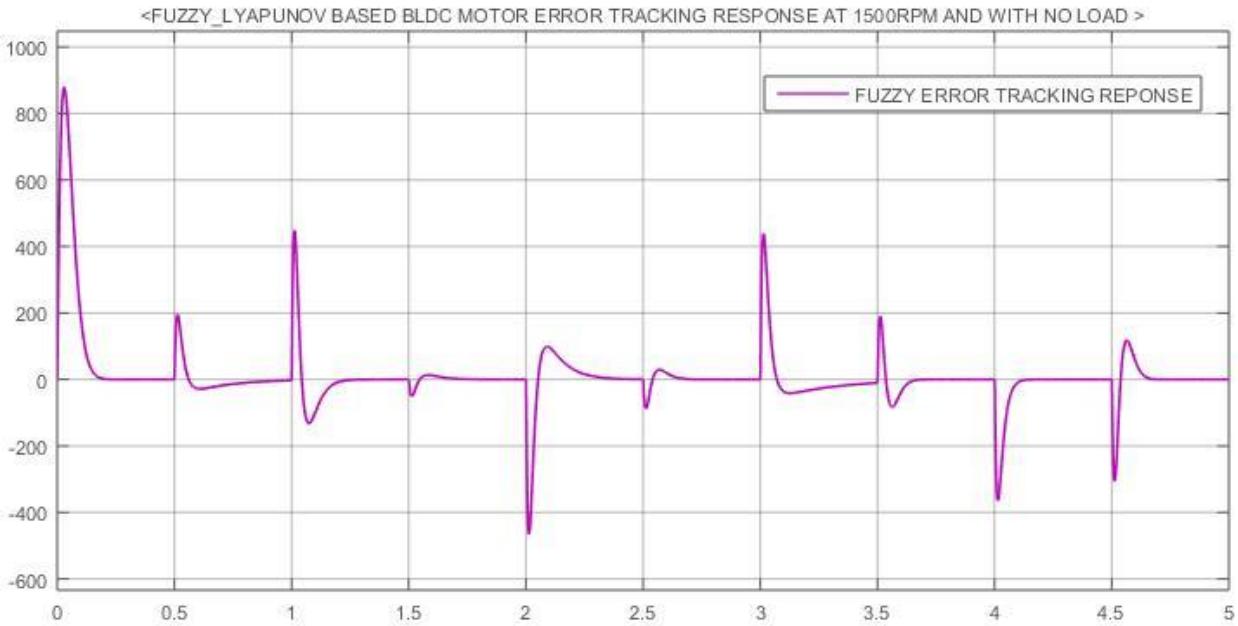

Figure 0.30 No load error tracking response of Fuzzy based MRAC system at 1500rpm rated speed

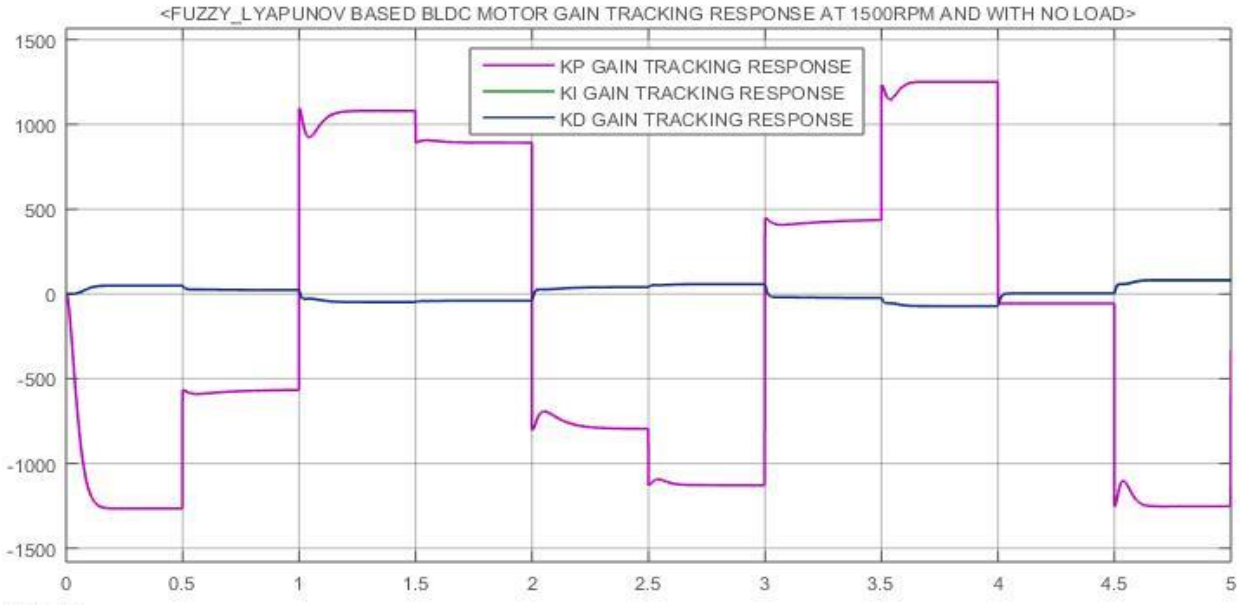

Figure 0.31 No load Gain tracking response of Fuzzy based MRAC system at 1500rpm rated speed

5.6.3.2 Load Tracking Response at 1500rpm and with load change Of Proposed System

The following tracking response based on load change on the plant shows the tracking response of proposed control system with a good response of tracking and almost a small error change observed as the result of the control system with load torque of 300Nm.

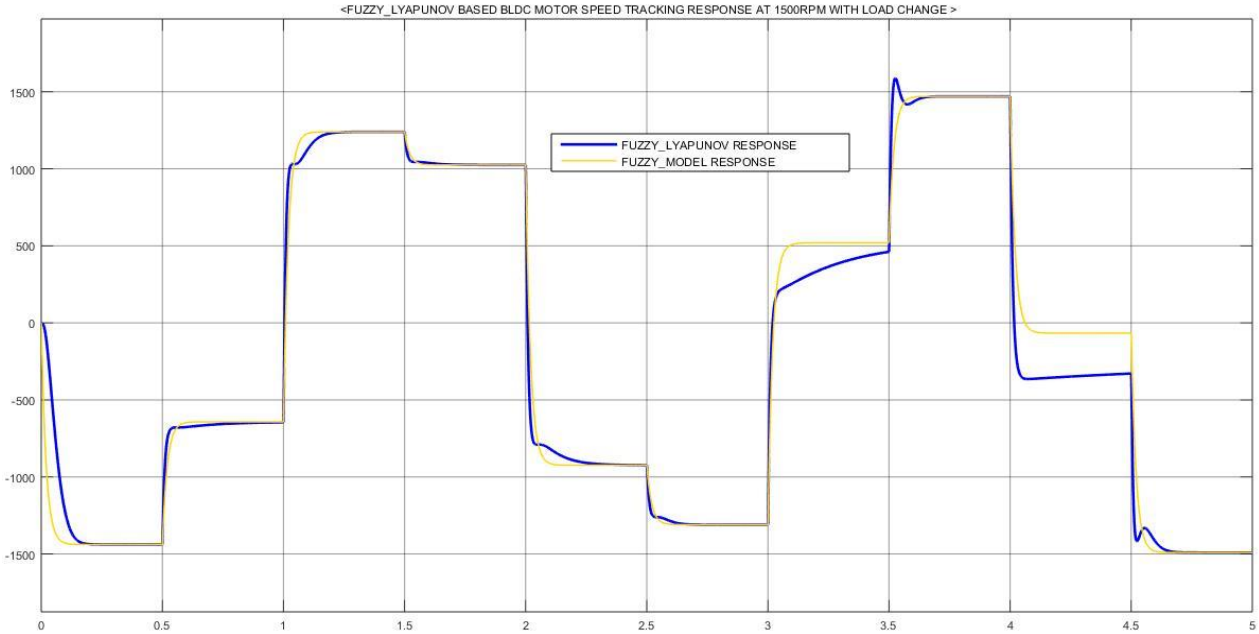

Figure 0.32 sudden load speed tracking response of Fuzzy based MRAC system

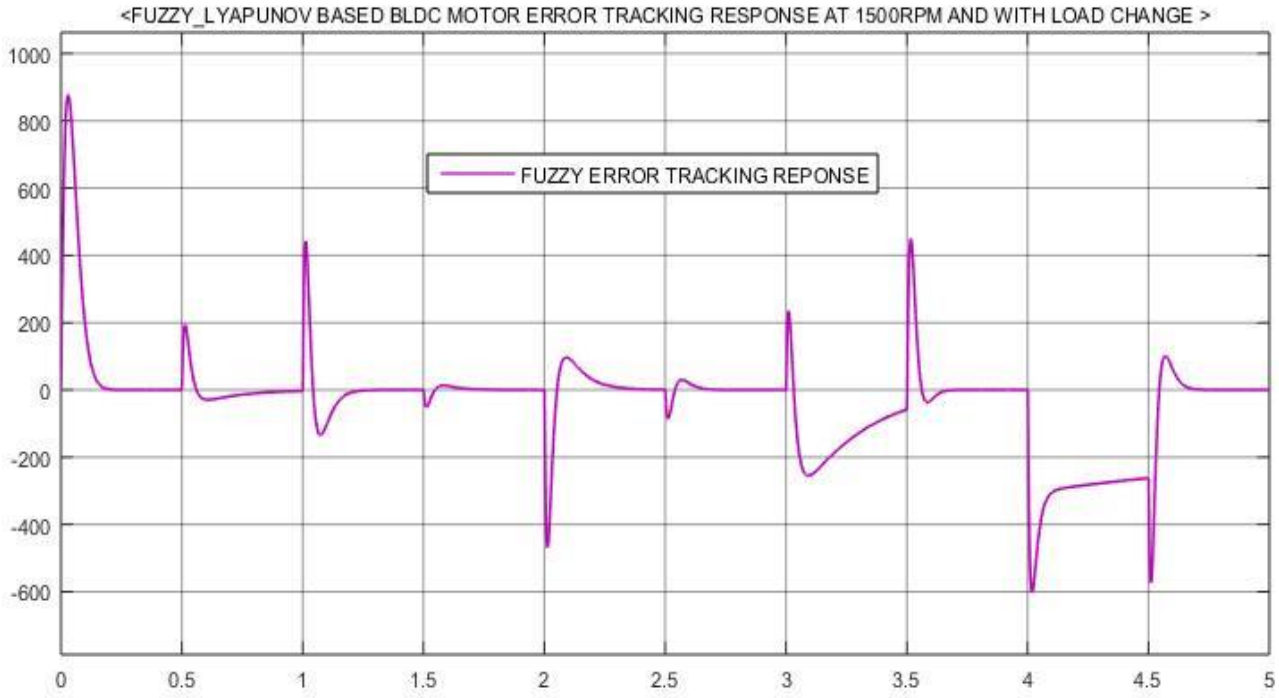

Figure 0.33 Error tracking response of Fuzzy based MRAC system with load change at rated speed

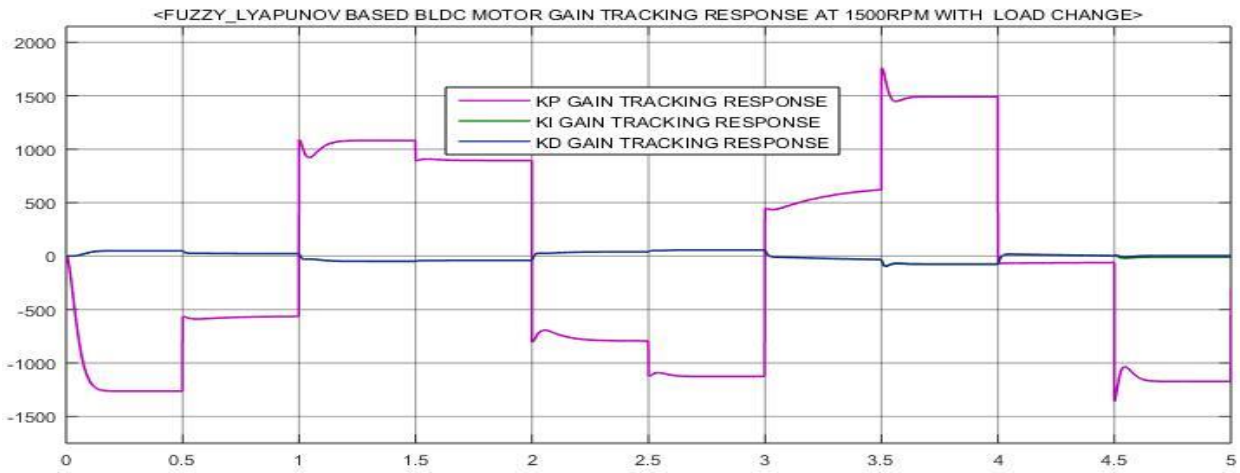

Figure 0.34 Gain tracking response of Fuzzy based MRAC controller system with load change at rated speed.

5.7 Proposed System Result Comparisons

5.7.1 No Load result comparison at rated speed of 1500rpm

The following system result indicates the comparison of output signal of the plant which have been indicate in the above but to show how much the proposed system responds to the applied rated speed with no load condition in the same plane with steady state performance characteristics.

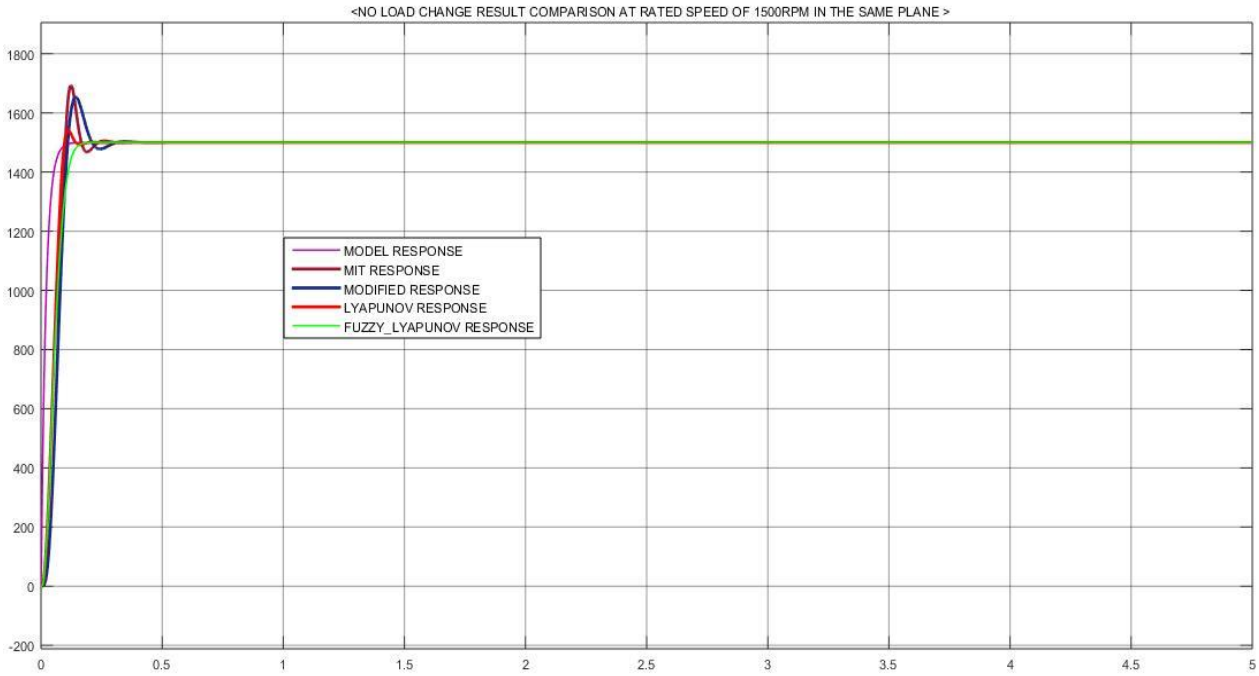

Figure 0.35 No load performance result comparison of each control system

5.7.2 With Load Change Result Comparison at Rated Speed of 1500rpm

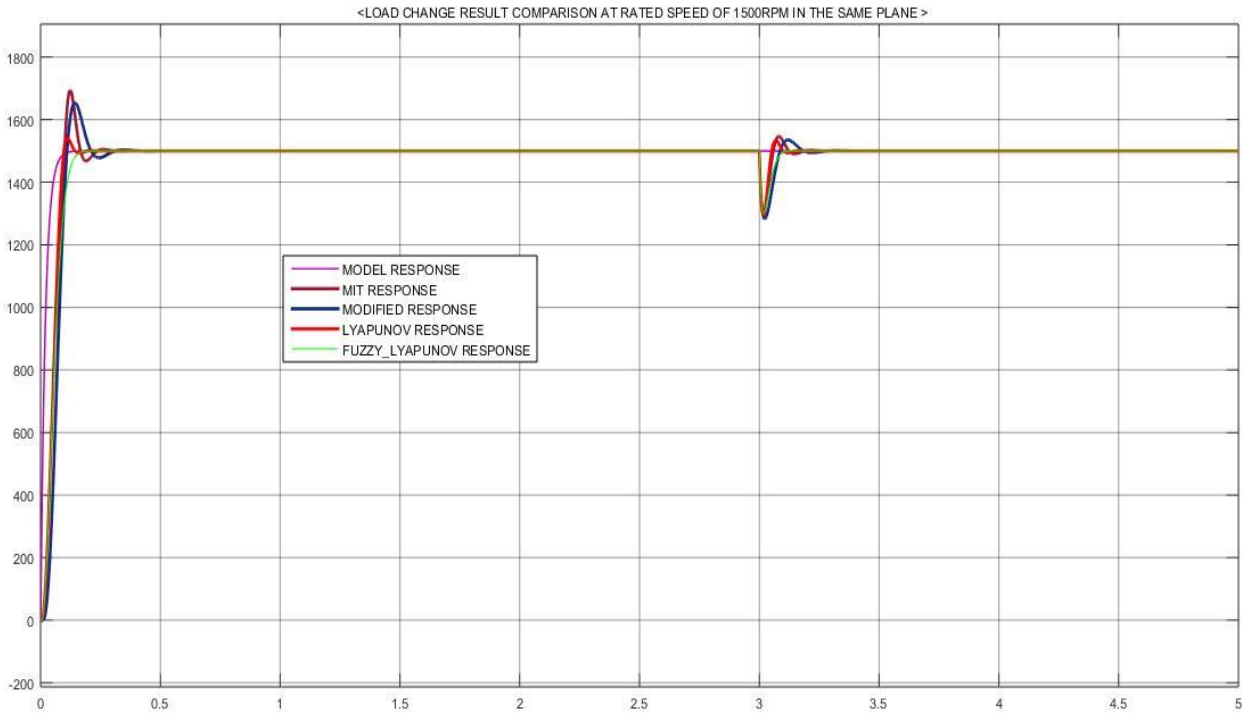

Figure 0.36 performance result comparison of each control system in the same plane with load change

5.8 Numerical Performance Comparison

The model reference adaptive control using Lyapunov stability method shows considerably reduced percentage overshoot and good tracking control with stability is ensured. Thus Fuzzy based Model Reference Adaptive Control using Lyapunov Stability Method shows the best control and tracking performance as compared to PID controller and simple MIT rule methods so the given table 7 below shows the Comparison between the performance characteristics of each controllers at rated speed of the motor.

5.8.1 No Load Numerical Comparisons at Rated Speed

Table 0.1 No load numerical Comparison between the characteristics of each controllers at 1500rpm rated speed.

Performance Characteristics	PID controller	MRAS with MIT rule	MRAS With Lyapunov Stability Method	Fuzzy based MRAS controller
Maximum Overshoot (%)	18.452	13.068	2.577	0.505
Rise time (sec)	0.00552	0.0567	0.0596	0.0784
Settling time (sec)	0.012	0.4580	0.195	0.200
Preshoot (%)	0.595	0.568	0.515	0.505
Undershoot (%)	-3.436	2.090	1.513	1.433

5.8.2 Load Change Based Numerical Comparisons at 1500rpm Rated Speed

Table 0.2 load change based performance comparisons at rated speed

Performance Characteristics	PID controller	MRAS with MIT rule	MRAS With Lyapunov Stability Method	Fuzzy based MRAS controller
Maximum Overshoot (%)	18.452	13.068	2.577	0.474
Rise time (sec)	0.00255	0.0565	0.0596	0.0784
Settling time (sec)	0.01214	3.41	3.30	3.102
Preshoot (%)	0.595	0.568	0.515	0.505
Undershoot (%)	-3.295	2.064	1.656	1.502

From numerical performance comparison characteristics a Fuzzy based MRAS controller shows better performance result and as given in the above Figures and tables result of performance listed than simple MRAS and conventional PID controller, only some percentage undershoot is observed.

CHAPTER SIX

CONCLUSION AND FUTURE WORK

6.1 Conclusion

The model of BLDC motor is developed with its dynamic characteristics and a controller is designed by using PID controller, Model Reference Adaptive controller algorithm with MIT rule as well as Lyapunov Stability method and Fuzzy based MRAC with Lyapunov stability method such that the speed control is obtained and is implemented using MATLAB/Simulink software. A comparative study between these three techniques were undergone and which shows that Fuzzy based Model Reference Adaptive controller with Lyapunov Stability method shows better results as it reduces the maximum overshoot and also disturbances are reduced almost rejected. Then there is considerable reduction in steady state error as well as settling time with some undershoot consideration. The stability of the system is also ensured using this type of controller and we have improved the existing system based on the numerical analysis and accurate percentage overshoot with god steady state response.

6.2 Future Work

In these thesis we tried to analysis the speed control of BLDC motor only on MATLAB Toolbox to conclude that Fuzzy based MRAS controller is better result than simple MRAS and conventional PID controller in performance and efficiency improvement. However, the simulation result of the controller can't be good in real time application or have to be done in experimental analysis, so we recommend that applying the proposed method to real time system and conduct full analysis of other power quality issues such as

- harmonic distortion,
- voltage imbalance, and
- Flux improvements of the motor.

To get a better performance and efficiency of the BLDC motor in a simple manner.

Additionally, system protection should take into consideration both under and over voltage conditions and also when the system runs there must be a continuous electric power, no voltage fluctuation occurred around the system area.

REFERENCES

[1] Vinod Kr Singh Patel, A.K.Pandey, "Modelling andSimulation of Brushless DC Motor Using PWM ControlTechnique", International Journal of Engineering Researchand Applications, Vol. 3, Issue 3, May-Jun 2013, pp.612-620., 2005.

[2] K. Ang, G. Chong, Y. Li, 'PID control system analysis, design, and technology', IEEE Trans. Control System Technology, Volume 13, pp. 559 – 576, 2005.

[3] Atef Saleh Othman Al-Mashakbeh, "Proportional Integral and Derivative Control of Brushless DC Motor", European Journal of Scientific Research 26-28 July 2009, vol.35, pg 198-203.

[4] Manafeddin Namazov, DC motor position control using fuzzy proportional-derivative controllers with different defuzzification methods, Turkish Journal of Fuzzy Systems, Vol.1, No.1, pp. 36-54, 2010.

[5] "Modelling and Control of Three Phase BLDC Motor using PID with Genetic Algorithm", UK Sim 13 the International Conference on Modelling and Simulation, pp.189-194, 2011. And Simulation, pp.189-194, 2011.

[6] Anjali.A.R "Control Of Three Phase BLDC Motor Using Fuzzy Logic Controller" International Journal of Engineering Research &Technology (IJERT), Vol. 2, Issue 7, July 2013.

[7] R. Kandiban, R. Arulmozhiyal "Design of Adaptive Fuzzy PID Controller for Speed control of BLDC Motor" International Journal of Soft Computing and Engineering ,Volume-2, Issue-1, March 2012

[8] J. J. E.Slotine, W. Li, "Composite Adaptive Control of Robot manipulators," Automatica, Vol. 25, pp. 509-519, 1991.

[9] Adel A.El-samahy and Mohamed A.Shamseldin, "BLDC motor tracking control using self-tuning fuzzy PID control and model reference adaptive control" Ain Shams university ,Ain Shams Engineering Journal (2018) 9,341-352.

[10] Thasneem. And Shalu George K."Speed Control of Brushless DC Motor Using Model Reference Adaptive Control", International Journal of Advanced Research in Electrical, Electronics and Instrumentation Engineering, Vol. 6, Issue 5, May 2017

[11] Lei Jin-li, "Adaptive Control for Brushless DC Motor Based on Fuzzy Inference". TELKOMNIKA Indonesian Journal of Electrical Engineering, 12(5): 3392-3398, 2014.

[12] M. A. Shamseldin, and A. M. A. Ghany, M. A. A. Ghany, "Performance Study of Enhanced Non-Linear PID Control Applied on Brushless DC Motor," International Journal of Power Electronics and Drive System (IJPEDS), vol. 9, no.2, pp. 536–545, 2018

[13] Murali Dasari,A Sreenivasula Reddy and M Vijayakumar, "Modelingof a commercial BLDC motor and control using GA-ANFIS tuned PID controller" - IEEE International Conference on Innovative Research In Electrical Sciences (IICIRES), 2017.

[14] Adel A.El-samahy. and Mohammed A.Shamseldin," Brushless DC Motor tracking control using self-tuning fuzzy PID control and model reference adaptive control ", Ain Shams Engineering Journal (2018), 22 march 2016.

[15] John Wiley & Sons Singapore "PERMANENT MAGNET BRUSHLESS DC MOTOR DRIVES AND CONTROLS" First Edition. Chang-liang Xia.pp 26-52, Science Press. Published 2012.

[16] Walter, N. A., Stephen, L. H. (2003) Electric Motor Control. Thomson/Delmar Learning, Australia.

[17] Krause, P. C. (1986) Analysis of Electric Machinery. Kinsport Press Inc., Kinsport Town.

[18] Pillay, P., Krishnan, R. (1989) Modeling, simulation, and analysis of permanent-magnet motor drives, part I: the permanent-magnet synchronous motor drive. IEEE Transactions on Industry Application, 25(2), 265–273.

[19] Gao,J.,D.,Wang,X.H.,Li,F.H.(2005) AC Motor and Its Analysis.(2nd edition) Tsinghua University press, Beijing (Chinese).

[20] I. Press, L. Shafer, G. W. Arnold, and D. Jacobson, ANALYSIS OF ELECTRIC MACHINERY AND DRIVE SYSTEMS. 2013.

[21] Mohamed. A.Shamseldin, M. Abdullah Eissa, and Adel. A. EL-Samahy, "A Modified Model Reference Adaptive Controller for Brushless DC Motor", 17th International Middle East Power Systems Conference, Mansoura University, Egypt, December 15-17, 2015.

[22] C. Mohankrishna, N. Rajesh Kumar Gowd, A. Ramesh, and G. Subba Rao Gupta, "Modelling and Simulation of BLDC Motor Using State Space Approach", International Journal of Innovative Research in Electrical, Electronics, Instrumentation and Control Engineering, Vol. 4, Issue 5, May 2016.

[23] Murali Dasari et al," GA-ANFIS PID compensated model reference adaptive control for BLDC motor" International Journal of Power Electronics and Drive System (IJPEDS), Vol. 10, No. 1, March 2019, pp. 265~276.

APPENDIX A

Programing with MATLAB Code:

To simulate the fuzzy controller in MATLAB, first the rules have to be coded.

Coded rules:

[System]

Name='rules'

Type='mamdani'

Version=2.0

NumInputs=2

NumOutputs=1

NumRules=49

AndMethod='min'

OrMethod='max'

ImpMethod='min'

AggMethod='max'

DefuzzMethod='centroid'

[Input1]

Name='Error',

Range=[-0.8 0.8]

NumMFs=7

MF1='NL':'trapmf',[-0.8 -0.8 -0.6 -0.4]

MF2='NM':'trimf',[-0.4 -0.2 -0.02]

MF3='NS':'trimf',[-0.2 -0.1 0]

MF4='ZE':'trimf',[-0.02 0 0.02]

MF5='PS':'trimf',[0 0.1 0.2]

MF6='PM':'trimf',[0.02 0.2 0.4]

MF7='PL':'trapmf',[0.4 0.6 0.8 0.8]

[Input2] Name='ChangeInError'

Range=[-0.8 0.8] NumMFs=7

MF1='NL':'trapmf',[-0.8 -0.8 -0.6 -0.4]

MF2='NM':'trimf',[-0.4 -0.2 -0.02]

MF3='NS':'trimf',[-0.2 -0.1 0]

MF4='ZE':'trimf',[-0.02 0 0.02]

MF5='PS':'trimf',[0 0.1 0.2]

[Output1]

Name='ChangeOfControl'

Range=[-1 1] NumMFs=11

MF1='NL':'trimf',[-1 -1 -0.8]

MF2='NLM':'trimf',[-0.7 -0.5 -0.3]

MF3='NM':'trimf',[-0.6 -0.4 -0.2]

MF4='NMS':'trimf',[-0.3 -0.2 -0.1]

MF5='NS':'trimf',[-0.4 -0.2 0]

MF6='ZE':'trimf',[-0.2 0 0.2]

MF7='PS':'trimf',[0 0.2 0.4]

MF8='PSM':'trimf',[0.1 0.2 0.3]

MF9='PM':'trimf',[0.2 0.4 0.6]

MF10='PML':'trimf',[0.3 0.5 0.7]

MF11='PL':'trimf',[0.8 1 1]

APPENDIX B

```
% ---------- Unit-step response ---- ------
% ***** Enter numerators and denominators of systems with
% z = 0,0.2,0.4,0.6,0.8 and z=1, respectively. *****
 num1= [0 0 100];
den1 = [1 0 100];
num2 = [0 0 100];
den2 = [1 4 100];
num3 = [0 0 100];
den3 = [1 8 100];
num4 = [0 0 100];
den4 = [1 12 100];
num5 = [0 0 100];
den5 = [1 16 100];
num6 = [0 0 100];
den6 = [1 20 100];
t = 0:0.125:10;
[c1 ,x1 ,t] = step(num1 ,den1 ,t);
[c2,x2,t] = step(num2,den2,t);
[c3 ,x3 ,t] = step(num3 ,den3 ,t);
[c4,x4,t] = step(num4,den4,t);
[c5 ,x5 ,t] = step(num5 ,den5 ,t);
[c6,x6,t] = step(num6,den6,t);
plot(t,c1 ,t,c2, t,c3,t,c4,t,c5,t,c6)
text(1,1.65,'z = 0')
text(0.5,1.39,'z = 0.2')
 text(0.5,1.26,'z = 0.4')
  text(0.5,1.16,'z = 0.6')
  text(0.5,1.06,'z = 0.8')
  text(0.40,0.92,'z = 1')
```

```
grid
title('Unit-step Responses of six Systems')
xlabel('t Sec')
ylabel('speed 0utputs of z=0,0.2,0.4,0.6,0.8 and 1')
```